Cannat, M., Karson, J.A., Miller, D.J., et al., 1995
Proceedings of the Ocean Drilling Program, Initial Reports, Vol. 153

5. SITE 922[1]

Shipboard Scientific Party[2]

HOLE 922A

Date occupied: 29 December 1993

Date departed: 1 January 1994

Time on hole: 2 days, 22 hr, 52 min

Position: 23°33.162′N, 45°1.926′W

Bottom felt (drill-pipe measurement from rig floor, m): 2612.0

Distance between rig floor and sea level (m): 11.10

Water depth (drill-pipe measurement from sea level, m): 2600.9

Total depth (from rig floor, m): 2626.60

Penetration (m): 14.60

Number of cores (including cores having no recovery): 3

Total length of cored section (m): 14.60

Total core recovered (m): 9.23

Core recovery (%): 63

Oldest sediment cored: None

Hard rock:
Depth (mbsf): 14.50
Nature: Troctolite, olivine gabbro, gabbro
Measured velocity (km/s): 5.00–5.77

HOLE 922B

Date occupied: 1 January 1994

Date departed: 7 January 1994

Time on hole: 5 days, 20 hr, 03 min

Position: 23°31.368′N, 45°1.926′W

Bottom felt (drill-pipe measurement from rig floor, m): 2612.0

Distance between rig floor and sea level (m): 11.20

Water depth (drill-pipe measurement from sea level, m): 2600.8

Total depth (from rig floor, m): 2649.40

Penetration (m): 37.40

Number of cores (including cores having no recovery): 5

Total length of cored section (m): 37.40

Total core recovered (m): 11.93

Core recovery (%): 31

Hard rock:
Depth (mbsf): 37.40
Nature: Troctolite, metatroctolite, olivine gabbro, gabbro, oxide gabbro, metagabbro
Measured velocity (km/s): 4.7–5.9

Principal results: Site 922 is located about 2 km south of Site 921 at 23°31.37′N, 45°01.93′W, on the western median valley wall of the Mid-Atlantic Ridge (MAR; Fig. 1, "Site 921" chapter, this volume). This site lies among extensive outcrops of massive to foliated gabbroic(?) rocks on a terrace sloping 15° to 25° to the east near the top of a prominent cliff. A pilot hole, Hole 922A, reached a depth of 14.6 mbsf and yielded 9.23 m of gabbroic rock. Based on the favorable drilling conditions in Hole 922A and the relatively subdued terrain, deployment of a hard-rock guide base (HRGB) was attempted at Site 922. Deployment of the HRGB failed, however, and an attempt to re-enter Hole 922A resulted in spudding Hole 922B less than 1 m away.

Hole 922A penetrated to 14.6 mbsf with a cumulative recovery of 9.23 m (63.2%). Hole 922B reached a depth of 37.4 mbsf and recovered 11.93 m (31%, excluding the first wash core) of gabbroic material (Table 1). The upper portions of both cores, as expected, are very similar; however, they show minor differences in alteration reflecting the heterogeneous nature of fracturing and hydration in this terrane.

Cores from the uppermost part of both holes are composed of intensely hydrothermally altered (total alteration ranges from 30% to 95%) rocks considered to have been derived mostly from a troctolitic protolith. Mafic minerals are nearly completely replaced by a fine mesh of chlorite and actinolite. Olivine exhibits complex and variably developed coronas of iddingsite, talc, tremolite, smectite, pyrite, and iron oxide minerals, and it is commonly rimmed by chlorite. Plagioclase is only moderately altered, except in the vicinity of thin chlorite-coated veinlets.

Below these highly altered rocks, fresher troctolite and olivine gabbro intervals with well preserved igneous and structural features were recovered. Poikilitic olivine gabbro with very coarse (up to 15 cm) clinopyroxene crystals as well as lesser metatroctolite were also sampled. Locally, these rocks contain centimeter- to decimeter-sized patches and irregular layers and veins of oxide-bearing gabbro or metagabbro, with abundant apatite and zircon. Leucocratic veins a few centimeters wide also occur locally in the core.

In the less altered intervals, plagioclase is commonly relatively fresh, with chlorite-actinolite rims and a trace of epidote replacement. Secondary minerals after clinopyroxene include brown amphibole, actinolite, and iron oxide minerals. Hairline to centimeter-wide veins of actinolite, actinolite ± chlorite, and chlorite occur throughout the core. Rare epidote ± prehnite veinlets occur locally.

Shape preferred orientations, inferred to have resulted from magmatic flow, are scarce in gabbroic rocks from Site 922. Crystal-plastic deformation is concentrated predominantly in discrete shear zones, typically a few centimeters to a few decimeters wide, which display well-defined sharp boundaries and strong grain-size reduction. They form anastomosing networks and have no consistent dip throughout the cores. Some of these are localized in intervals of oxide-bearing gabbro. Brittle deformation throughout most of the troctolite and olivine gabbro intervals is restricted to arrays of microcracks, closely spaced fracture networks, and several generations of veins. Some sheared actinolite veins also occur.

Remanence data from both the archive half-cores and discrete samples from Site 922 indicate predominantly normal magnetic polarity. The majority of samples, with a mean inclination ($42.2° \pm 3.6°$, $n = 15$) are similar to the expected dipole inclination (41°) at Site 922. However, two samples have high-stability components of shallow negative inclinations. These negative inclinations may reflect either tectonic rotations or the incomplete isolation of reversed polarity characteristic remanence as a

[1] Cannat, M., Karson, J.A., Miller, D.J., et al., 1995. *Proc. ODP, Init. Repts.*, 153: College Station, TX (Ocean Drilling Program).

[2] Shipboard Scientific Party is given in the list of participants preceding the contents.

Table 1. Coring summary, Holes 922A and 922B.

Core	Date	Time (UTC)	Depth (mbsf)	Cored (m)	Recovered (m)	Recovery (%)
153-922A-						
1R	31 Dec 1993	1300	0.0–6.6	6.6	1.26	19.1
2R	01 Jan 1994	1425	6.6–13.5	6.9	6.93	100.0
3R	01 Jan 1994	1855	13.5–14.6	1.1	1.04	94.5
Coring totals				14.6	9.23	63.2
153-922B-						
1W	04 Jan 1994	1635	0.0–14.0	14.0	2.40	
2R	05 Jan 1994	0930	14.0–19.0	5.0	3.37	67.4
3R	05 Jan 1994	1750	19.0–24.0	5.0	2.67	53.4
4R	06 Jan 1994	0805	24.0–33.5	9.5	3.41	35.9
5R	06 Jan 1994	1935	33.5–37.4	3.9	0.08	2.1
Coring totals				23.4	9.53	40.7
Washing totals				14.0	2.40	
Combined totals				37.4	11.93	

result of a significant normal polarity low-stability component. The mean NRM intensity (arithmetic mean = 1.45 A/m ± 1.4) and Koenigsberger ratio (3.95) are similar to the values obtained from Site 921 gabbroic rocks.

Gabbroic rocks recovered at Site 922 have grain densities between 2.8 and 3.0 g/cm^3 and relatively low porosities (0.23% to 1.23%). V_p ranges from 5.0 to 6.16 km/s. The densities and velocities of these rocks are lower than observed at Site 921, and porosity is slightly higher.

OPERATIONS

Site 921 Transit to Site 922 (MK-1)

As the drill string was being retrieved from Hole 921E the vessel was offset in DP mode approximately 0.9 nmi to the south. A positioning beacon was dropped at 1720 hr, 29 December, initiating Site 922. Because none of the pilot holes (Holes 921A, 921B, 921C, 921D, and 921E) indicated a favorable location for setting the HRGB, the decision was made to investigate a new site. After reviewing *Nautile* dive tapes of the area, Site 922 was chosen.

Hole 922A

A new rotary core barrel bottom-hole assembly (RCB BHA) was made up and deployed. The VIT was then lowered down the drill string for a seafloor survey. After 21 hr, 30 min of surveying the bit was set on the seafloor to attempt spudding Hole 922A. A jet test was performed at 350 gpm with 10,000 lb weight on bit (WOB) resulting in virtually zero penetration. As the VIT was being retrieved in preparation for spudding the hole, the bit slid downhill 9.5 m. The VIT was run back to bottom to inspect the BHA. The BHA was found intact and the bit was repositioned for spudding. Another jet test was performed with similar results. The VIT was then retrieved and Hole 922A was spudded at 2156 hr, 30 December.

Hole 922A seafloor depth was determined by drill-pipe measurement to be 2612 mbrf (2600.9 mbsl). Hole 922A was cored three times to a total depth of 2626.6 mbrf (14.6 mbsf) recovering 9.23 m of metamorphosed gabbro (Table 1). The overall penetration rate was approximately 0.3 m/hr. The decision was made to pull out of the hole and set the HRGB. The bit cleared the seafloor at 1612 hr, 1 January, ending Hole 922A.

The drill string was retrieved in preparation for deploying the HRGB. The same HRGB that was deployed at Hole 920C was picked up and lowered to the seafloor without incident. The HRGB was landed on the seafloor 13 times in 5 hr and 15 min as the ship was offset between each landing. Each time the HRGB was landed a slope of greater than 22.5° was indicated. With ever-increasing odds of damaging the HRGB due to heave while landing, the decision was made to abort the landing and retrieve the HRGB.

Hole 922B

After recovering the HRGB, a new RCB BHA was made up. The BHA and VIT were lowered to the seafloor. A search was then made for Hole 922A with the intent of reentering and deepening it. The first attempt at reentering what appeared to be Hole 922A was unsuccessful. After 2 hr of searching, another attempt was made at reentering what was believed to be Hole 922A. When the BHA landed on the seafloor without reentering the hole the decision was made to spud Hole 922B at that location.

Hole 922B was spudded at 0900 hr, 3 January. Hole 922B seafloor depth was determined by drill-pipe measurement to be 2612 mbrf (2600.8 mbsl). The first core (Core 153-922B-1W) had to be cored to 14 mbsf before a drill-pipe connection could be made without the bit heaving out of the hole. The hole was cored to 2649.4 mbrf (37.4 mbsf) recovering 9.53 m of gabbro. An additional 2.42 m of gabbro was recovered in the wash core. The penetration rate was 0.3 m/hr throughout most of the drilling in the hole.

With 75.1 rotating hours on the bit the decision was made to pull out of the hole for a bit change and attempt a reentry. Hole 922B was successfully reentered without a reentry funnel. However, when the hole was reamed to 12 mbsf the BHA top sub box failed, leaving the outer core barrel assembly in the hole. With the loss of the outer core barrel assembly, the hole could not be advanced. The drill string was pulled out of the hole clearing the seafloor at 1215 hr, 7 January, ending Hole 922B.

Camera Survey

A VIT camera survey was conducted to locate a suitable site for Hole 922A 1.8 km (1 nmi) south of Site 921. This additional site was necessary to provide an alternative drilling target for deep penetration of gabbroic rocks and for deployment of a HRGB. A positioning beacon was dropped at 23°31.45′N, 45°01.72′W, at a water depth of 2745 m (Fig. 1). This position is in the vicinity of extensive gabbro exposures documented by *Alvin* dive 1012 (Karson and Dick, 1983) and *Nautile* dive HS 17 (Mével et al., 1991) between depths of 3000 and 2200 m.

The first several hours of the survey traversed huge detached blocks of massive to foliated rock presumed to be gabbro. This mega-talus was composed of blocks ranging from 1 to more than 10 m across. A variable thickness of pelagic ooze, generally less than a few tens of centimeters thick, covers subhorizontal surfaces. Steep faces of blocks are completely devoid of sediment.

A traverse of about 200 m to the west climbed this talus ramp in search of the headwalls of scarps from which it had been derived. Along this traverse, at a depth of about 2600 m, the seafloor slope decreases abruptly and traverses were made to the north and south following this distinct break in slope. At a point about 270 m west and 140 m south of the beacon, a series of steep, rugged scarps exposing massive gabbroic(?) rocks was encountered. In this vicinity, the acoustic signal from the positioning beacon became erratic and unreliable so a second beacon was deployed. After resetting the navigational reference system and completing a brief survey, it was determined that the scarps in this area were too steep to be likely drilling targets. The survey proceeded generally upslope over a heavily sedimented seafloor to the west. At about 100 m west of the new beacon, an isolated southeast-trending scarp in massive (gabbroic) rock was found emerging from the otherwise smoothly sedimented bottom. This scarp was briefly surveyed and abandoned when no subhorizontal outcrop surfaces were found. The survey continued north about 50 m and then upslope to the west another 70 m to a depth of approximately 2435 m. Only smooth pelagic ooze with widely dispersed cobbles to boulders of rock were observed. Failing to locate potential drilling sites led to the decision to return to the scarps near the second beacon.

Some 60 m south of the beacon along the edge of the steep scarp, a series of relatively gently sloping rock benches was found (Fig. 1). These proved to extend at least several tens of meters south and were subsequently surveyed in detail to define their lateral extent, geological characteristics, and inclination. This area is located near a rounded corner defined by a broad, moderately sloping, east-facing scarp and a steeper, more abrupt, south-facing scarp. Above these cliffs, the slope of the outcrop surface diminishes gradually, producing a broad, rounded shoulder. West of the cliffs are a series of smooth-looking bare-rock terraces. These terraces are 5–10 m wide and separated by steep, contour-parallel steps 1–2 m high. The terraces appear to have progressively less steeply inclined surfaces upslope to the west and north. Isolated cobbles and boulders are strewn across the rock surfaces and there is a minimal (few tens of centimeters) cover of pelagic ooze. These ledges were considered to be potential sites for the deployment of an HRGB.

About 10 m upslope from the edge of the cliff, a rounded step 2 m high marks the beginning of an area of more continuous boulders and rubble separated by pockets of smooth sediment. No basement surfaces are visible upslope from this point and it appears that there is a continuous layer of poorly consolidated rubble, ranging up to a few meters thick, covering any outcrops. The surface of this area is much more irregular than the rock ledges below; however, relatively smooth pockets of sediment between steeper areas with more rubble are common. Upslope, the rubble is completely blanketed by smooth to rippled and bioturbated pelagic ooze.

Lowering the drill bit to the seafloor at numerous points and recording the bit depths yielded estimates of the slopes across this shoulder. These estimates ranged from 6° to 25°, though this method is regarded to have an error of at least 5°. Several observations supported the view that slopes in this area are 20° or less. First, subangular boulders rest directly on top of relatively smooth, flat outcrop surfaces, suggesting that the surfaces are well below the maximum angle of repose. Some of the boulders were nudged by the drill string and did not roll down the slope. Low-density sediment, when disturbed by the drill bit, flowed slowly downslope in a sluggish turbidity flow. Based on observations of these types of flows on different slopes at Sites 920 and 921, the slope in this area appeared to be only slightly steeper than previously drilled sites.

A first attempt to spud a hole was made in the rubble just above the smooth rock ledges along the cliff edge. An attempt to jet-in at this point demonstrated that there was no significant rubble or sediment but that there was a significant slope, probably at least 15°–20° to the south. Unfortunately the drill bit slid off the outcrop before drilling could begin. A second spot was chosen about 20 m west of the cliff edge, well back into the rubble and sediment-covered area upslope. Another jet test showed only very limited sediment cover but still a significant slope, probably in the range of 15°–20°. Drilling began smoothly at this point and it became immediately apparent from drilling characteristics that there was virtually no rubble in this location. These results suggested that despite the rubbly look of the surface even 10 to 20 m from the cliff, bare rock outcrop is exposed beneath a very thin and discontinuous cover of pelagic ooze and isolated rock fragments.

Following a successful, shallow (14.6 m) pilot hole (Hole 922A), a brief VIT camera survey was made to find an optimal location for a guide base. During this survey the area immediately around Hole 922A was deemed suitable. The area was mapped in detail so that sufficient landmarks would be available for positioning the guide base. Subsequent attempts to deploy the guide base and later to re-enter Hole 922A were also monitored with the VIT camera. Having the HRGB hanging from the drill string hindered the view, and only a few of the landmarks identified during the previous survey could be recognized. It appeared that failure to settle the HRGB at a safe angle was due in part to the general slope being steeper than estimated, but also to the rugged, angular small-scale topography of the seafloor.

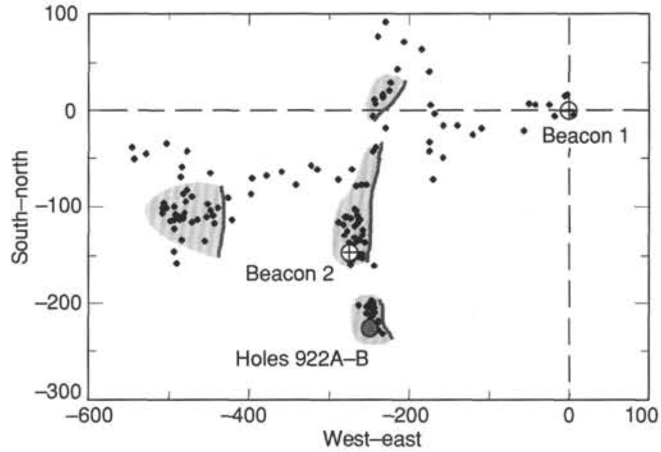

Figure 1. Map view of traverse from original Site 922 positioning beacon (Beacon 1) to Holes 922A and 922B (23°31.362′N, 45°01.926′W). Dots represent positions determined by navigation during the survey. Shaded areas represent outcrops, and thick lines are inferred faults bounding these outcrops.

Lithologic Units

Hole 922A

Two lithologic units have been defined in Hole 922A (Table 2; Fig. 2). The uppermost 6.9 m of the core recovered consists of highly altered gabbroic rocks, probably metatroctolite (Unit 1). Hand specimens of these extensively altered rocks are gray-green. Mafic phases and plagioclase near mafic grains are almost completely altered to various amphiboles and chlorite so that the protolith and possible variability of protoliths within the unit are difficult to assess in hand specimens. Thin sections of rocks from this unit show that minor relict clinopyroxene and substantial plagioclase remain, and suggest that olivine, now 100% altered, was also abundant. The degree of alteration drops substantially between Pieces 3 and 4 in Section 153-922A-2R-1, and below this point the protolith can be unequivocally identified. Because of the uncertainty about the nature of the protoliths of these rocks and their distinct visual appearance, they have been grouped as a single unit. The contact between this highly altered unit and the underlying troctolite and olivine gabbro of Unit 2 was not recovered.

Unit 2 in Hole 922A is dominated by troctolite and olivine gabbro but also includes numerous small intrusive and sheared intervals of oxide gabbro and gabbronorite. Interlayering of olivine gabbro and troctolite is common, and grain-size layering is also observed. Clinopyroxene is present as a fine-grained interstitial phase throughout much of this unit, and its relative abundance determines the change from troctolite to olivine gabbro.

Hole 922B

In Hole 922B, two units have been defined (Table 2), although both of these units are, in detail, lithologically complex. The unit designations indicate the dominant rock types, and other rock types present are noted in the sections where these units are fully described. Unit 1 consists of troctolite and olivine gabbro, but also includes metatroctolite (Fig. 3), oxide gabbro and oxide gabbronorite, as well as felsic veins, some of which are oxide-mineral-rich. As in Hole 922A, troctolite and olivine gabbro are intimately mixed in this unit, with the rock type changing as the proportion of fine-grained, interstitial clinopyroxene changes. In Section 153-922B-2R-2 within this unit, several pieces consist of both meta-olivine gabbro and gneissic oxide gabbronorite, which are juxtaposed along sheared, possibly intrusive, contacts. The boundary between Unit 1 and the underlying poikilitic olivine gabbro of Unit 2 was not recovered.

Table 2. Summary of lithologic units defined for Holes 922A and 922B.

Hole	Unit	Name	Cored interval From	Cored interval To	Curatorial depth to top of unit (mbsf)	Recovered (m)	Recovery (approx. %)
922A	1	Meta-troctolite (?)	1R-1(1)	2R-1(3)	0.00	1.57	19.10
	2	Troctolite and olivine gabbro	2R-1(4)	3R-1(4)	6.91	7.66	99.20
922B	1	Troctolite and olivine gabbro	1W-1(1)	2R-3(4)	0.00	5.77	30.40
	2	Poikilitic olivine gabbro	3R-1(1)	5R-1(1)	19.00	6.16	41.90

Note: Total depth of penetration for Hole 922A was 14.6 mbsf and for Hole 922B was 37.4 mbsf.

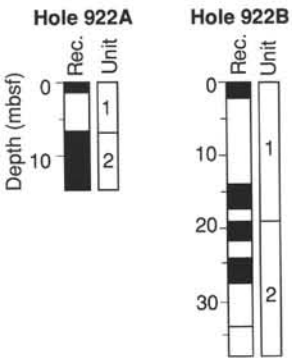

Figure 2. Columnar section showing the downhole recovery and lithological units in Holes 922A and 922B. Black bars indicate recovered intervals.

Unit 2 consists predominantly of medium- to coarse-grained olivine gabbro, with sparse, coarse to pegmatitic clinopyroxene grains (Fig. 4). The large clinopyroxene grains are poikilitic to subophitic and partially enclose coarse, euhedral plagioclase grains. The large poikilitic clinopyroxene crystals are a distinctive characteristic of this unit. Within Unit 2, Sections 1 and 2 of Core 153-922B-4R are notable for their relative abundance of apatite and zircon in small magmatic veinlets (Fig. 5).

IGNEOUS PETROLOGY

Holes 922A and 922B were drilled ~1 m apart at 23°31.362′N, 45°01.926′W. From these holes, a variety of igneous rock types were recovered, including predominantly olivine gabbro, troctolite, and gabbro with minor oxide gabbro, oxide gabbronorite and crosscutting gabbroic and felsic magmatic veins. The high degree of alteration and locally strong deformation present in much of the recovered rock make it difficult to evaluate the primary modal abundances of parts of the core, both in hand specimen and in some thin sections. Nevertheless, parts of the core preserve classic examples of igneous cumulate textures and structures known from basic layered intrusions.

Magmatic fabrics, including alignment of elongate plagioclase and olivine grains, and poikilitic or interstitial clinopyroxene are common in descriptions of the cores. Clear examples of modal layering are observed within individual pieces and over longer sections of core. Much of the troctolite and olivine gabbro from these holes exhibit an unusual igneous texture that is similar to what has been called harrisitic or crescumulate texture in basic layered intrusions. Two different types of magmatic alignment of phases are observed; one type, in which the alignment of olivine and plagioclase is parallel to layer boundaries, and a second type, where the alignment is perpendicular to layer boundaries. The second type occurs in rocks with crescumulate textures; the first could represent alignment resulting from settling of inequant grains or magmatic flow. These features are clear evidence for the operation of the same types of cumulus processes of rock formation that are well known from layered intrusions.

Lithologic Descriptions

Metatroctolites

The uppermost core recovered from Holes 922A and 922B are extensively altered gabbroic rocks inferred to be metatroctolite(?) and meta-olivine gabbro (Fig. 3). These rocks have a distinctive green to gray-green appearance in hand specimen. In Hole 922A, the upper 1.6 m of recovered rocks are identified as metatroctolite(?). In Hole 922B, the first two pieces at the top of the hole (Section 153-922B-1W-1, Pieces 1 and 2A) are also inferred to be metatroctolite(?). The identification of troctolite as the igneous protolith must be viewed as tentative. Complete or very extensive alteration of the mafic phases to tremolite-actinolite and chlorite (see "Metamorphic Petrology") makes assessment of primary modal proportions for these rocks extremely difficult. The identification of troctolite as the protolith of these rocks rests partly on the clear recognition of troctolite in the underlying, less altered material into which they grade in both holes. In addition, the textural appearance of altered rock and the less altered troctolite is very similar. Abundant plagioclase remains after alteration, although much of the relict plagioclase has a milky, cloudy appearance in hand specimen and is partially altered.

It appears from thin section observations that both olivine and clinopyroxene react to form very similar alteration assemblages in these rocks. In particular, coronas with tremolite-actinolite cores and chlorite rims form from both phases. Only in those cases where relict primary phases remain, or where alteration assemblages unique to a particular primary phase are observed, is it possible to unequivocally identify mafic primocrysts. For example, in cases where talc and magnetite are identified in hand specimen or in thin section, it is clear that olivine was the primary phase, and better estimates of primary modes were made. Given the small-scale heterogeneity of rock types observed in fresher parts of these holes, it is likely that the metatroctolite(?) rocks include both troctolitic and gabbroic protoliths.

Troctolites and Olivine Gabbros

Troctolites recovered from Hole 922A and 922B are mottled gray and white in hand-specimen. Their most common textural features are alignments of elongate subhedral plagioclase and elongate anhedral olivine crystals, perpendicular to layer boundaries in some rocks and parallel to layer boundaries in other rocks. Clinopyroxene occurs predominantly as interstitial or poikilitic crystals, with individual angular grains or subgrains set in an matrix of subhedral interlocking plagioclase. Disseminated primary iron oxide minerals occur throughout troctolite and olivine gabbro as interstitial grains. Brown hornblende is commonly seen rimming, or partially rimming the oxide mineral grains, partially replacing or rimming interstitial clinopyroxene, and also as rare discrete interstitial grains with no associated oxide minerals or clinopyroxene. Rarely, exsolution features are observed in these oxide minerals. Modal proportions are quite variable, with plagioclase ranging from 50% to 70%, olivine from 5% to 40%, clinopyroxene from 2% to 35%, and traces of disseminated oxide and sulfide minerals.

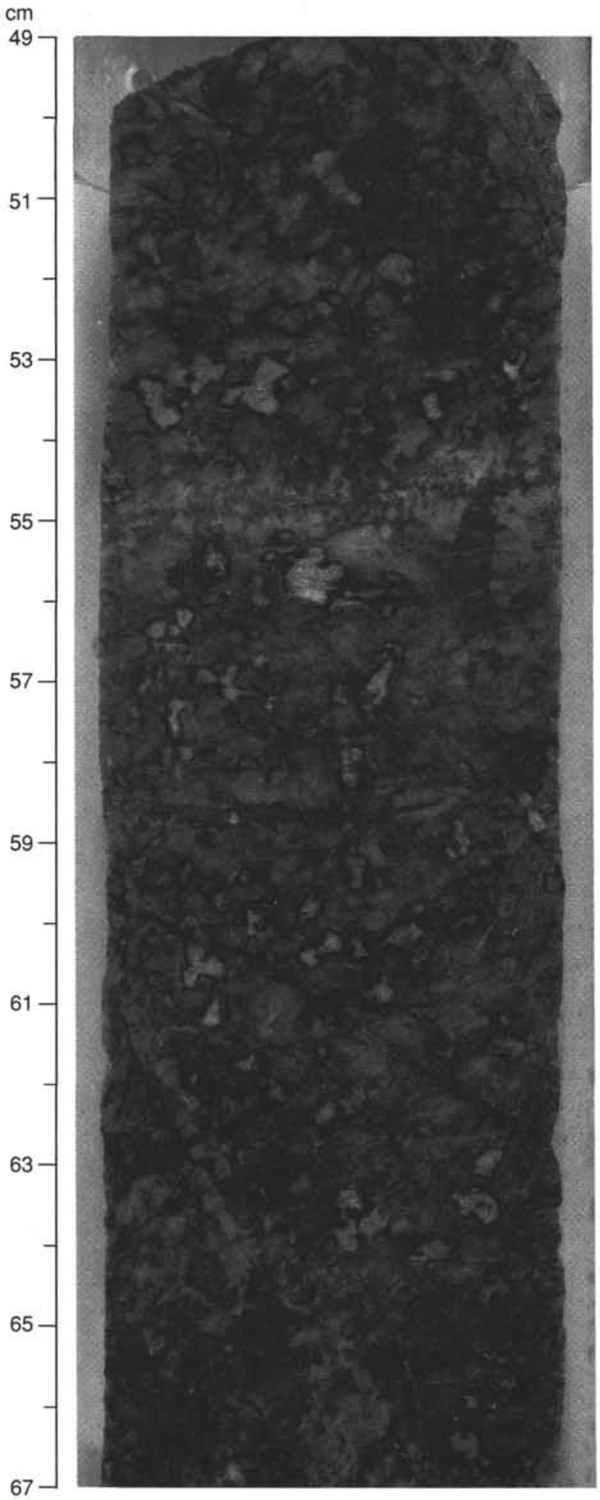

Figure 3. Altered coarse-grained olivine gabbro to troctolite. Note dark coronas around relict olivine grains and numerous dark veins of actinolite and/or chlorite. Olivine in this sample exhibits well-developed coronas of talc, tremolite, iron oxide minerals, pyrite, and chlorite. Chlorite forms dark rims around altered olivine. Subhorizontal dark green actinolite and chlorite veins and veinlets are abundant. This type of alteration is typical of many parts of the cores from both Holes 922A and 922B. The sample is cut by a magmatic vein (54–55 cm) that consists of pervasive replacement by actinolite-tremolite and chlorite after mafic phases. Sample 153-922B-4R-1, 49–67 cm.

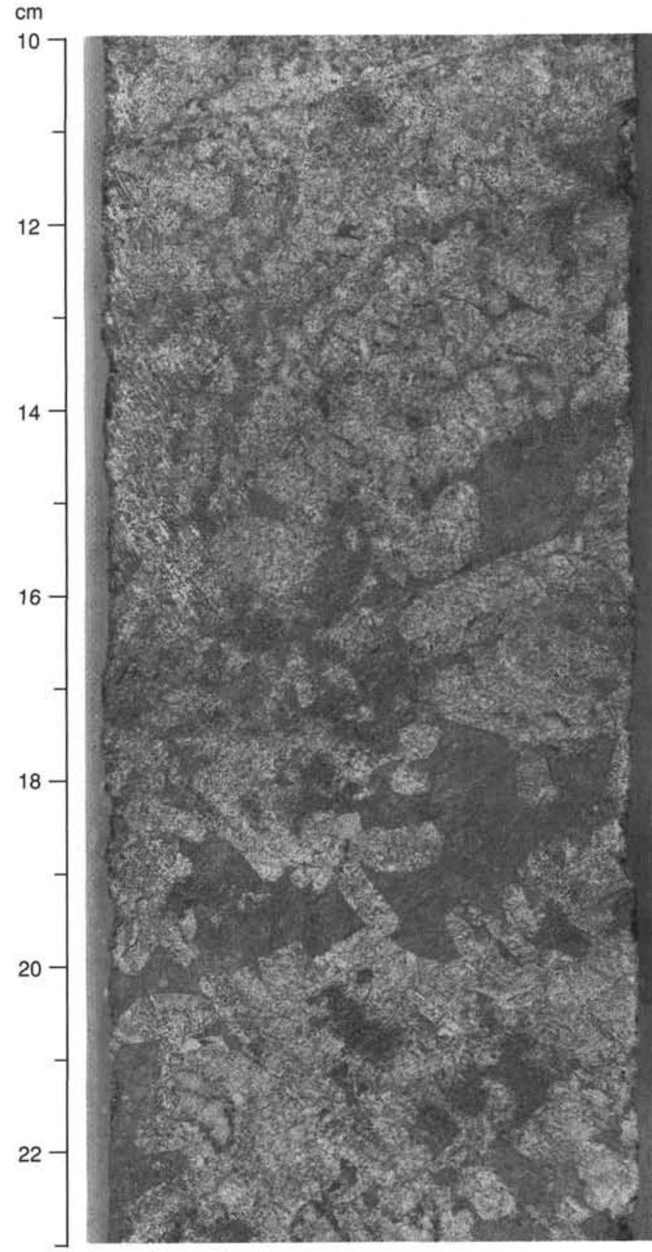

Figure 4. Coarse-grained to pegmatitic olivine gabbro with distinctive large clinopyroxene crystals (gray) that enclose sparse, euhedral plagioclase crystals (white). Medium- to coarse-grained plagioclase, clinopyroxene, and altered olivine make up the bulk of the rock. Sample 153-922B-3R-2, 10–23 cm.

Fine-grained clinopyroxene is commonly interstitial to plagioclase in rocks that have been termed troctolite, with olivine crystals concentrated in large clusters surrounded by the plagioclase plus clinopyroxene matrix. The specific rock name assigned depends on the scale of observation made in assigning the name (i.e., in thin section or in small pieces, the local mode is not always characteristic of larger portions of rock), with local variation over the scale of centimeters from troctolite to olivine gabbro in many pieces. Troctolite grades into olivine gabbro as the proportion of interstitial clinopyroxene increases. In view of the gradational nature of the relationship between these different rock types, and of the arbitrary boundary set in naming them, they are considered together in this section.

Clear examples of modal layering within individual pieces have been observed in the rocks from Holes 922A and 922B. Such layering

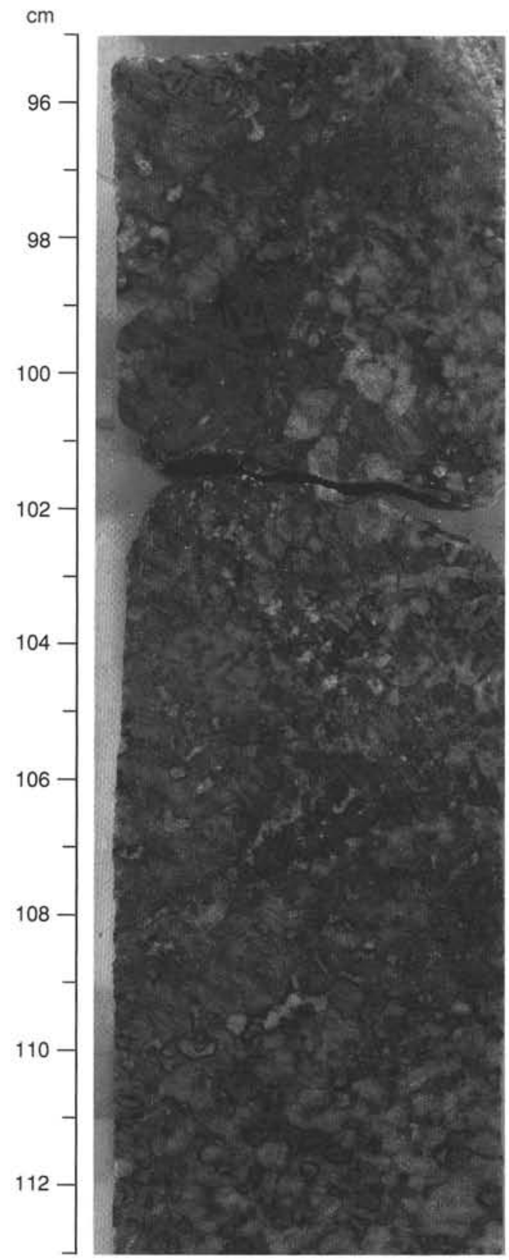

Figure 5. Small magmatic vein containing abundant apatite and zircon in coarse-grained, poikilitic olivine gabbro of Unit 2, Hole 922B. Apatite crystals (white) are clearly visible in the interval 103–104 cm. Sample 153-922B-4R-1, 95–113 cm.

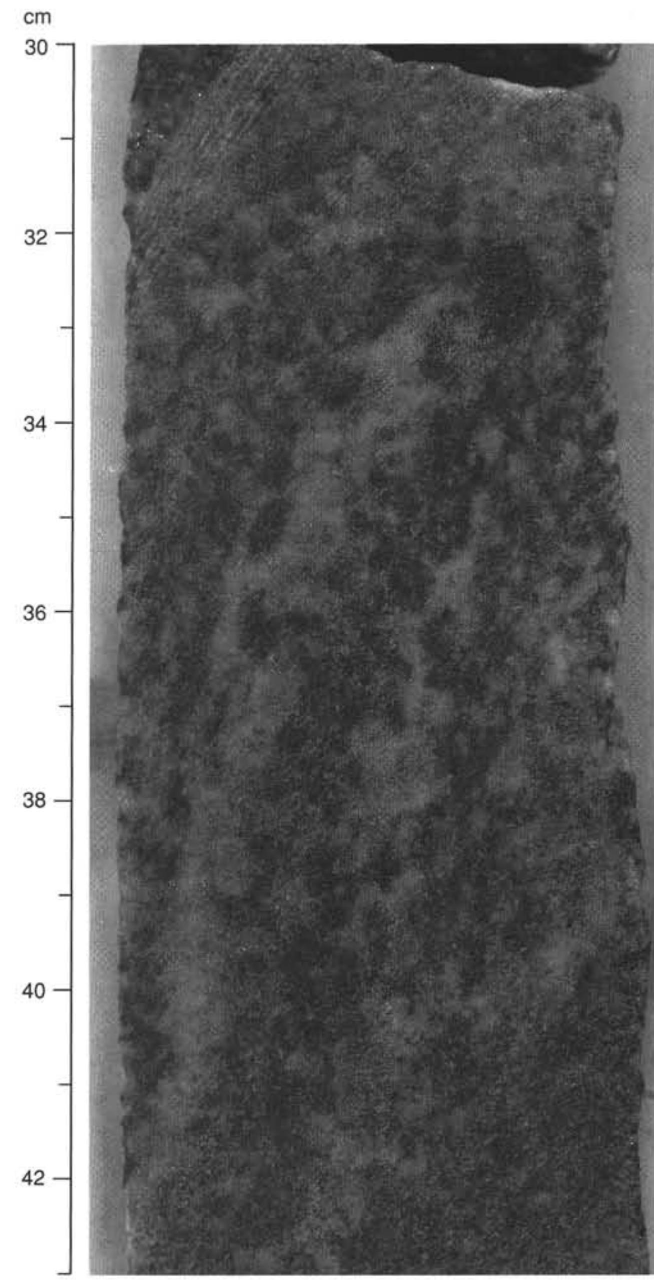

Figure 6. Core photograph of alternating plagioclase-rich and olivine-rich layers in troctolite in Sample 153-922B-1W-1 (Piece 2B, 30–43 cm). Three to four pairs of plagioclase-rich and olivine-rich layers are shown. Layer repetition occurs on the scale of 0.5 to 1 cm. Modal layering is one of the characteristic textural features of rocks formed by crystal accumulation in basaltic magma chambers.

is defined by changes in modal composition, with planar or near-planar boundaries between lithologies with different modes. An example of this type of igneous layering is shown in Figure 6. Centimeter-scale banding occurs because of the repetition of olivine-rich and plagioclase-rich layers. These layers dip approximately 80° relative to the axis of the core in the example shown in Figure 6. Olivine-rich layers contain some plagioclase and plagioclase-rich layers contain some olivine, and minor interstitial clinopyroxene is also present. The layer boundaries in this interval are not perfectly planar, but undulate gently along the length of the piece. The sharpness of layer boundaries is variable along individual layers, as olivine or plagioclase crystals or clumps of crystals extend above or below layer boundaries. Magmatic alignment of plagioclase and olivine parallel to layer boundaries occurs in this interval. Figure 7 illustrates a more subtle compositional layering in troctolite, defined by gradual changes in modal composition. The upper portion of the piece is relatively plagioclase-rich, grading downwards into relatively olivine-rich rock.

Magmatic alignment of elongate plagioclase crystals, with the direction of elongation parallel to layer boundaries, is illustrated from thin sections in Figure 8. Plagioclase grains are subhedral to euhedral. Some variability in the attitude of plagioclase grains occurs in these examples of magmatic alignment, but the orientation of grains show a shape preferred orientation. The rocks appear to consist of a framework of near-parallel elongate plagioclase and elongate olivine grains or grain clusters, with space-filling by intercumulus, interstitial clinopyroxene, and overgrowths of olivine on olivine cumulus crystals.

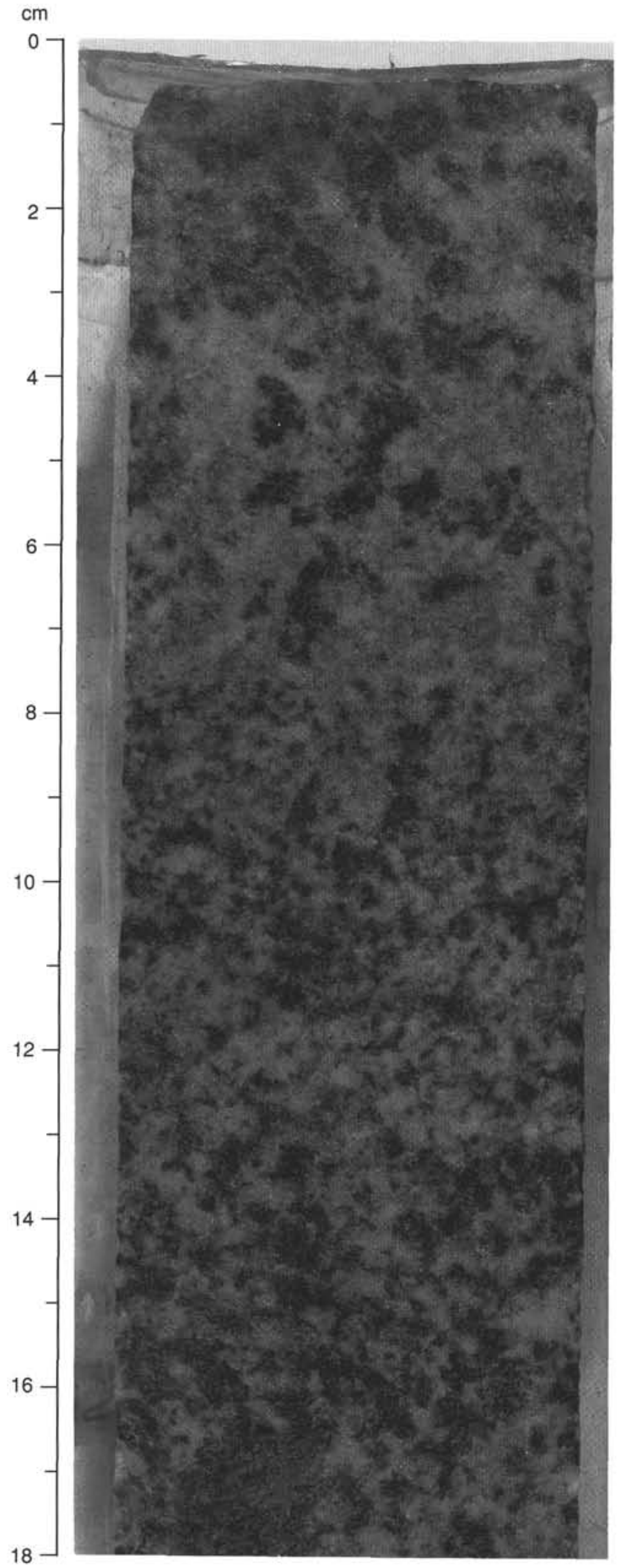

Figure 7. Core photograph of modal variations in troctolite in Sample 153-922A-2R-3 (Piece 1, 0–18 cm). Plagioclase-rich troctolite (3–11 cm) grades into relatively olivine-rich troctolite.

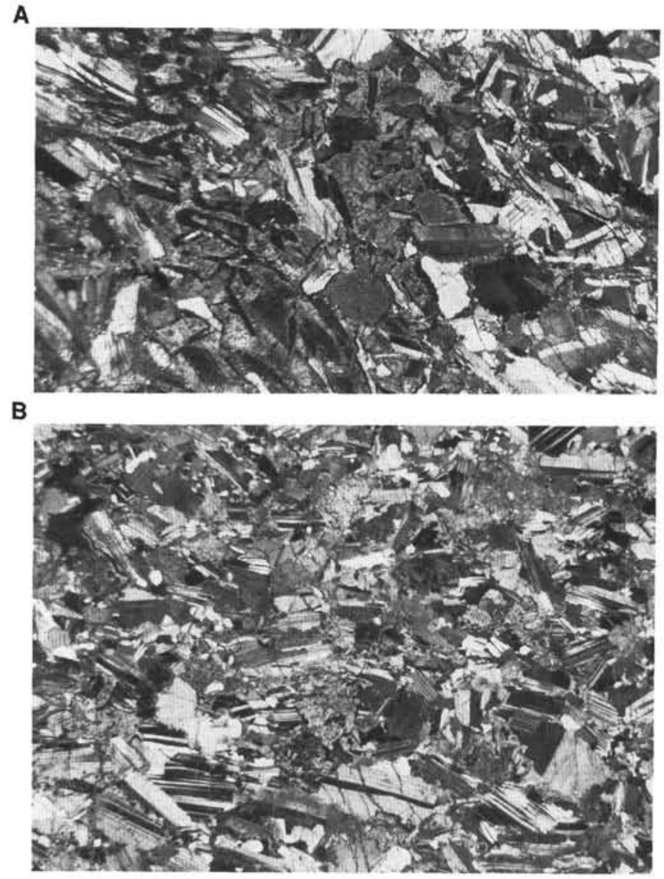

Figure 8. Photomicrographs of magmatic alignment of plagioclase in troctolite and olivine gabbro. **A.** Sample 153-922A-2R-5 (Piece 1, 30–35 cm). Width of field is 5 cm. **B.** Sample 153-922B-1W-1 (Piece 5, 66–73 cm). Width of field of view is 1.5 mm.

Another notable type of cumulate texture was best observed in Sample 153-922B-2R-1 (Piece 2A, 10–23 cm) and is shown in Figure 9. In this textural type, large (10–15 mm) elongate olivine grains have amoeboid, lobate-branching, quasi-dendritic grain shapes. Olivine crystals are intergrown with elongate, radiating blooms and clusters of large (10–15 mm) plagioclase grains. The margins between plagioclase and olivine are complex, interdigitated, and appear serrated in hand specimen (Fig. 10), with olivine lobes and branches embaying plagioclase grains. These textural features are common in thin sections from the troctolitic rocks in Holes 922A and 922B. In a thin section from the interval depicted in Figure 9, it is clear that large branching olivines noted in hand specimens are single, optically continuous grains. An example of this texture observed in thin section from the crescumulate rocks is shown in Figure 11. The olivine grains do not show fine skeletal or dendritic shapes, but rather lobate, branching, amoeboid shapes (Fig. 12). Some olivine grains appear to be rooted on or to have nucleated on plagioclase grains. These observations suggest harrisitic or crescumulate textures such as those described from the Rhum layered intrusion (Wadsworth, 1961). Clinopyroxene in the crescumulate troctolites and olivine gabbros is interstitial, poikilitic, and commonly lines the boundaries between olivine and plagioclase, in addition to forming larger interstitial, poikilitic grains. Subtle layer boundaries appear to be present in some pieces with crescumulate textures, but well-defined layering is not observed.

Troctolite in Holes 922A and 922B are intimately mixed with olivine gabbro. Troctolite grades into olivine gabbro in these rocks as the proportion of fine-grained interstitial clinopyroxene increases. All troctolite contains some clinopyroxene. Figure 13 shows olivine gabbro in which the olivine is distributed in patches which are surrounded

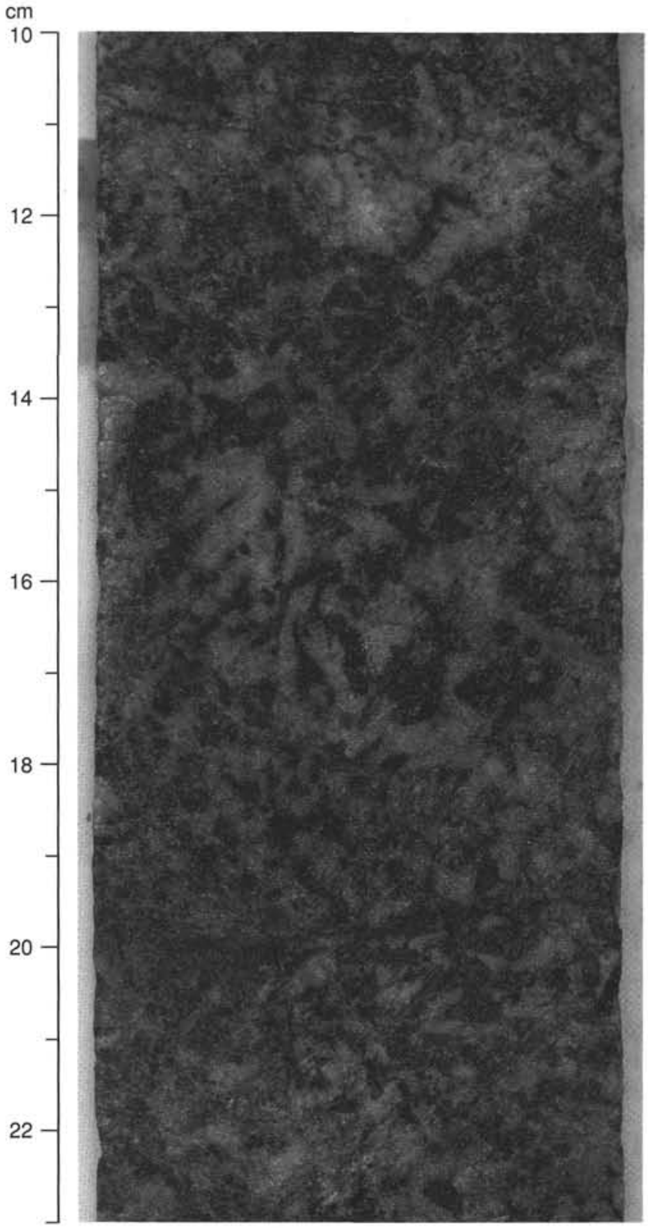

Figure 9. Core photograph of radial plagioclase and quasi-dendritic olivine crystals in troctolite. Olivine crystals consist of elongate grains with lobate, branching textures. Individual olivine grains observed in thin section from this sample have lengths of up to 15 mm. Plagioclase grains are elongated and reach lengths of up to 20 mm. They are elongated parallel to nearby olivine crystals. The phases show mutually interfering grain boundaries. Clinopyroxene is interstitial to the olivine and plagioclase and is poikilitic. Sample 153-922B-2R-1 (Piece 1A, 10–23 cm).

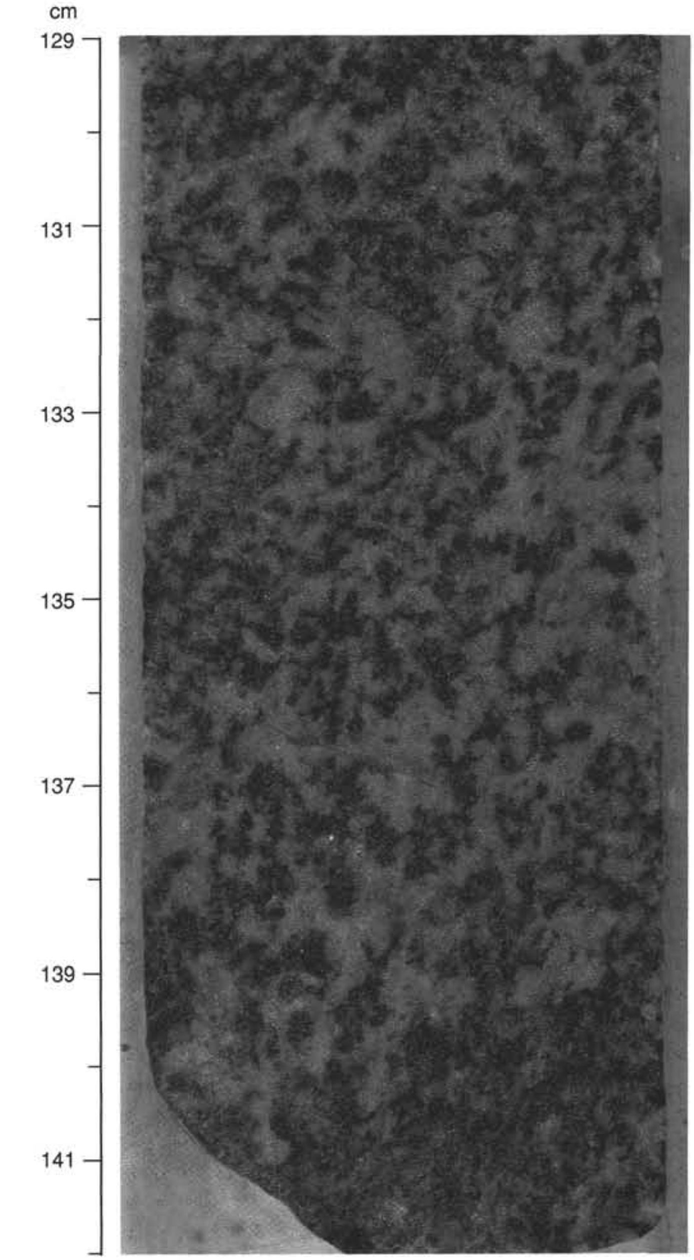

Figure 10. Core photograph of crescumulate texture in Sample 153-922A-2R-1 (Piece 8, 129–142 cm). Complex boundaries between olivine and plagioclase are well displayed in this example.

by plagioclase-rich regions with fine-grained interstitial clinopyroxene. Clinopyroxene in the troctolite from the upper sections of Holes 922A and 922B appears to be exclusively poikilitic or interstitial, but coarse oikocrystic clinopyroxene is not present. Below the troctolite-rich sequence encountered in Hole 922B, a sequence of olivine gabbro with very coarse poikilitic clinopyroxene is present. These rocks are described in the following section.

Poikilitic Olivine Gabbro

Sections 153-922B-3R-1 and -3R-2 consist of olivine gabbro that contains very coarse to pegmatitic (up to 20 cm) interstitial, poikilitic and subophitic grains of green clinopyroxene. The primary mineralogy consists of 52% to 64% plagioclase, 5% to 23% olivine and 14% to 32% clinopyroxene, with disseminated iron oxide minerals. Pervasive alteration of olivine and clinopyroxene has produced a green spotted appearance on the cores. Both olivine and clinopyroxene are present as interstitial grains between subhedral to euhedral plagioclase. Plagioclase compositions, based on shipboard optical determinations, are variable from sample to sample and range from An_{50-80} (thin sections of Samples 153-922B-3R-1, Piece 3, 44–50 cm, 3R-2, Piece 1, 0–5 cm, and 3R-2, Piece 3A, 54–58 cm).

The poikilitic olivine gabbro is generally coarse-grained, but contains patches ranging from 5 to 15 cm in diameter in which the grain size is very coarse to pegmatitic. Very coarse-grained to pegmatitic oikocrysts of clinopyroxene up to 20 cm long are, in all cases, associated with these patches. In Figure 14, an oikocryst of pegmatitic

A

B

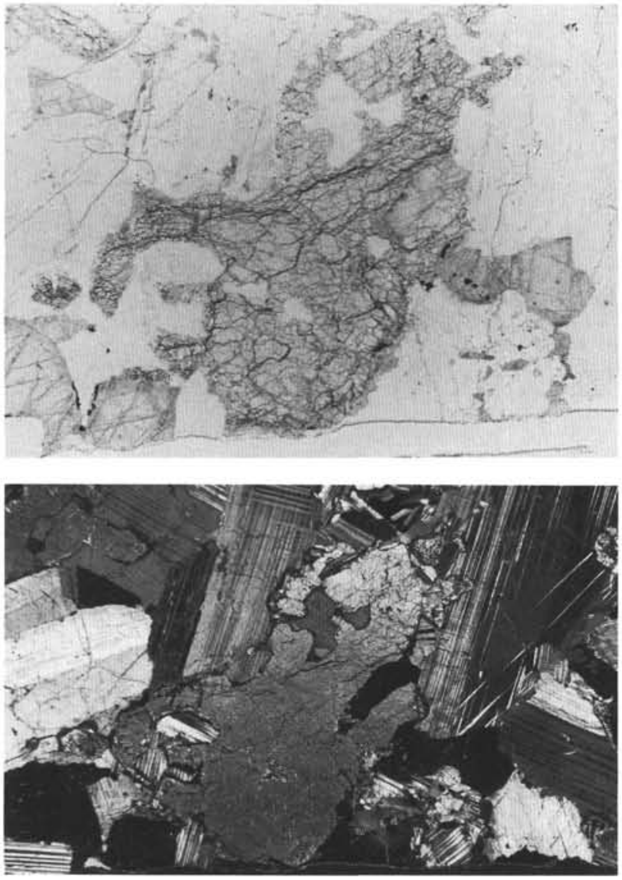

Figure 11. Photomicrographs of sample with crescumulate texture. Elongate branching-amoeboid olivine is in center of field of view. Sample 153-922B-2R-1 (Piece 1A, 12–17 cm). Field length is 1.2 cm wide. **A.** Plane polarized light. **B.** Crossed polars.

clinopyroxene is shown, with the piece oriented such that the common crystallographic orientation of spatially separated clinopyroxene grains is apparent, based on the fact that cleavage faces in these grains reflect light simultaneously. The largest patches contain randomly oriented, very coarse-grained euhedral plagioclase (up to 32 mm) and pervasively altered interstitial clinopyroxene. Individual arms, or branches, of clinopyroxene oikocrysts range in thickness to 25 mm. The large chadacryst-free cores of some oikocrystic clinopyroxene grains in Cores 153-922B-3R and -4R is notable. Poikilitic crystal habit is often interpreted to result from purely intercumulus growth of poikilitic phases, but the presence of such large inclusion-free cores of oikocrysts suggests the possibility that rare clinopyroxene cumulus grains could have been nuclei for growth of oikocrysts. It is unlikely that the plagioclase framework could have supported pore space large enough for the growth of the pegmatitic chadacryst-free clinopyroxene oikocrysts.

At the base of Section 153-922B-3R-2, in Piece 4, a clinopyroxene oikocryst is developed adjacent to a thin (<1 cm) vein of oxide mineral- and clinopyroxene-rich material (30% iron oxide minerals). Some coarse-grained patches have sharp margins, and consist of coarse (10–15 cm) subhedral clinopyroxene and up to 15% iron oxide minerals. The iron oxide minerals occur as coarse interstitial grains. Two layers of anorthositic gabbro occur on the adjacent ends of three consecutive pieces (153-922B-3R-1, Pieces 4A and 4B, and the top of -3R-2, Piece 1). The recovered thickness of these layers is 0.5 to 3 cm. They consist of euhedral plagioclase up to 12 mm in size, and altered interstitial clinopyroxene up to 8 mm in size. A small (<3 cm) vein of plagioclase extends into the adjacent olivine gabbro below the layer formed at the top of Section 153-922B-3R-2, Piece 4B.

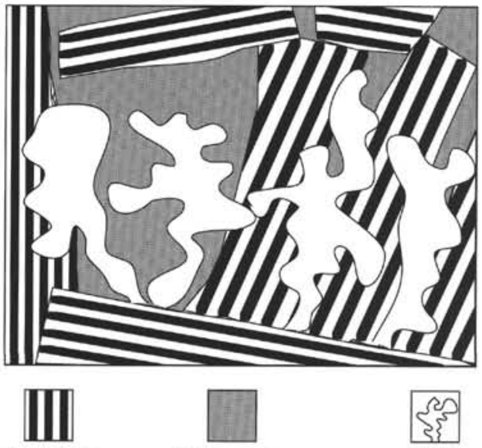

Figure 12. Illustration showing crescumulate textures observed in thin section in troctolites and olivine gabbros from Holes 922A and 922B. Elongate, amoeboid olivines are single grains in optical continuity that grew subparallel to elongate, radiating plagioclase grains. Interstitial space between olivine and plagioclase is commonly filled with poikilitic or interstitial clinopyroxene.

Late-Stage Magmatic Veins and Oxide-Bearing Intrusives

Magmatic veins of a variety of late stage and fractionated melts have intruded gabbroic rocks from Holes 922A and 922B. Generally they are coarse-grained or pegmatitic. The mineral assemblages that make up the gabbroic veins are varied and lithologies include gabbro, oxide gabbro, hornblende gabbro, and oxide-hornblende gabbro. More evolved veins of diorite, quartz diorite, and trondhjemite also are present. Grain sizes vary between 15–35 mm for gabbroic compositions, but are finer for diorites and trondhjemites. The gabbroic veins are typically coarser grained than the adjacent wall rock and are obvious in hand sample.

One example of this type of vein can be observed in Section 153-922B-4R-1 (Pieces 8A and 8B; Fig. 5). The top of Piece 8B and the base of Piece 8A contain an intrusive coarse-grained composite vein and small evolved magmatic pocket several centimeters across. At its center, it contains euhedral blocky, rather than tabular, plagioclase grains with intergranular clinopyroxene grains. On the margin of the pocket (base of Piece 8A), clinopyroxene grains (cores now altered to actinolite) are rimmed by magmatic hornblende and are associated with discrete grains of euhedral to subhedral prismatic hornblende up to 11 mm long within interstitial areas. This zone appears to have solidified on the edge of the intrusive pocket. The intrusive pocket also has abundant apatite (in places making up 10% to 15% of the pocket and vein at the top of Piece 8B) as inclusions within amphibole or as discrete grains. A thin vein that appears to feed the intrusive pocket and larger vein cuts obliquely across the top of Piece 8B and appears to link directly with the pocket described above. The vein is very narrow and is easily seen as a line of smaller apatite and larger pyroxene-amphibole grains with minor amounts of plagioclase. The apatite crystals appear to be interstitial to clinopyroxene and form a trail extending to the clot above. The linking vein is narrow (several millimeters across).

Similar veins elsewhere in the cores show gradations in composition from the edge of the vein to the center, the more fractionated solidification products are commonly toward the center. Two coarser-grained gabbroic veins also cut across Piece 6A in the same section of the core. The evolved nature of these melt products is apparent as they typically contain oxide minerals, magmatic amphibole, apatite, and

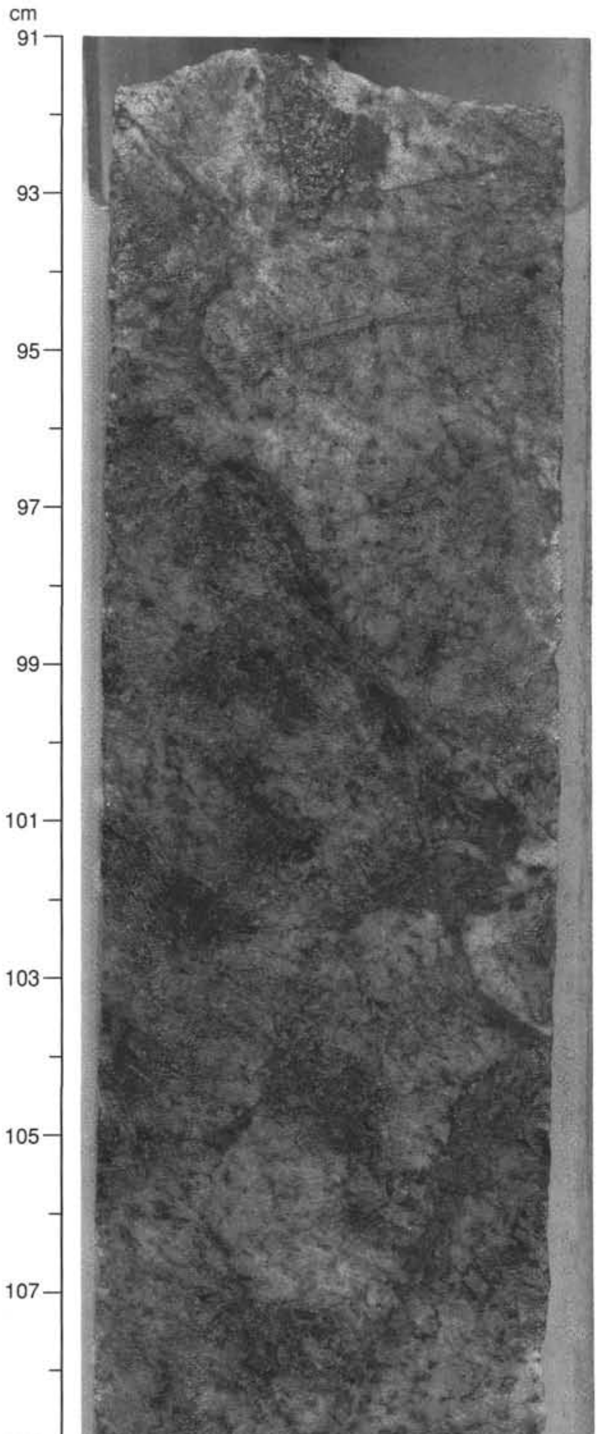

Figure 13. Patchy distribution of olivine in olivine gabbro. Large, dark olivine patches are separated by light areas that consist of plagioclase with interstitial clinopyroxene. In places, olivine shows growth patterns similar to that shown in Figure 12, with elongate, lobate-dendritic shapes. A small patch of oxide- and apatite-rich material (91–93 cm) appears near the top of this photo associated with a small shear zone. Other thin shear zones and veins dipping in the opposite direction are also visible in this sample. Sample 153-922B-2R-1 (Piece 2A, 91–110 cm).

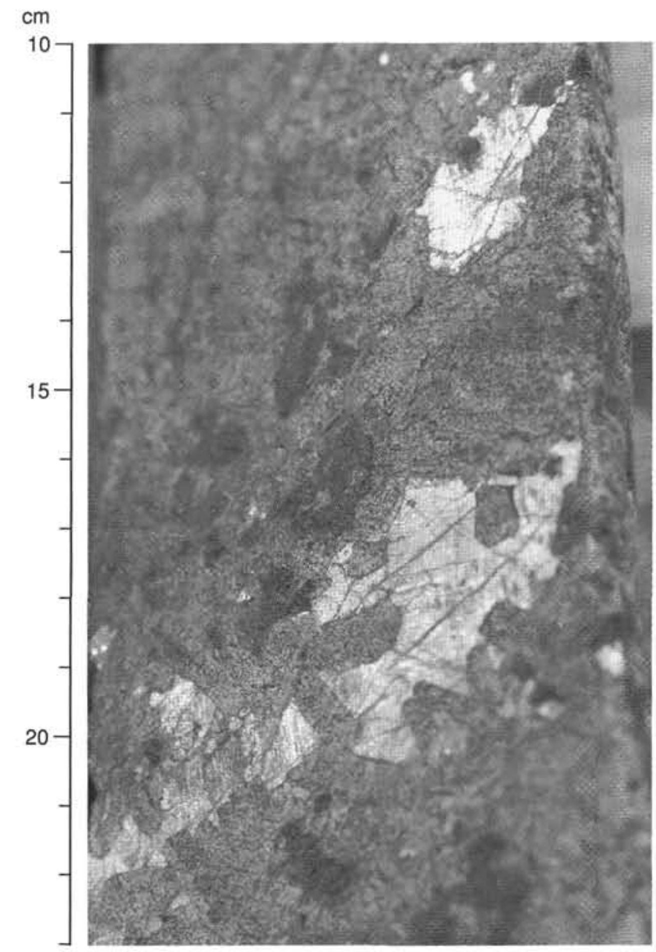

Figure 14. Core photograph showing large poikilitic clinopyroxene grain, illuminated because the core has been rotated to the appropriate orientation where cleavage faces in crystallographically aligned clinopyroxene grains all reflect in the same orientation. The reflecting grains of clinopyroxene that are physically separated in the surface of this core presumably are physically connected elsewhere. These poikilitic grains have complex three-dimensional shapes. They either completely or partially enclose large plagioclase grains in the poikilitic rocks from Hole 922B. A flat lying photograph of the same interval of core is pictured in Figure 4. Sample 153-922B-3R-2 (Piece 1, 10–23 cm).

zircon. These evolved melts are observed as small melt trails and larger veins in much of the gabbroic rock sampled from Holes 922A and 922B. Apatite and zircon have been commonly observed in thin section and hand specimens of Hole 922A and 922B rocks, and are commonly associated with oxide mineral-rich shear zones, and with coarse-grained intrusive dikes.

Many examples of oxide gabbro and gabbronorite occur in rocks sampled from Holes 922A and 922B. These oxide-rich zones generally occur as sheared, relatively evolved magmatic intrusives that cut the troctolite and olivine gabbro host rocks. The mineralogy of these oxide mineral-rich intrusive bodies generally consists of plagioclase, clinopyroxene, orthopyroxene, titanomagnetite ± ilmenite ± apatite ± zircon. Oxide-mineral-bearing zones also commonly have relatively abundant sulfide minerals.

In virtually every piece of Section 153-922A-2R-2 sheared, oxide-mineral-bearing zones occur. Volumetrically, the most significant occurrence of oxide-rich gabbro and gabbronorite in Holes 922A and 922B are observed in Section 153-922B-2R-2. Within this section, a series of gneissic to porphyroclastic oxide gabbros is juxtaposed with olivine gabbro host rocks. A vertical contact separating oxide-rich gabbronorite and olivine gabbro is illustrated in Figure 15. The con-

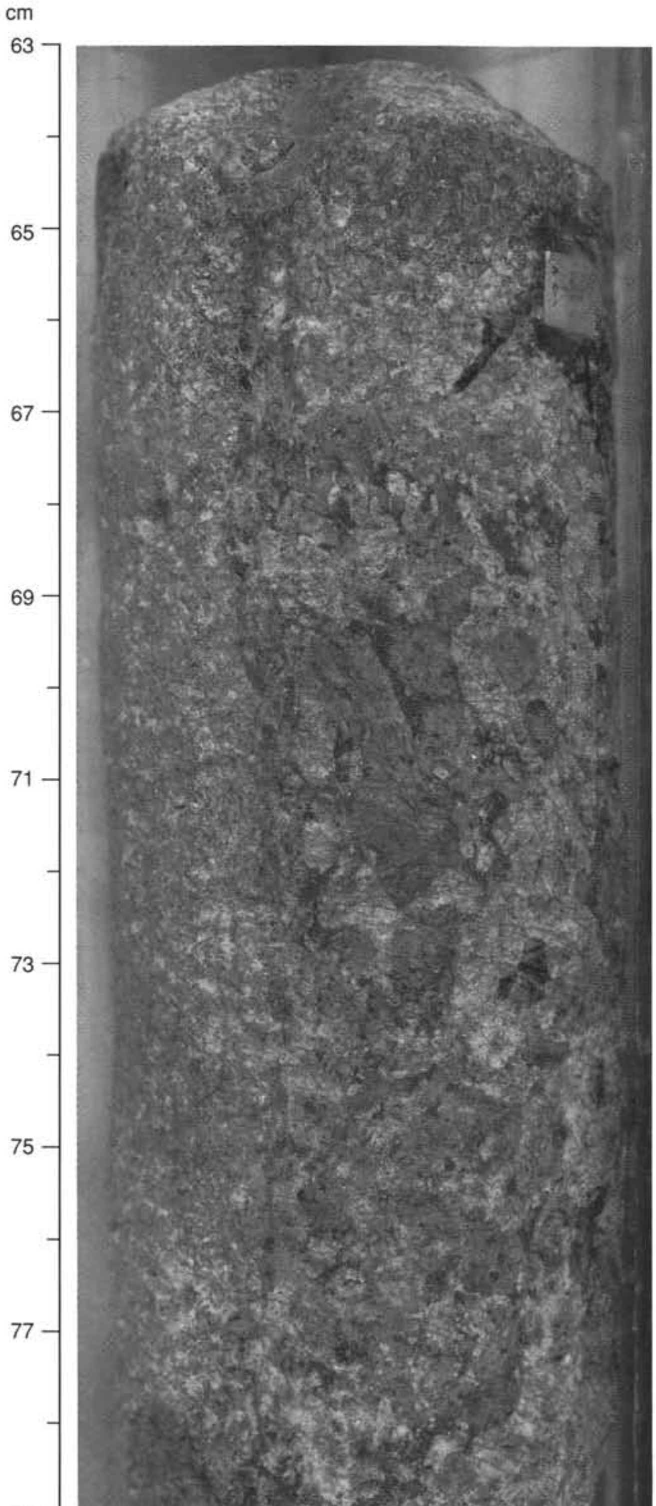

Figure 15. Intrusive, sheared vertical contact between oxide gabbronorite (right side) and olivine gabbro (left side) in Sample 153-922B-2R-2 (Piece 7, 63–79 cm). The oxide-mineral-bearing rocks are strongly deformed, whereas olivine gabbro is relatively undeformed. Alteration is high in both rock types.

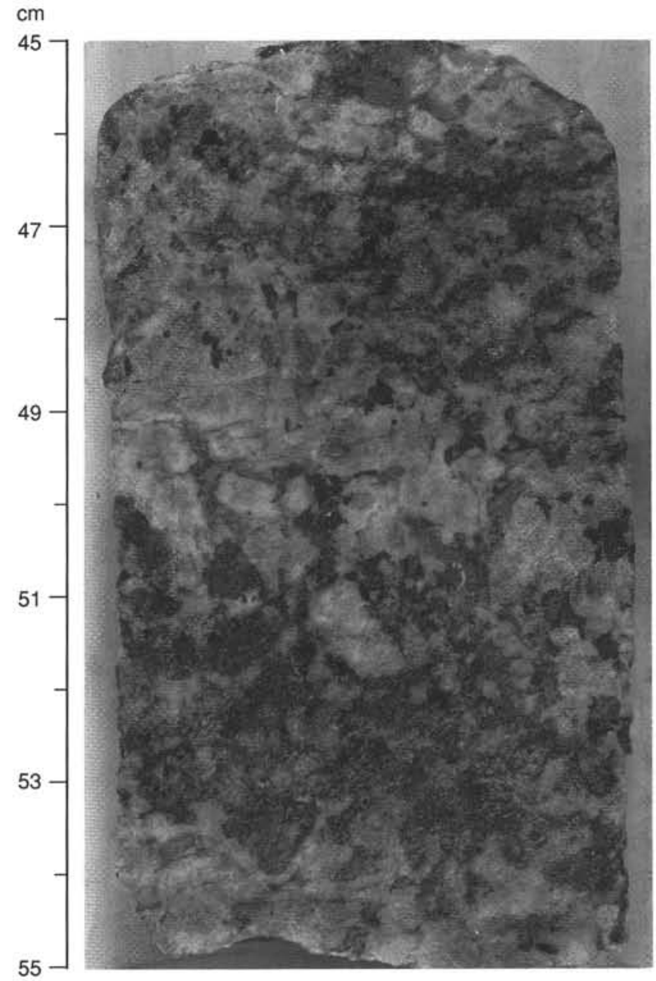

Figure 16. Bands of oxide mineral-rich and plagioclase-rich gabbro in moderately altered olivine gabbro, Sample 153-922B-1W-1 (Piece 3, 45–55 cm). Plagioclase grains are subhedral to euhedral and appear to be zoned. The margins of these bands are lined with Fe-Ti oxide minerals and much of the interstitial space among the plagioclase crystals is filled with oxides. This is a rare example of undeformed oxide-rich rock occurring in Hole 922B. Olivine grains in this sample exhibit variably developed coronas composed of talc, tremolite-actinolite, and chlorite.

tact is sharp, with some evidence for shearing (see "Structural Geology," this chapter). Olivine gabbro is relatively undeformed, but the adjacent oxide gabbronorite is strongly deformed.

An example of coarse-grained, relatively undeformed oxide mineral-rich bands occurs in Sample 153-922B-1W-1 (Piece 3, 45–55 cm; Fig. 16). Several bands of coarse, euhedral to subhedral, plagioclase-rich material occur within olivine gabbro rock occur adjacent to the oxide mineral-rich zones. Within these bands, high modal proportions (10 to ~20 modal%) of interstitial oxide minerals surround the plagioclase grains. The margins of the large band of euhedral plagioclase-rich rock in the central portion of this sample is lined, above and below, with iron-titanium-oxide minerals. The dark bands separating the plagioclase-rich material are olivine gabbro to troctolite and represent the dominant rock types within this interval.

In most cases, it appears that oxide mineral-bearing bands are localized within oxide-poor gabbroic rocks. Iron-titanium oxide minerals occur interstitially within gabbronorite and as schlieren within shear zones. Silicate porphyroclasts and recrystallized, commonly porphyroclastic mylonitic zones are concentrated in the vicinity of oxide-mineral-rich schlieren (Fig. 17). The complicated structures

A

B

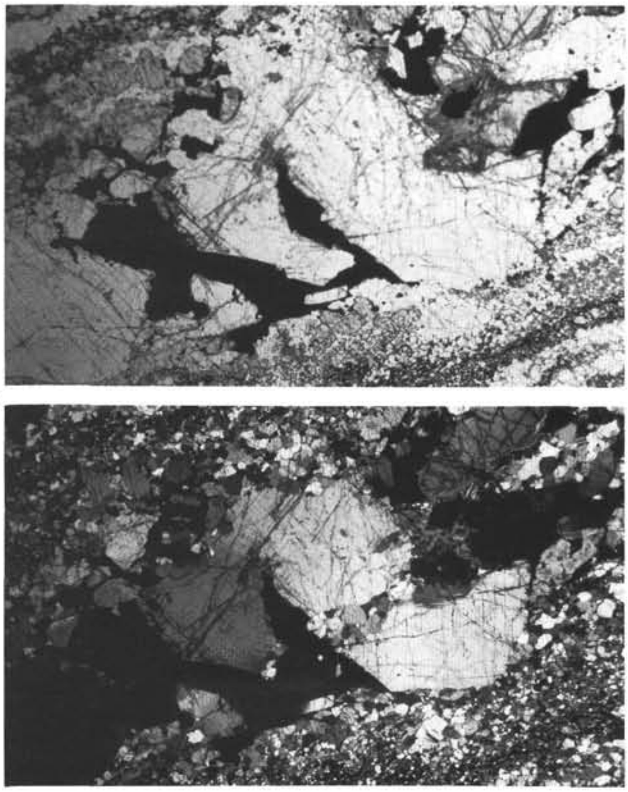

Figure 17. Iron oxide minerals concentrated in a porphyroclastic zone in gabbronorite intrusive vein into troctolite. Oxide minerals are interstitial to large plagioclase porphyroclasts and are relatively undeformed. Adjacent to the oxide-mineral-bearing zone, an olivine and clinopyroxene-bearing amphibolitized, mylonitic shear zone is observed. Field length is 8 mm. Sample 153-922B-1W-1 (Piece 8, 105–112 cm). **A.** Plane polarized light. **B.** Crossed polars.

A

B

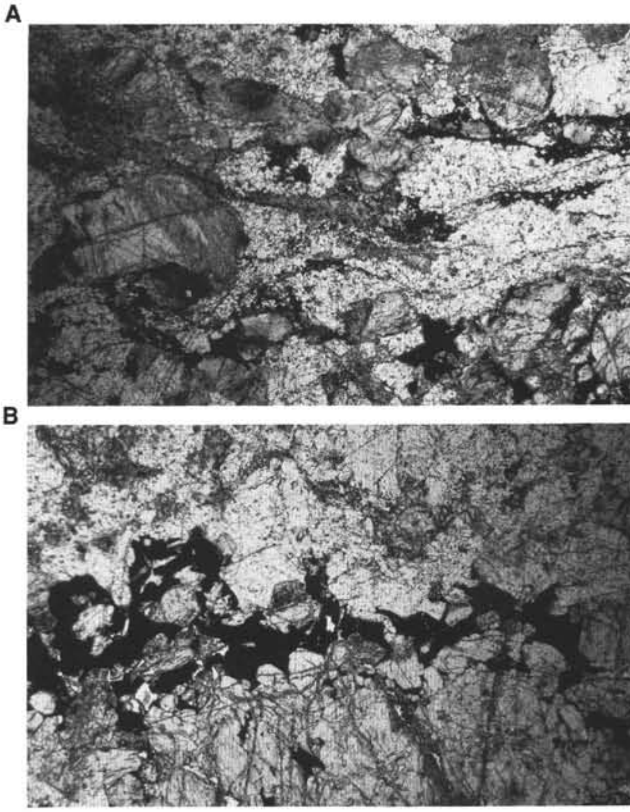

Figure 18. Photomicrographs of oxide-mineral-rich zones in Sample 153-922B-1W-1 (Piece 5, 66–73 cm). The oxide minerals are cross cut by a shear zone in (**A**), but are relatively undeformed in (**B**). Field length is 8 mm wide in both (**A**) and (**B**).

observed in these rocks make it difficult to reach conclusions about the relationship of the oxide gabbros to the dominant lithologies in the section (i.e., whether the oxide-rich material originated during normal cumulative processes or represents an allochthonous melt phase that has impregnated the gabbroic rock). In thin section, examples have been noted where oxide minerals are included in shear zones, with apparent grain-size reduction of both silicate and oxide minerals, and in other cases oxide minerals are concentrated near shear zones but appear not to have been as strongly sheared as the nearby silicate submylonitic zones. In one case, both sheared and unsheared oxide mineral-rich zones are observed in one thin section (Fig. 18).

Lithologic Units

Table 2 shows units, extent of units, depths of unit boundaries, and recovery for Holes 922A and 922B. Figure 2 shows lithologic columns with unit boundaries for these holes, along with core recovery and depth of penetration. The two lithologic units defined in core recovered from Hole 922A are (1) metatroctolite(?) and (2) troctolite and olivine gabbro. In metatroctolite(?), mafic phases and plagioclase near mafic grains are altered to actinolite and/or tremolite rimmed by chlorite, so that the relative proportions of olivine to clinopyroxene are difficult to assess. Thin sections of rocks from this unit show that both olivine and clinopyroxene were present, and that minor relict clinopyroxene and substantial plagioclase remain. Because of the uncertainty about the nature of the protoliths of these rocks and their distinct visual appearance relative to the underlying rocks, metatroctolites(?) have been defined as a single unit. No contact between this unit and the underlying troctolite and olivine gabbro unit was recovered. From Piece 3 of Section 153-922A-2R-1, to Piece 4, the level of alteration drops substantially, and proceeding down within this section, alteration is much lower, relict primary phases are more abundant, and the nature of the protolith can be determined with greater confidence.

Unit 2 in core from Hole 922A consists predominantly of troctolite and less abundant olivine gabbro, but also includes numerous small intrusive, porphyroclastic oxide gabbros and gabbronorites in Sections 153-922A-2R-2 and 2R-3. Grain-size layering and modal layering are observed. Clinopyroxene is present as a fine-grained interstitial phase throughout much of this unit, and troctolite grades into olivine gabbro as the abundance of interstitial clinopyroxene increases.

Two units are defined in gabbroic rocks from Hole 922B, although both these units are lithologically diverse. The upper unit in Hole 922B consists of troctolite and olivine gabbro, but also includes metatroctolite, oxide gabbro, and oxide gabbronorite, as well as various gabbroic veins and anorthositic, oxide-rich bands. As in Hole 922A, troctolite and olivine gabbro grade into each other as the proportion of fine-grained, interstitial clinopyroxene changes. In Section 153-922B-2R-2 within Unit 1, several pieces consist of both meta-olivine gabbro and gneissic-oxide gabbronorite, which are juxtaposed along sheared contacts. The boundary between Unit 1 and the underlying poikilitic olivine gabbro of Unit 2 has been placed between the bottom of Section 153-922B-2R-3 and the top of Section 3R-1; no contact was recovered between these two units.

Unit 2 in core from Hole 922B is dominated by olivine gabbro, in which sparse, very coarse to pegmatitic (up to 15 cm) poikilitic to subophitic clinopyroxene grains occur in a medium- to coarse-grained matrix of altered olivine, clinopyroxene and plagioclase. The poikilitic clinopyroxene commonly occurs in the vicinity of 15–25 mm plagioclase grains, which they partially enclose. These coarse to pegmatitic, poikilitic clinopyroxene grains are characteristic of the lower portion of the core in Hole 922B, so that this unit has been designated as poikilitic olivine gabbro, although significant lithologic diversity is observed in this unit. The abundance of these coarse poikilitic to subophitic grains is not high. Sections 1 and 2 of Core 153-922B0-4R are notable because they contain abundant apatite and zircon in very small magmatic veinlets and larger dikes. Near the base of Unit 2, Section 4R-3 consists of metagabbro; almost no olivine was present in the protolith. These rocks, like most of Cores 3R and 4R from Hole 922B are extensively altered, with nearly complete replacement of mafic phases, and the development of chlorite coronae around replaced mafic grains leads to the partial replacement of adjacent plagioclase grains. The occurrence of the pegmatitic clinopyroxene grains decreases downward in Core 4, and virtually no poikilitic to subophitic clinopyroxene grains are present in Section 4R-3.

Modal variations among the most abundant primary constituent minerals, plagioclase, clinopyroxene, and olivine, are shown in Figure 19 for Holes 922A and 922B. These modes were estimated from visual core descriptions. The dominant rock types in these holes are olivine gabbro and troctolite. Olivine-poor to olivine-free gabbro was recovered from near the base of Hole 922B. It must be noted again that these visual estimates were made on altered rocks whose primary modes were difficult to judge; thus these modes should be regarded as rough estimates. No clear modal distinctions exist between the units in these holes, as the units were defined on the basis of metamorphic character, or on the basis of textural distinctions (olivine gabbro vs. poikilitic olivine gabbro), so the units are not differentiated on Figure 19.

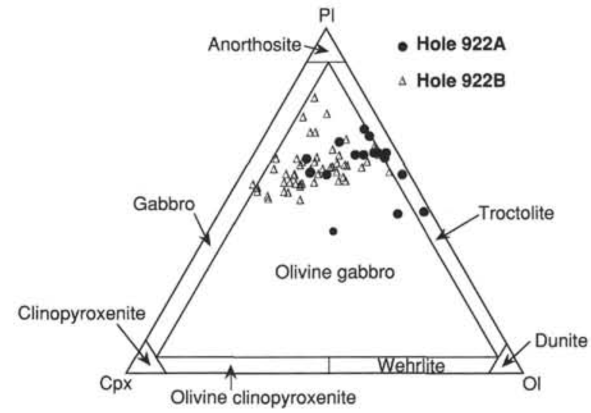

Figure 19. Ternary plot of modal variations in Holes 922A and 922B. Both holes are dominated by olivine gabbro and troctolite. Hole 922B includes gabbro and metagabbro near the base of the hole.

Cross-hole Correlations

Hole 922A and 922B, being only 1 m apart, do not display significant cross-hole correlation, and the units named in these holes are not equivalent. Unit 1 metatroctolite rocks of Hole 922A (Fig. 2) were identified in Hole 922B, but only two small fragments of extensively altered gabbroic rocks, inferred to be metatroctolite, were recovered in the top core of Hole 922B. Unit 2 of Hole 922A (troctolite and olivine gabbro) is equivalent to Unit 1 of Hole 922B, and this small volume of material did not merit separation into a separate unit in Hole 922B.

Geochemistry

A total of nine whole-rock samples from Site 922 were analyzed for major element oxide and trace element abundances by X-ray fluorescence (XRF) spectroscopy (Table 3). Five of these samples were from cores from Hole 922A and four were from gabbroic rocks recovered from Hole 922B. Sample weights ranged from 24.5 to 82.3 g and were typically 50–65 g (six samples). Sample preparation techniques and analytical procedures are described in the "Introduction" and "Explanatory Notes" (this volume). For Rb, Nb, Ce, and Ba measured abundances are generally near or below the detection limits (see "Explanatory Notes," this volume, and "Geochemistry," this chapter).

The main objective of sampling and geochemical analysis of material from the two holes at Site 922 was to establish the primary chemical characteristics of the main lithologies encountered, although most samples have been significantly altered (Table 4) and this alteration can affect the geochemistry of the rocks.

Results

Most of the analyzed samples are significantly altered. Loss on ignition (LOI) in these samples varies from 0.3% to 3.4%. Both petrographic observations, in which abundant hydrous alteration phases after mafic minerals are described, and the LOI values indicate that the gabbroic rocks sampled from Holes 922A and 922B are significantly more altered than most samples from the holes at Site 921.

Major element oxide and trace element abundances are presented in Table 3 with depth (mbsf), rock type, and lithologic unit for each sample. The petrographic characteristics of these samples are summarized in Table 4. With respect to the lithological units assigned to the recovered material at Site 922, one sample from Unit 1 of Hole 922A (a meta-olivine gabbro) and four samples from Unit 2 were analyzed, yielding a downhole sequence of a troctolite, an oxide gabbro, an olivine gabbro, and an oxide gabbronorite. In rocks from Hole 922B, one sample, a gabbronorite, from Unit 1 and three olivine gabbro samples from Unit 2 were analyzed.

Five of the nine samples analyzed were olivine gabbros. Major element oxide variations in the olivine gabbros are relatively small for SiO_2 (47%–47.8%), Al_2O_3 (21.5%–22.4%), and CaO (10.7%–11.8%); K_2O and P_2O_5 are uniformly low with values at or below detection limits. If Sample 153-922B-3R-2 (Piece 3, 44–50 cm) is excluded, variations in TiO_2 (0.3%–0.4%), Fe_2O_3 (5.1%–5.9%), MgO (11.56%–12.43%), and Na_2O (1.45%–1.75%) are also small. Compared to other olivine gabbro samples from Holes 922A and 922B, Sample 153-922B-3R-2 (Piece 3, 44–50 cm) has a slightly more evolved composition with high TiO_2 (1.05%), Fe_2O_3 (7.32%), and Na_2O (2.1%), and low MgO (9.43%); this is reflected by higher abundances of iron oxide minerals. Trace element concentrations are more variable with both the relatively evolved sample (Sample 153-922B-3R-2, Piece 3, 44–50 cm) and the meta-olivine gabbro adding to the range of trace element abundances. In the case of the meta-olivine gabbro this may be due to alteration. Incompatible trace element abundances are low; Zr = 29–35 ppm and Y = 9–10 ppm, and compatible trace element abundances are moderately high, with Ni = 376–403 ppm and Cr = 105–233 ppm. The more evolved olivine gabbro has a slightly higher abundance of Y and a dramatically higher abundance of Zr (60 ppm) and significantly lower Ni and Cr abundances, 290 and 83, respectively.

The troctolite, as might be expected, has a slightly less evolved composition than the olivine gabbro. It has lower SiO_2, TiO_2, Al_2O_3 and Na_2O, and higher MgO. Likewise, it has similar incompatible trace element (Zr and Y) and Sr abundances and higher compatible trace elements abundances (Ni and Cr) than the least evolved olivine gabbro.

The two oxide gabbro samples and the gabbronorite exhibit a wide range of both major element oxide and trace element abundances. In comparison to olivine gabbro, the two oxide gabbro samples and the gabbronorite have high TiO_2, Fe_2O_3, Na_2O, and P_2O_5 and lower Al_2O_3, MgO, and CaO abundances. The two oxide gabbros have lower SiO_2 than the olivine gabbro, while the gabbronorite has higher SiO_2. These features reflect both the more evolved character of these rocks (high Na_2O) and the variable modal abundances of accumulated orthopyroxene, iron oxide minerals and apatite (SiO_2, TiO_2, and P_2O_5). Incompatible trace element (Zr and Y) abundances are much higher than in the less evolved olivine gabbro, and compatible trace element (Ni and Cr) abundances are much lower.

Table 3. Major element oxides and trace element abundances, Holes 922A and 922B.

Hole:	922A	922A	922A	922A	922A	922B	922B	922B	922B
Core, section:	1R-1	2R-1	2R-2	2R-5	3R-1	2R-2	3R-1	4R-2	4R-3
Interval (cm):	130–133	122–129	106–111	0.2–9	104–109	81–87	44–50	16–22	70–76
Piece:	9	8	2	1A	4B	8	3	1A	4B
Depth (mbsf):	1.3	7.82	9.08	11.96	14.54	16.3	19.44	25.45	27.3
Unit:	1	2	2	2	2	1	2	2	2
Rock type:	MOLGAB	TROC	OXGAB	OLGAB	OXGAB	GABNOR	OLGAB	OLGAB	OLGAB
Major element oxides (wt%)									
SiO_2	47.79	46.41	44.21	47.59	40.22	48.27	47.17	47.58	47.04
TiO_2	0.27	0.19	2.06	0.38	5.14	2.26	1.05	0.41	0.39
Al_2O_3	22.38	18.50	18.14	21.50	12.60	15.22	21.46	22.33	21.63
Fe_2O_3	5.14	6.15	13.17	5.24	18.57	12.25	7.32	5.93	5.48
MnO	0.11	0.11	0.19	0.09	0.32	0.23	0.11	0.08	0.09
MgO	11.81	17.05	7.26	12.43	6.80	7.97	9.43	11.56	12.21
Ca0	11.39	10.81	9.75	11.78	9.83	10.47	10.98	10.69	11.44
Na_2O	1.70	1.29	2.54	1.57	2.25	2.96	2.10	1.75	1.44
K_2O	0.03	0.03	0.03	0.03	0.03	0.03	0.04	0.01	0.01
P_2O_5	0.00	0.01	1.50	0.02	3.35	1.53	0.03	0.00	0.02
Total	100.63	100.55	98.85	100.63	99.11	101.19	99.68	100.32	99.75
LOI	3.35	0.86	0.34	3.37	0.33	1.16	1.94	2.83	3.11
Trace elements (ppm)									
Nb	BDL	BDL	5	BDL	22	8	2	BDL	BDL
Zr	71	29	52	35	145	113	60	33	29
Y	7	8	57	9	75	72	12	9	10
Sr	145	132	170	132	129	173	169	136	148
Rb	BDL	BDL	2	BDL	2	BDL	BDL	BDL	BDL
Zn	35	39	101	37	170	83	41	18	30
Cu	36	51	79	23	99	93	229	10	20
Ni	335	554	213	376	139	162	290	403	379
Cr	109	581	28	233	58	48	83	114	105
Ce	BDL	BDL	32	BDL	83	34	BDL	BDL	BDL
Ba	BDL	BDL	BDL	BDL	69	3	BDL	BDL	BDL
Mg#	0.84	0.87	0.56	0.85	0.46	0.60	0.75	0.82	0.84
Zr/Y	10.1	3.6	0.9	3.9	1.9	1.6	5.0	3.7	2.9
Cr/Ni	0.33	1.05	0.13	0.62	0.42	0.30	0.29	0.28	0.28

Notes: Unit = lithological unit defined on the basis of mineralogical characteristics; LOI = loss on ignition; BDL = below detection limits. See "Geochemistry" section of "Explanatory Notes" for detection limits; Mg# = magnesium number calculated as the molar ratio of Mg/[Mg + 0.85*Fe (total)]; Rock type codes: MOLGAB = meta-olivine gabbro, TROC = troctolite, OXGAB = oxide gabbro, OLGAB = olivine gabbro, GABNOR = gabbronorite.

Table 4. Estimated mineral modes, alteration, and petrographic summary for Site 922 XRF samples.

						Olivine		Cpx		Opx		Plagioclase		Accessory minerals				
Core, section	Piece	Depth (mbsf)	Unit	Rock name	Alteration (%)	Original	Relict	Original	Relict	Original	Relict	Original	Relict	Hornblende	Apatite	Zircon	Sulfide minerals	Oxide minerals
153-922A-																		
1R-1	9	1.30	1	Meta-olivine gabbro	51	35	0	15	4			50	45					
2R-1	8	7.82	2	Troctolite	1	17	16	3	3			79	79	0.5				0.4
2R-1	8	7.82	2	Olivine gabbro	2	28	27	12	12			58	58	1.0			tr	0.3
2R-2	2	9.08	2	Oxide gabbro	0	15	15	6	6	10	10	62	62		tr		tr	6.0
2R-5	1A	11.96	2	Olivine gabbro	30	20	0	15	10			65	60					0.5
3R-1	4B	14.54	2	Oxide gabbronorite	19	3	1	15	5	12	10	60	55		tr		tr	10.0
153-922B-																		
2R-2	8	16.36	1	Gabbronorite	16			15	10	10	2	73	70			tr	tr	2.0
3R-1	3	19.44	2	Olivine gabbro	22	12	6	24	17			60	51					3.0
4R-2	1A	25.45	2	Olivine gabbro	33	10	0	23	5			65	60			tr		2.5
4R-3	4B	27.27	2	Gabbro	39	10	0	25	1			65	60					0.8

Notes: All modes are visually estimated from thin section. Where there is significant modal heterogeneity on the scale of the thin section, estimates are given for each domain. Unit = lithologic unit defined on the basis of mineralogical characteristics, tr = trace.

Discussion

Throughout most of the sequence of rocks recovered from Holes 922A and 922B, the cumulus phases were olivine and plagioclase. Most unaltered grains of clinopyroxene noted in thin section in these rocks are interstitial. Notable exceptions occur in Sections 153-922B-4R-2 and 4R-3. Given the extensive alteration of mafic phases, it is uncertain whether cumulus clinopyroxene was present in these holes. The only rocks that appear to have clinopyroxene grains that are clearly cumulus are oxide mineral-bearing rocks. In cases where a group of clinopyroxene grains in one region has a common crystallographic orientation, they are described as poikilitic, and are interpreted to have mostly crystallized after accumulation of the olivine and plagioclase. Such poikilitic grains are often interpreted to represent grain growth from trapped or circulating pore melts. Detailed mineral chemistry studies are required to assess whether such post-cumulus clinopyroxene represents trapped liquid or heteradcumulus growth. If these grains crystallized from trapped liquid, then cumulus crystal compositions could reflect re-equilibration with this trapped liquid. If clinopyroxene grains represent heteradcumulus growth, then the cumulus crystals could have retained primary magmatic compositions.

In some cases, clinopyroxene is interstitial to plagioclase, not as groups of grains with common crystallographic orientations, but rather as single grains that do not show common orientations with neighboring clinopyroxene grains. In these cases, clinopyroxene could be a cumulus phase. The interstitial texture of these clinopyroxene crystals could result if post-cumulus overgrowths formed on clinopyroxene, but not on plagioclase. Plagioclase crystals would retain their original euhedral to subhedral shapes and clinopyroxene overgrowths would fill in the remaining pore space.

Modal layering is a typical feature in cumulate rocks but the origins of this layering are not well understood. Recent interpretations suggest that cumulate rocks form by heterogeneous nucleation in boundary layers near the floor and walls of magma chambers rather than by homogeneous nucleation throughout the chamber. In this scenario, small-scale modal layering reflects differences in the crystallizing assemblage with time, rather than separation of phases by differences in settling rate. These issues cannot be resolved based on textural features alone.

The observation of crescumulate textures in cumulate rocks is commonly interpreted to indicate rapid crystal growth into supersaturated melt present at the cumulate-magma interface. Rapid crystal growth leads to the production of dendritic crystal habits, with the long axis of the grains aligned in the direction of most rapid crystal growth. This type of crystallization occurs by nucleation of crystals on preexisting cumulus crystals, with crystal growth into the magma body.

The occurrence of numerous small, intrusive, evolved differentiates, such as oxide gabbronorite and trondhjemite, indicates that magma evolution somewhere in the magmatic system in the MARK area has proceeded down-temperature to extreme values (85%–99% crystallization of primary magmas). The source of such highly evolved liquids is not known. Mobilization and injection of extremely evolved differentiates occurred before extensive cooling of these rocks, because such injections are frequently associated with high-temperature ductile shear zones and relatively coarse grain sizes of solidification products. In-situ crystallization within pore spaces in cumulate rock could produce such differentiates, but a resolution of this question will require shore-based studies. If pore space evolution is responsible for the production of these evolved melts, one would expect to find evidence for extreme evolution within the cumulate rocks. Zoning of plagioclase over very wide ranges of anorthite content, for example, would provide evidence for extreme differentiation of interstitial pore melts. The widespread occurrence of poikilitic clinopyroxene in these rocks might be interpreted as evidence for substantial down-temperature crystal growth during the solidification; however, such poikilitic grains can form by adcumulus or heteradcumulus growth. Poikilitic grains observed in thin section are not strongly zoned in major elements in the majority of cases, based on optical observations. Zoning in plagioclase is commonly oscillatory, with anorthitic cores, intermediate zones that are more albitic and rims that are similar in composition to grain cores.

Gabbroic rocks recovered from Holes 922A and 922B, when compared with those from holes at Site 921 (see "Igneous Petrology," "Site 921" chapter, this volume) and from Hole 735B, show a wide range of compositions (Fig. 20). They extend from slightly less evolved compositions (troctolite: Mg number = 0.87) to significantly more evolved compositions (oxide gabbro: Mg numbers = 0.46–0.5). In terms of major element oxide trends there are too few data on evolved compositions to make a valid comparison between Sites 921 and 922; however, using data from gabbroic rocks at Hole 735B as a basis for comparison, there are some striking differences, both between Sites 921 and 922 and between Site 922 and Hole 735B.

For some major element oxides, both Sites 921 and 922 fall within or close to the field of Hole 735B data (e.g., Fig. 20). However, for SiO_2 vs. Mg number (Fig. 21) Hole 922B gabbroic rocks include an oxide gabbro with lower SiO_2 than Hole 735B oxide gabbro. This geochemical difference probably reflects differences in primary modal compositions of cumulate rocks between the various localities. The host rocks of oxide gabbronorites at Site 922 are troctolite or olivine-rich olivine gabbro, and mini-cores taken for XRF analysis encompassed both the oxide-mineral rich horizon and the olivine-bearing host. Low silica in rocks from Site 922 could reflect higher modal olivine and iron titanium oxide mineral abundances throughout the sequence. Olivine and oxide minerals will lower bulk silica contents. The Site 922 rocks are extensively altered, which could play a role in the low silica abundances as well.

Site 922 gabbroic rocks are also distinct from Site 921 and Hole 735B gabbros in terms of some incompatible trace element variations. For example, troctolite and olivine gabbro displays Y–Mg number variations comparable to Site 921 and Hole 735B gabbros (Fig. 21), but the oxide gabbro and gabbronorite have much higher Y abundances at a given Mg number. High Y abundances are correlated with high P_2O_5 contents (Table 3). The higher Y in these rocks reflects high modal apatite in the analyzed samples, as Y, like the rare earth elements, is a compatible element in apatite. They are also distinct in compatible trace element characteristics, having higher Ni abundances at a given Mg number than either Site 921 or Hole 735B gabbros (Fig. 21). The higher Ni abundances are consistent with the olivine-rich nature of rocks chosen for analysis.

The high Cr/Ni Type 2 gabbro of Site 921 (see "Igneous Petrology," "Site 921" chapter, this volume) is not represented in the analyzed samples at Site 922 (Fig. 22). Poikilitic olivine gabbro with the characteristic green clinopyroxene oikocrysts is present at Site 922, but the poikilitic zones were not sampled for shipboard analysis. Further geochemical studies are needed to determine whether they have the chemical characteristics of the mineralogically and texturally similar poikilitic olivine gabbros of Site 921.

In Site 921 gabbroic rocks, TiO_2 is generally less than 1 wt% with one outlying sample at 3.4 wt%; all have uniformly low (<0.05 wt% P_2O_5; Fig. 23). In contrast, Site 922 gabbros display two trends. The low P_2O_5 trend comparable to Site 921 gabbros is represented by one high TiO_2 olivine gabbro (Section 153-922B-3R-2, Piece 3; TiO_2 = 1.05 wt%), the remaining high TiO_2 samples (oxide gabbro and the gabbronorite) fall on a high P_2O_5 trend. This trend is consistent with thin section observations that apatite often occurs in association with iron oxide minerals in Site 922 samples. Hole 735B gabbro also shows these two trends, although the high P_2O_5 trend is less well developed. These two trends are also seen in incompatible trace elements (e.g., Fig. 23) where the high P_2O_5/high TiO_2 gabbro is characterized by high Zr and Y abundances. Again, this is consistent with thin-section observation of zircon and apatite in some gabbronorite samples from Site 922.

There are two types of occurrence of oxide gabbro at Sites 921 and 922. The first exists as oxide gabbro layers, the second as zones of sheared oxide gabbro zones that may have originated as magmatic veins (see "Igneous Petrology" and "Structural Geology," "Site 921" chapter, this volume). Further geochemical characterization of these two groups of TiO_2-rich gabbros is necessary in order to determine whether they represent two intrinsically different lithologies or result solely from the heterogeneous distribution of accessory minerals. The compositions of cumulate rock samples are a function of the modal compositions of the samples, the compositions of the minerals that comprise the samples, and also the quantity of trapped melts, or evolved overgrowths on minerals crystallized from intercumulus melts. Shore-based microanalytical studies are needed to understand the composition of these rocks.

METAMORPHIC PETROLOGY

Introduction

Variably altered and deformed gabbroic rocks recovered from Holes 922A and 922B record a complex history of interaction between deformational and hydrothermal processes. The rocks are gen-

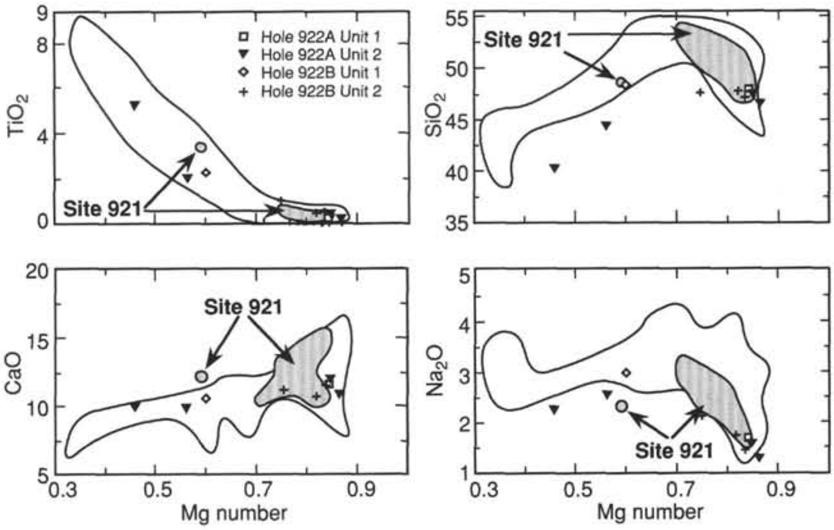

Figure 20. Major element variation diagrams vs. magnesium number (Mg number). White field = Hole 735B data from Leg 118, *Initial Reports;* gray field = Site 921 data from "Igneous Petrology" section, "Site 921" chapter, this volume. Gabbroic rocks from Site 922 show trends similar to those determined at Site 735B for Mg number vs. TiO_2 and Mg number vs. CaO, but have lower SiO_2 and lower Na_2O at low Mg numbers.

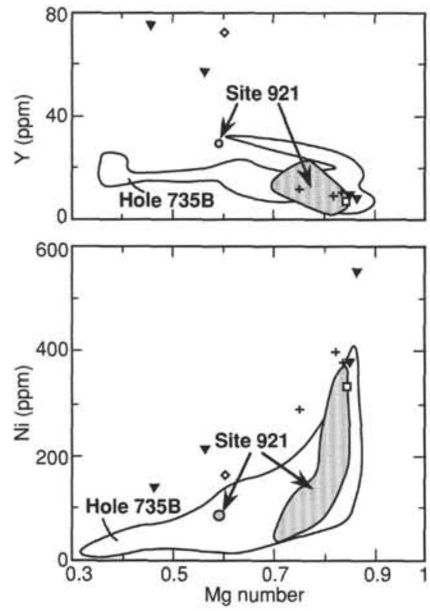

Figure 21. Trace element variation diagrams vs. magnesium number (Mg#). Gabbroic rocks from Site 922 have higher Y in evolved oxide gabbronorites, relative to Site 735B (white field). They also have higher Ni contents at all stages of evolution. Symbols as in Figure 20.

erally characterized by moderate to high alteration intensities (20%–50%), with localized intervals of pervasive alteration (80%–100%) in which primary textures and mineralogy are obscured. Background static metamorphism of the gabbro, olivine gabbro, and troctolite is heterogeneous and variable both on a centimeter to meter scale and downsection, reflecting variation in fracturing and attendant hydration. This overprinting by brittle failure of high-temperature metamorphic events resulted in the moderate to high intensity static background alteration of primary textures and mineralogy.

Secondary minerals include abundant actinolite-tremolite and chlorite and lesser amounts of talc, cummingtonite, epidote, smectite, carbonate minerals, zeolite minerals, and clay minerals. Alteration is commonly associated with brittle deformation in the form of singular, amphibole ± chlorite veins, and fine vein networks. Locally, pervasive alteration is associated with magmatic veins and pods that contain plagioclase, pyroxene, hornblende, and abundant accessory phases consisting of apatite, zircon, and oxide minerals. Secondary minerals in these compositionally evolved rocks include abundant actinolite-tremolite, chlorite, secondary plagioclase, and hydrothermal clinopyroxene, with lesser amounts of epidote, prehnite, carbonate minerals, and titanite. In zones of negligible to high alteration intensity, brown hornblende as an interstitial phase and as discontinuous rims around clinopyroxene and olivine is common.

Vein distribution and abundance in Holes 922A and 922B are heterogeneous with the highest abundances associated with highly deformed, oxide-bearing shear zones. Background mineral assemblages of the veins and wall rock require that fluid circulation in the gabbroic rocks occurred at temperatures >500°C, and that attendant alteration occurred under greenschist facies conditions (300°–400°C). Though alteration assemblages in this suite of rocks are generally similar in character to those observed in crustal rocks recovered by dredging and submersible from the ridge-transform massif (Gillis et al., 1993b; Kelley et al., 1993; Marion et al., 1991; Marion, 1992; Gallinatti, 1984; Karson and Dick, 1983), higher temperature mineral assemblages are better preserved, and alteration intensities are generally lower in gabbroic rocks recovered from Holes 922A and 922B.

In the following discussion, alteration mineral assemblages and textural relations within the gabbroic rocks from Site 922 are described. Downhole and inter-hole variations of secondary phases between the gabbroic, troctolitic, and olivine gabbroic rocks are characterized and a summary of the metamorphic and hydrothermal history preserved in these rocks is presented.

Alteration of Primary Phases in the Gabbroic Rocks

The plutonic suite recovered from Holes 922A and 922B include olivine gabbro, gabbronorite, olivine gabbronorite, gabbro, and oxide-bearing gabbro, which are commonly moderately to highly altered (Fig. 24 and Table 5). At least 40% of the gabbroic rocks recovered are affected by 65% background alteration. Mineral assemblages defining distinct metamorphic zones are generally absent and alteration is commonly heterogeneous. Secondary minerals reflecting high-grade thermal metamorphism are associated with mylonite zones in olivine gabbronorite and oxide-gabbronorite intervals and indicate that dynamic metamorphism occurred under amphibolite to transitional granulite facies conditions. Retrograde alteration in the highly deformed zones is commonly slight. Local intervals, which exhibit 80%–100% replacement, are related to densely veined and oxide-rich intervals of deformation with high-temperature alteration assemblages generally overprinted by lower temperature secondary phases. In general, background alteration is governed by replacement of olivine, followed by clinopyroxene, and disequilibrium textures are common (Figs. 25 and 26).

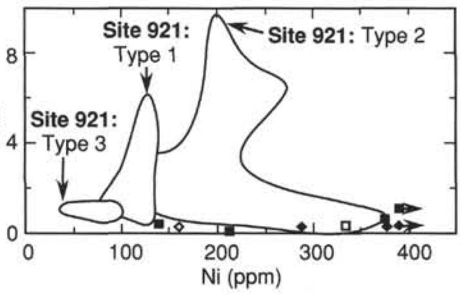

Figure 22. Cr/Ni vs. Ni. Clinopyroxene-rich samples with high Cr/Ni analyzed from Site 921 were not sampled at Site 922. Olivine-rich, clinopyroxene-poor samples have high Ni and low Cr because Ni is strongly compatible in olivine, whereas Cr is strongly compatible in clinopyroxene. Symbols as in Figure 20.

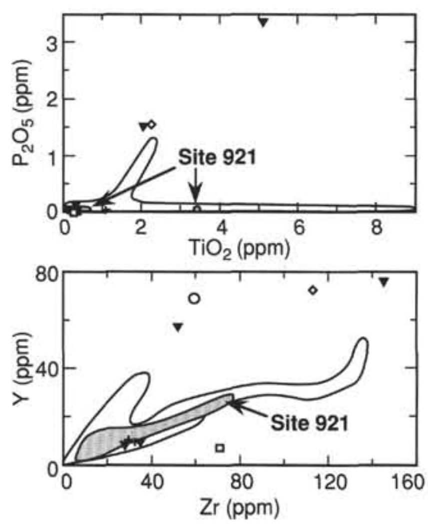

Figure 23. TiO_2 vs. P_2O_5 and Zr vs. Y. Apatite-rich oxide gabbronorites form a trend of steeply increasing P_2O_5 with increasing TiO_2. Oxide-rich samples also have high Zr and Y because these elements are compatible in Fe-Ti oxides and apatite, respectively. Symbols and fields as in Figure 20.

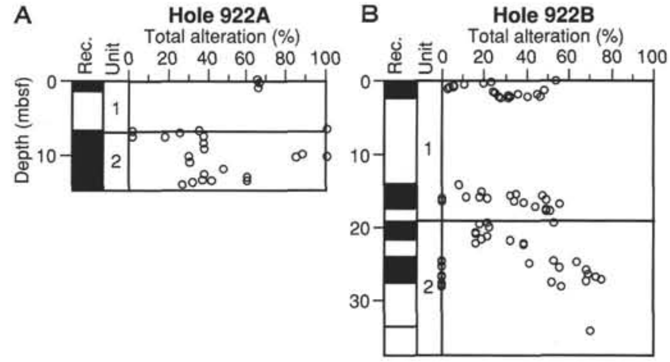

Figure 24. Depth vs. abundance of secondary minerals in percent, estimated from core samples, for (**A**) Holes 922A and (**B**) 922B. Lithologic units are described in "Igneous Petrology," this chapter. Core recovery for these sections is indicated by black bars. Alteration intensities are generally similar between Holes 922A and 922B and there are no apparent differences in the occurrences of alteration minerals downhole.

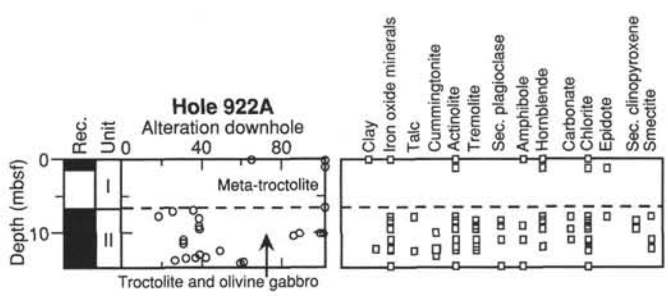

Figure 25. Alteration intensities and occurrences of secondary minerals with depth in gabbroic rocks recovered from Hole 922A.

Olivine

In the gabbroic rocks, alteration intensity of olivine is commonly high to pervasive (40%–80%); however, some samples contain up to 90% relict olivine. Complex coronitic replacement after olivine forms a macroscopically striking feature of gabbroic sections from Holes 922A and 922B (Figs. 3, 15, and 27). Initial stages of olivine alteration involves formation of a microvein network containing fine-grained magnetite. With progressive alteration, talc and iron oxide minerals line the microfractures and develop discontinuous rims around grain boundaries. In more highly altered grains, irregular, concentric zoning of olivine involves cores of intergrown tremolitic to actinolitic amphibole and fine-grained magnetite (Figs. 27 and 28). The amphiboles form fibrous sprays, which radiate inward from chloritic rims, and are locally intergrown with variable amounts of pale yellow, mixed-layer chlorite-smectite, olive brown to yellow smectite, iddingsite, chlorite, and talc, with traces of pyrite (Figs. 27–29). Locally, carbonate minerals occur as fine grains within the coronas and discontinuously rim corona margins (e.g., Sample 153-922B-3R-2, Piece 3A, 54–58 cm). Where olivine grains are in contact with plagioclase, rimming chlorite forms millimeter-wide bands, which exhibit compositional zonation from innermost bands composed of Mg-rich-chlorite, with anomalous olive-green birefringence, to an outer rim of Fe-rich, dark green chlorite with anomalous blue birefringence (Figs. 27–29). Brown amphibole partially rims olivine locally and occurs as an interstitial phase.

In highly altered samples, fine-grained magnetite is pervasive along crosscutting microfractures and as concentrated bands that mimic original grain boundaries. Locally, magnetite forms composite, elongate "feathery" to dendritic grains that are associated with tremolite and radiate into the cores of coronas (e.g., Sample 153-922A-2R-5, Piece 1, 30–35 cm). Where olivine is completely replaced, the talc and magnetite assemblage is generally absent, and alteration is dominated either by intergrown chlorite and tremolite that form large felted mats, or by pods of smectite, pyrite, and chlorite. In any one sample these mineral zonations are highly variable and one or more alteration phases may be absent. Similar zonation of secondary phases after olivine has been described for gabbros collected during submersible dives in the MARK area (Marion, 1992; Gillis et al., 1993b) at Sites 894 and 735, at the Hess Deep and Southwest Indian Ridge, respectively (Gillis, Mével, Allan, et al., 1993a; Stakes et al., 1991), and at the Mid-Cayman Rise (Ito and Anderson, 1983).

In hand sample, altered olivine is characterized by an iron red color because of replacement by iddingsite, and coarse-grained pyrite is common. In some sections this style of alteration gives the core a mottled and oxidized appearance. The alteration is associated with development of an orange clay mineral(?), which forms net veins in plagioclase (e.g., Section 153-922B-1W-2). In pervasively altered gabbroic samples, interconnected coronas form distinctive amoeboid-shaped, fibrous pods with dark green chloritic rims (Fig. 28). The amphibole and chlorite-rich pods commonly enclose anhedral plagioclase with embayed grain boundaries and clean cores. Actinolite and chlorite microveinlets typically cut the plagioclase, radiating inward from the rimming actinolite and chlorite (Fig. 29). Well-

Table 5. Metamorphic summary for Holes 922A and B.

Primary mineralogy	Secondary mineralogy	Fluid inclusions
Olivine	Coronitic, tremolite-actinolite, talc, carbonate, magnetite, pyrite, iddingsite, iron-oxide minerals	Vapor-dominated along healed microfractures
Clinopyroxene	Brown amphibole, green to yellow-green amphibole, secondary clinopyroxene, pyrite, magnetite	Primary vapor-dominated, low-salinity inclusions
Orthopyroxene	Pale green amphibole (cummingtonite?), talc, chlorite	
Plagioclase	Secondary plagioclase, zeolite, clay, actinolite, chlorite, epidote, prehnite	Plagioclase contains secondary vapor to liquid-dominated inclusions
Apatite, Zircon, Titanite, Magnetite		Apatite contains vapor and liquid-dominated inclusions

Vein types	Facies and intensity
Magmatic: plagioclase, amphibole, cpx	Transitional granulite to greenschist facies, <5%–100% altered
Hydrothermal: actinolite, chlorite + actinolite, rare epidote ± prehnite, calcite veins	

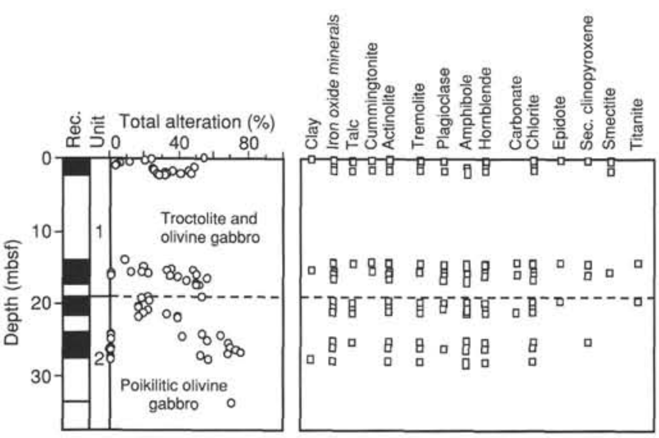

Figure 26. Alteration intensities and occurrences of secondary minerals with depth in gabbroic rocks recovered from Hole 922B.

developed actinolite-tremolite and chlorite coronas form ellipse-shaped pods in association with shear zones (e.g., Section 153-922-2R-1). In highly deformed zones, olivine forms fine-grained neoblasts, which exhibit a mosaic texture and are commonly enclosed by iron oxide minerals. Coarser grained crystals in these zones form aggregates that are slightly altered to talc and iron oxide minerals.

Clinopyroxene

Alteration of clinopyroxene in Holes 922A and 922B dominates alteration intensity in gabbro, oxide gabbro, and to a lesser extent olivine gabbro, where pyroxene replacement varies from <10% to 100%. Brown hornblende after clinopyroxene and as an interstitial phase is pervasive throughout gabbroic rocks from this site. Hornblende forms the earliest alteration phase after clinopyroxene, where it occurs both as fine-grained, brown inclusions within clinopyroxene, which are commonly associated with magnetite, and as discontinuous rims around clinopyroxene grain margins (Figs. 25 and 26). With progressive alteration, clinopyroxene grains become turbid and green brown due to abundant micron-sized (<1–5 μm), anhedral, magnetite grains, and intergrowths of very fine-grained fibrous pale green to yellow amphibole. Felted actinolitic mats after clinopyroxene form distinctive amoeboid-shaped pods, similar to those after olivine, and contain abundant, fine-grained iron oxide minerals and traces of blebs of brown amphibole.

Amphibole after clinopyroxene exhibits complicated and diverse optical zonation and crystal habits. It typically forms fine-grained, fibrous, pale green to colorless radiating actinolite-tremolite mats, which rim or completely pseudomorph clinopyroxene. Fine-grained anhedral pyrite and magnetite are commonly associated with fibrous

Figure 27. Moderately well-developed coronitic replacement of olivine (Sample 153-922B-3R-2, Piece 3, 54–58 cm). Field length is 1.5 mm long. Slightly altered olivine in the core of the corona is cut by fine, iron oxide mineral-filled veinlets. Olivine is rimmed by talc and tremolite-actinolite, with a well-developed outer rim of zoned chlorite. Fine veinlets of intergrown actinolite and chlorite radiate outward from the edge of the corona into adjacent plagioclase grains.

actinolite rims and as inclusions in clinopyroxene. In pervasively altered sections, such as those that occur at the top of Hole 922A, extensive development of actinolite-tremolite pods, which are rimmed by chlorite, completely obscures the primary mineralogy. Pale green to dark green chlorite with anomalous blue to low first-order birefringence after actinolite is common in these zones and is best developed where bounded by both clinopyroxene and plagioclase. Coarser grained aggregates of bladed amphibole after clinopyroxene locally exhibit well-developed cleavage and are commonly green-yellow, or dark green to blue-green. These amphiboles are especially well developed in compositionally evolved patches and veins containing accessory minerals consisting of apatite, zircon, and magnetite. Formation of coarse-grained, actinolitic patches, which are locally rimmed by chlorite, are particularly well developed adjacent to macroscopic magmatic veins and later fractures filled with actinolite ± chlorite.

Secondary hydrothermal clinopyroxene occurs in minor amounts throughout Holes 922A and 922B (Figs. 25 and 26), where it is associated with oxide-rich gabbros, gabbronorites, compositionally evolved patches, and felsic veins, and in alteration halos adjacent to these veins. In these rocks, secondary clinopyroxene commonly forms as "dusty" inclusion-filled patches and rims around primary clinopyroxene, where it locally results in 50%–60% replacement (e.g., Sample 153-922B-2R-2, Piece 3, 20–23 cm). Vapor-dominated fluid inclusions and very fine-grained oxide minerals are ubiquitous in the secondary clinopyroxene. The secondary clinopyroxene is commonly associated with well-developed, dark green to blue-green amphibole, which forms coarse rims around clinopyroxene. In well-crystallized zones, secondary clinopyroxene forms clear, colorless to pale green patches within primary clinopyroxene grains. The secondary pyroxenes are petrographically similar to those in gabbros from the Skaergaard Intrusion (Manning and Bird, 1986), to those in plutonic rocks from Sites 894 and 735 at Hess Deep (Gillis, Mével, Allan, et al., 1993a), and at the Southwest Indian Ridge, respectively (Stakes et al., 1991; Mével and Cannat, 1991), and in gabbros recovered from the MARK area just north of Site 922 (Gillis et al., 1993b).

Orthopyroxene

Orthopyroxene alteration intensity is highly variable (<10%–100%), and finer grains are commonly more pervasively altered. In slightly to moderately altered grains, cummingtonite and fine-grained oxide minerals fill microfractures cutting orthopyroxene grains, form narrow rims around pyroxene grains, and occur as isolated intergrown fibrous patches within the grains. In highly deformed zones, orthopyroxene porphyroclasts exhibit bent deformation lamellae and are rimmed by fine stringers of iron oxide minerals and cummingtonite or tremolite. Along localized deformation zones, neoblastic polygonal grains are overprinted by pale green amphibole and chlorite. In these zones, coarser grained porphyroclasts exhibit cummingtonite along grain boundaries and are locally pervasively replaced by cummingtonite. Fine-grained orthopyroxene crystals are enclosed in mats of cummingtonite and are cut by rare veinlets of brown amphibole. In pervasively altered samples, felted mats of tremolite are overgrown by chlorite in orthopyroxene pseudomorphs (e.g., Sample 922B-2R-2, Piece 3, 20–23 cm).

Plagioclase

Plagioclase alteration ranges from <10% to 100% and predominantly involves the formation of secondary plagioclase, with minor amounts of epidote, prehnite, and chlorite in pervasively altered zones. In general, plagioclase is strikingly fresh, with pervasive alteration typically constrained to alteration halos associated with intrusion of magmatic veins and millimeter-wide actinolite ± chlorite veinlets. In highly altered zones, plagioclase is typically turbid due to abundant fine-grained inclusions of chlorite, amphibole, and clay minerals. Secondary plagioclase commonly forms irregular micro-veinlets and patches that crosscut and rim primary plagioclase, respectively. Locally, in extensively altered patches and adjacent to crosscutting veins, secondary plagioclase contains abundant, anhedral to euhedral, liquid-dominated fluid inclusions. Fine-grained, fibrous sprays of actinolite commonly replace plagioclase grain boundaries and radiate from adjacent altered pyroxene and olivine grains. Pale green amphibole and chlorite veinlets, most commonly associated with oxide-rich deformation zones, form anastomosing veinlets cutting plagioclase, and actinolite rimming plagioclase grain boundaries is common. Traces of epidote, typically associated with magmatic veins and in mylonite zones, forms fine-grained, granular, pale green inclusions in plagioclase that are locally associated with prehnite. Chlorite after plagioclase is common in olivine gabbros, where it is associated with coronitic replacement of olivine.

Static and Dynamic Metamorphism of Gabbroic Rocks

The gabbroic rocks recovered from Site 922 were affected by variable degrees of alteration and deformation, which in the initial stages involved crystal-plastic deformation. This high-temperature deformation was subsequently overprinted by brittle deformation, which resulted in the formation of millimeter-wide actinolite and actinolite + chlorite veins. These veins, which locally form dense anastomosing networks, resulted in moderate to high intensities of static background metamorphism from amphibolite- down to greenschist-facies conditions. In the following discussion, mineral assemblages and deformational relationships are presented in terms of igneous rock types.

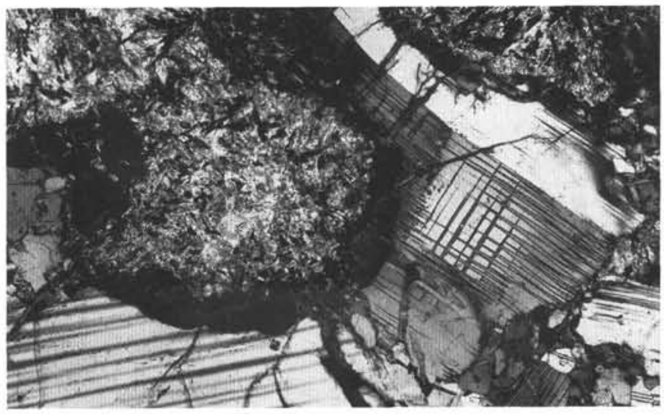

Figure 28. Pervasively altered olivine grains with secondary minerals forming a network of amoeboid-shaped pods, which enclose plagioclase (Sample 153-922B-1W-2, Piece 3, 44–50 cm). Field length is 3 mm long. Felted mats composed of fibrous intergrowths of tremolite-actinolite, talc, and fine-grained iron oxide minerals rimmed by dark green chlorite, bound plagioclase grain boundaries.

Figure 29. Outer margin of a corona after olivine. Zoned chlorite forming the outer margin is bounded by well developed inwardly radiating sprays of tremolite + iron oxide minerals, which pervasively replace olivine (Sample 153-922A-2R-2, Piece 3, 30–35 cm). Field length is 3 mm long.

Troctolitic Gabbro

Troctolitic rocks recovered from Holes 922A and 922B exhibit highly variable and heterogeneous alteration intensities ranging from ~20% to 100%, with highest intensities associated with deformation zones and intrusion of magmatic veins (Fig. 30). Alteration of the troctolites is dominated by variable development of coronitic replacement after olivine (Fig. 27). The coronas are composed of variable modal amounts of talc, iron oxide minerals, tremolite-actinolite, and traces of smectite, with commonly well-developed zoned rims of chlorite (Figs. 27–29). In some samples associated with magmatic veins, talc forms coarse grains with birds-eye extinction and is intergrown with tremolite. In the most pervasively altered samples, talc is absent and coronas are dominantly composed of tremolite-actinolite and chlorite. Troctolites recovered from the top portion of Holes 922A and 922B are highly to pervasively altered, with alteration dominated by formation of actinolite-tremolite-rich pods, rimmed by chlorite. Primary mineralogy of mafic phases in these rocks is commonly completely obscured by secondary phases. The amoeboid-shaped amphibole pods enclose anhedral plagioclase grains, which are relatively free of alteration in the cores. Olivine grains in less altered portions of the core are commonly only slightly altered (<10%), with minor rims of tremolite, or talc, and crosscutting microfractures filled with

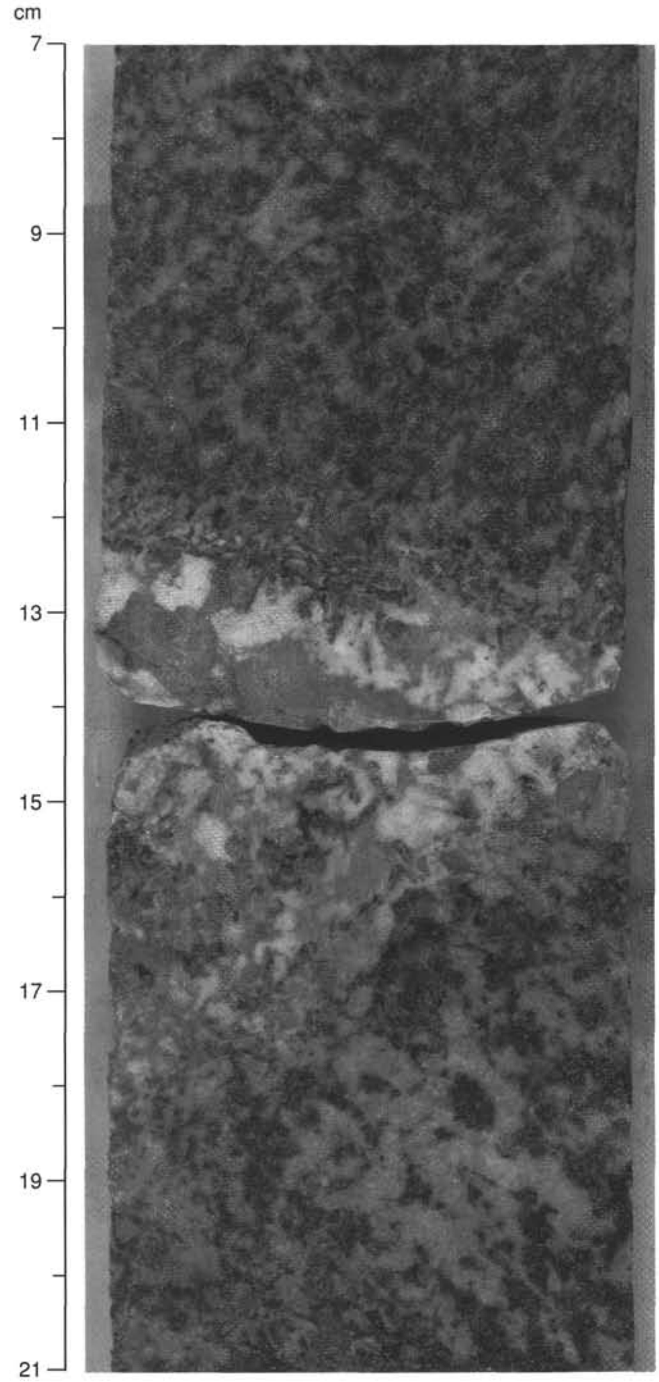

Figure 30. Felsic magmatic vein cutting moderately altered troctolitic gabbro in Unit 2 of Hole 922A (Sample 153-922A-2R-2, Piece 1, 7–21 cm). The vein is composed of intergrown felted mats of actinolite + iron oxide minerals and brown hornblende after clinopyroxene. Chalk-white plagioclase is pervasively altered to secondary plagioclase, with minor epidote and prehnite. Other primary phases include apatite, zircon, and quartz. The vein margin is marked by pervasive alteration of the troctolitic host rock.

iron oxide minerals are common. Well-crystallized brown hornblende is pervasive in the troctolitic gabbros, where it occurs as partial rims, or encloses olivine and clinopyroxene grains, forms fine blebs in clinopyroxene, and less commonly occurs as an interstitial phase. It is most abundant in zones cut by magmatic veins and is generally associated with fine-grained magnetite. In many samples, mineralogical evidence indicating retrograde alteration of the hornblende is absent.

Plagioclase in the troctolites is generally only slightly to moderately altered, with alteration most intense adjacent to magmatic veins (Fig. 30). In these aureoles, plagioclase is typically dusty in appearance due to abundant fluid inclusions and fine-grained clay minerals, and grain boundaries are altered to chlorite ± amphibole. Plagioclase minerals in localized deformation zones exhibit patchy extinction, sutured grain boundaries, deformation twins, and are rimmed by neoblastic plagioclase. Retrograde alteration of these phases is commonly minor and limited to fine crosscutting veins of actinolite, and actinolite + chlorite. Rare prehnite locally replaces plagioclase adjacent to the veins. Alteration of accessory phases in the troctolites includes amphibole and titanite after titanomagnetite (Fig. 31).

In the bottom of Hole 922B, intense deformation of the troctolites has resulted in the formation of porphyroclastic mylonite (e.g., Sample 153-922B-4R-1, Piece 6A, 59–63 cm). The localized mylonitic zones are comprised of clinopyroxene-rich zones, millimeters in width, which are enclosed in a fine-grained matrix of neoblastic plagioclase. The mylonites are bounded on either side by relatively undeformed coarse-grained troctolite containing pervasively altered olivine. A well-developed wrapping foliation in the mylonite is defined by fine-grained and well-crystallized green to olive green amphibole, with trace amounts of brown amphibole. The amphibole-rich stringers wrap plagioclase and clinopyroxene porphyroclasts and pseudomorphically replace olivine grains. The amphibole-rich bands form alternating lenses with fine-grained, neoblastic plagioclase, which exhibit a mosaic texture.

Plagioclase porphyroclasts in the deformed zone form elongate and en-echelon, highly strained grains, which are cut by fine microfractures filled with amphibole. The porphyroclasts exhibit patchy extinction, sutured grain boundaries, glide twins, and contain embayments filled with fine-grained, neoblastic plagioclase. Clinopyroxene porphyroclasts are pervasively replaced by dark to pale green amphibole and are rimmed by amphibole. Pseudomorphically replaced olivine porphyroclasts form rounded pods completely replaced by tremolite-actinolite, chlorite, and fine-grained iron oxide minerals. Rare zircon occurs as an accessory phase in the mylonites.

The contact between mylonite zones and relatively undeformed troctolite is abrupt with adjacent plagioclase exhibiting minor glide twinning. Olivine grains in the undeformed troctolite are pervasively replaced and exhibit characteristic corona development of tremolite-actinolite, fine-grained iron oxide minerals, and chlorite. Both the mylonites and troctolites are cut by veinlets of fine-grained amphibole and chlorite and rare millimeter-wide veinlets of dark green to yellow green amphibole. The amphiboles commonly radiate away from altered olivine pods. The mineralogical assemblage and textural relationships defined by synkinematic, well-crystallized green amphibole and minor brown amphibole indicate that dynamic metamorphism in this zone occurred under amphibolite facies conditions (Spear, 1981). Alteration continued down into the greenschist facies as indicated by a strong overprint of the high-temperature phases by amphibole and chlorite.

Olivine Gabbro

The percentage of alteration of the olivine gabbros is heterogeneous, ranging from <10% to ~50%, with alteration dominated by replacement of olivine and formation of well-developed corona structures (Figs. 27–29). The olivine gabbros are strikingly fresh in some intervals, with alteration limited to fine anastomosing vein networks of iron oxide minerals in olivine and discontinuous rims of brown amphibole around olivine and minor clinopyroxene. With increasing alteration, talc, tremolite, and iron oxide minerals become significant secondary phases. In pervasively altered zones, olivine exhibits well-developed coronitic replacements, which in hand sample and thin section form a striking feature of the core (Fig. 32). The coronas are complex and consist of variable amounts of talc, tremolite, iron oxide minerals, and highly zoned, rimming bands of chlorite. The coronas

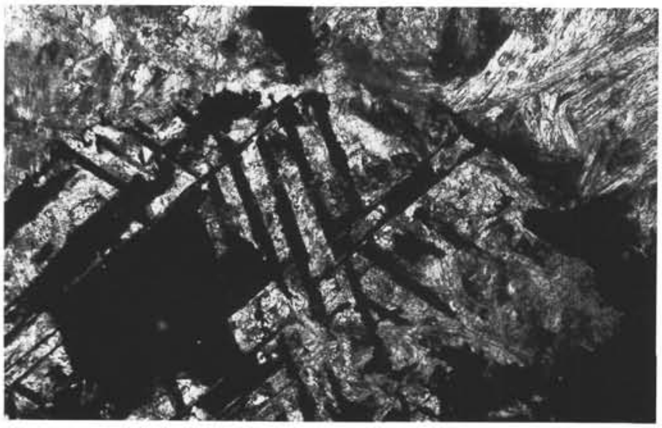

Figure 31. Ilmenite exsolution lamellae after titanomagnetite that are enclosed by secondary dark to light green, fibrous amphibole, with minor titanite (Sample 153-922B-3R-1, Piece 3, 44–50 cm). Field length is 3 mm long.

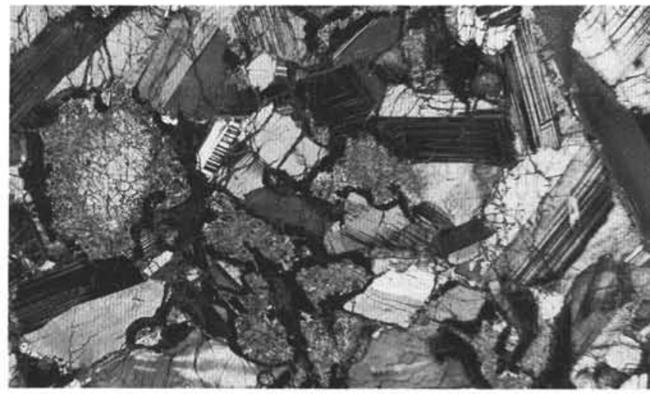

Figure 32. Heterogeneous alteration of olivine gabbro with characteristic development of coronitic replacement after olivine (Sample 153-922B-3R-2, Piece 3, 54–58 cm). Olivine in this sample is replaced by tremolite-actinolite, iron oxide minerals, and traces of talc and chlorite. Field of view is 24 mm.

are locally rimmed by well-developed brown hornblende and associated iron oxide minerals. In poikilitic olivine gabbros, pervasive alteration forms adjoining amoeboid shaped coronas that enclose plagioclase grains. Plagioclase grains in these zones commonly exhibit anhedral grain boundaries and are cut by fine veinlets of chlorite and actinolite. Plagioclase grains adjacent to these zones are typically rimmed by radiating sprays of actinolite and/or chlorite, and veinlets of chlorite and actinolite commonly shoot off from the coronas into the adjacent grains. Plagioclase in these areas typically hosts abundant, liquid-dominated fluid inclusions, which in some samples contain four to five birefringent daughter minerals. Clinopyroxene in the olivine gabbros is heterogeneously altered. In samples exhibiting slight alteration, brown hornblende as discontinuous rims and as fine-grained inclusions in clinopyroxene is common. With increasing alteration, actinolite and fine-grained iron oxide minerals progressively replace pyroxene.

Mylonite intervals within the olivine gabbros at the top of Hole 922B are composed of intercalated olivine and oxide gabbronorites that exhibit highly variable degrees of grain-size reduction on a local scale (<1 mm wide). In the mylonites, olivine-rich lenses with tapering lensoidal-shaped olivine porphyroclasts form anastomosing alternating bands with fine-grained neoblastic olivine and lenses dominated by neoblastic plagioclase. Recrystallized aggregates of olivine exhibit a mosaic texture and only very slight alteration in the form of microfractures filled with iron oxide minerals. Neoblastic olivine forms tails on highly strained olivine porphyroclasts, which exhibit deformation bands, patchy extinction, and sutured grain boundaries. Porphyroclasts of highly strained plagioclase are commonly elongate, sigmoidal in shape, and are enclosed in a fine- to very fine-grained matrix of neoblastic plagioclase. The porphyroclasts exhibit glide twinning, patchy extinction, and sutured grain boundaries in a manner similar to adjacent olivine porphyroclasts. Well-developed fine-grained brown hornblende and associated fine-grained iron oxide minerals form an anastomosing wrapping foliation around the olivine and plagioclase porphyroclasts. The synkinematic hornblende is overprinted by amphibole, which is fine grained and pale green.

In the oxide-rich zones, fine-grained olivine neoblasts are enclosed in oxide stringers. The neoblasts in these zones generally exhibit higher degrees of retrograde alteration than neoblasts that occur away from the oxide-rich bands. Alteration phases in these zones include brown amphibole, chlorite, tremolite-actinolite, and minor talc and iron oxide minerals. Locally, olivine is replaced by pseudomorphs of tremolitic amphibole. Orthopyroxene porphyroclasts in the oxide-rich zones are slightly to moderately altered to fine rims of cummingtonite(?), tremolite, and fine-grained iron oxide minerals.

Grain sizes in the mylonite zones vary on a submillimeter scale, with coarse-grained areas commonly adjacent to very fine-grained domains. Coarse-grained intervals are composed of discontinuous olivine aggregates and only minor stringers of rimming hornblende. Moderately coarse-grained plagioclase in these zones is highly strained and enclosed by localized elongate zones of neoblastic plagioclase. Alteration intensity in the coarser grained zones is generally higher than in the mylonitic zones, with rare pods of chlorite, minor talc, and fine-grained iron oxide minerals after olivine.

Mylonitic zones within the olivine gabbros exhibit slight to high intensities of alteration (e.g., Sample 153-922B-1W-1, Piece 10, 134–137 cm), where high alteration intensities are characterized by secondary minerals after olivine. Well-developed coronitic replacement of olivine by secondary phases is common. Medium-grained olivine porphyroclasts are pervasively altered (90%–100%) to amoeboid-shaped pods containing well-crystallized talc, intergrown with tremolite, and fine-grained iron oxide minerals. The walls of the pods contain inwardly radiating tremolite and intergrown iron oxide minerals, and outer rims of zoned chlorite. Olivine forms fine-grained, pervasively altered stringers, which are altered to tremolite, fine-grained iron oxide minerals, and minor chlorite. The stringers form alternating bands with neoblastic, fine-grained plagioclase grains that exhibit a mosaic texture and are commonly cut by fine veinlets of pale green amphibole and chlorite. Clinopyroxene alteration is highly variable, ranging from pervasive to slight, and alteration minerals include fine-grained fibrous green amphibole and fine-grained iron oxide minerals with localized rims of brown hornblende. Rounded to elongate plagioclase porphyroclasts exhibit glide twins, undulatory and patchy extinction, and sutured grain boundaries. They are commonly cut by chlorite veinlets, and the porphyroclasts are rimmed by a fine-grained mosaic of plagioclase neoblasts.

Gabbro

Slightly to moderately deformed gabbroic rocks recovered from Holes 922A and 922B exhibit alteration intensities ranging from 40% to 80%, with alteration characterized by well-developed coronitic replacement of olivine and to a lesser extent clinopyroxene. Coronitic replacement of olivine includes variable amounts of talc, tremolite-actinolite, fine-grained iron oxide minerals, and rare smectite with chlorite typically forming zoned outer rims. Pseudomorph pods form amoeboid-shaped patches in highly deformed zones. Clinopyroxene exhibits variably well-developed felted pods of actinolite-tremolite and intergrown chlorite, with coronitic rims of chlorite common. Fine-grained amphibole in these pods forms pseudomorphs of clinopyroxene and poikilitic clinopyroxene with inclusions of anhedral plagioclase. In isolated and compositionally evolved pods that contain apatite and zircon, clinopyroxene is typically replaced by well-developed green hornblende and associated oxide minerals. Plagio-

Figure 33. Photomicrograph of a mylonitic zone in gabbroic intervals in Hole 922B. Fine-grained neoblasts and plagioclase enclose clinopyroxene, plagioclase, and olivine porphyroclasts (Sample 153-922B-1W-2, Piece 2, 41–44 cm). Note glide twins in plagioclase porphyroclasts. Field length is 24 mm.

clase grains associated with these pods are cut by networks of veinlets composed of actinolite and chlorite, which radiate outward from the pseudomorphed pyroxene grains. Grain boundaries of plagioclase, associated with these zones, are commonly anhedral and embayed due to overgrowth by pale green chlorite.

Discrete shear zones occur locally throughout the gabbros (Fig. 33). Extensive grain-size reduction occurs on a millimeter to centimeter scale and results in formation of mylonite to protomylonite zones. Contacts with adjacent wall rocks are commonly abrupt, with bounding host rocks only slightly to moderately deformed. The mylonitic to protomylonitic zones are characterized by anastomosing bands of fine- to very fine-grained neoblastic plagioclase, which exhibit a well-developed mosaic texture. The plagioclase-rich bands commonly are interlayered with anastomosing bands of brown amphibole and fine-grained oxide minerals that are locally overprinted by fine-grained, fibrous green amphibole. The hornblende-rich bands form an anastomosing foliation that encloses porphyroclasts of pseudomorphically replaced olivine, aggregates of slightly altered neoblastic fine-grained olivine rounded to tapering porphyroclasts of clinopyroxene, and highly strained plagioclase grains. In highly retrograded zones, chlorite and actinolite-tremolite commonly overgrow the neoblasts near the margins of the deformation bands. The millimeter- to decimeter-wide shear zones are cut by anastomosing networks of apple green to dark green amphibole and chlorite. The boundary of the anastomosing mylonite zones are commonly abrupt, with only mild deformation of the bounding grains. Coarse- to moderately coarse-grained, strongly zoned plagioclase outside of these zones exhibits deformation bands, sutured grain boundaries, and patchy extinction. They are moderately replaced by secondary plagioclase, a trace of epidote, and prehnite. The grains are crosscut by abundant microfractures filled with actinolite, chlorite, and irregular patches and jagged veinlets of secondary plagioclase. The abundance of well-crystallized synkinematic hornblende in these zones, with minor overprints of green amphibole, indicates that deformation in these zones occurred under minimum temperatures of 700° to 900°C (Spear, 1981; Liou et al., 1974).

Gabbronorite and Oxide Gabbronorite, Oxide Gabbro

Gabbronorites and oxide gabbronorites, which occur locally throughout Units 1 and 2 in Holes 922A and 922B, are moderately to highly deformed and altered, with alteration intensities averaging ~30%. In localized zones of moderate to high deformation, coarse- to medium-grained plagioclase grains exhibit deformation twins, patchy extinction, and sutured grain boundaries. Porphyroclasts are commonly rimmed by localized zones of fine-grained neoblastic plagioclase, which exhibits a moderately well-developed mosaic texture. In these and undeformed zones, plagioclase is generally only slightly altered (<10%) with alteration limited to fine veinlets of green to pale blue-green amphibole and chlorite, which form sparse crosscutting networks. Clinopyroxene in the gabbronorites is slightly to pervasively altered (20%–100%). It is commonly replaced by fine-grained brown amphibole blebs and actinolite ± chlorite. In pervasively altered zones, pyroxene grains are replaced by pseudomorphs of actinolite and fine-grained iron oxide minerals, which form felted mats. Deformed pyroxene grains locally exhibit deformation lamellae and are partially recrystallized to fine-grained, clear clinopyroxene grains. In oxide gabbronorites, which commonly contain accessory minerals consisting of apatite and zircon, hydrothermal clinopyroxene is common. The hydrothermal clinopyroxenes are distinguished by containing abundant vapor-dominated fluid inclusions and very fine-grained oxide mineral inclusions, which give the pyroxene grains a dusty appearance. In these zones, well-developed green-brown amphibole forms coarse-grained rims after clinopyroxene. Orthopyroxene grains are variably altered (10%–100%), with fine grains commonly pervasively altered. Cummingtonite is the dominant alteration mineral after orthopyroxene; it forms narrow rims around orthopyroxene and occurs as fine, fibrous intergrowths with minor fine-grained oxide minerals. Iron oxide minerals are typically rimmed by pale green to blue green amphibole with lesser amounts of chlorite. Locally, these secondary phases fill fractures that cut the iron oxide minerals.

Core from near the middle of Hole 922A (Core 153-922A-2; ~9.1 mbsf) is composed of troctolitic gabbro and intervals of oxide gabbro and is cut by a narrow mylonite zone that contains abundant and well-crystallized synkinematic brown hornblende (Fig. 34). Plagioclase porphyroclasts in this zone are rounded to elongate and exhibit strong patchy extinction, sutured grain boundaries, and deformation twins. They are cut locally by microveins of actinolite and chlorite. Fine-grained, mosaic-textured neoblasts of plagioclase commonly enclose the porphyroclasts. Orthopyroxene porphyroclasts are elongate to sigmoidal in shape and are slightly to moderately altered to green amphibole. The porphyroclasts are typically rimmed by stringers of oxide minerals that define an anastomosing foliation. Locally orthopyroxene grains host apatite inclusions containing abundant primary, vapor-dominated fluid inclusions.

On either side of the oxide gabbronorite, recrystallized and highly strained olivine grains form fine-grained aggregates and near the oxide-mineral-rich zones are completely enclosed by oxide minerals. Olivine grains within the aggregates are only slightly altered to talc and fine-grained oxide minerals and are discontinuously rimmed by well-crystallized brown hornblende. Olivine grains commonly host abundant secondary vapor-dominated inclusions along healed microfractures. The fractures commonly terminate at olivine grain boundaries, suggesting that they predated deformation. Fine-grained hornblende forms discontinuous anastomosing stringers that are associated with and rim fine-grained iron oxide minerals. Away from the

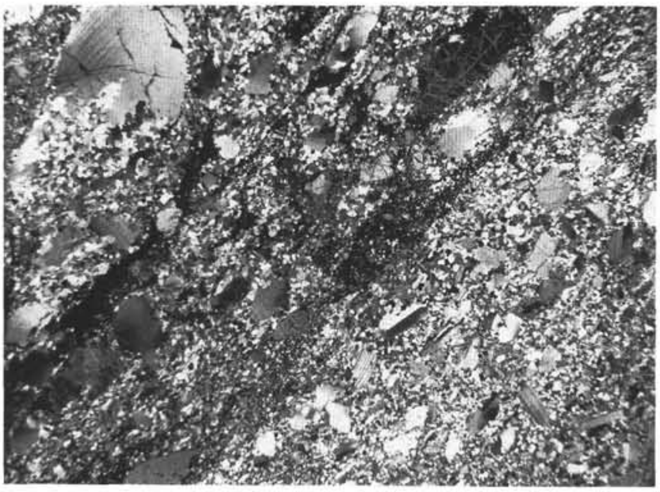

Figure 34. Deformed oxide-rich domain (middle) cutting diagonally across photo within a troctolitic interval in Unit 1 of Hole 922A. The highly deformed oxide gabbroic interval contains alternating bands of brown hornblende, plagioclase neoblasts, and stringers of oxide minerals, as well as plagioclase and clinopyroxene porphyroclasts (Sample 153-922A-2R-2, Piece 2, 106–111 cm). Field length is 24 mm.

mylonite zone, moderately coarse-grained olivine is slightly to pervasively altered to talc, fine-grained iron oxide minerals, and minor amphibole. Clinopyroxene is moderately to pervasively altered to fibrous mats of pale green amphibole and brown hornblende. The occurrence of neoblastic olivine and well-crystallized synkinematic brown hornblende after clinopyroxene in the mylonite zone indicates that dynamic metamorphism in this zone occurred under upper amphibolite to transitional granulite facies temperature conditions (600°–800°C) at low-pressure conditions.

Veins in the Gabbroic Rocks

Macroscopic veins are moderately abundant throughout the gabbroic rocks recovered from Holes 922A and 922B, and four generations have been identified based on crosscutting relationships. Mineralogy of the different vein generations was characterized in hand sample, and confirmed by thin-section analyses. In the following discussion, we describe the vein characteristics and provide a general chronology of the vein sets.

Magmatic Veins

Felsic magmatic veins compose less then 1% of the core recovered from Site 922 and are associated with pervasive alteration of the host gabbros (Figs. 3, 30, and 35). The veins are commonly either subhorizontal or subvertical and exhibit sharp boundaries with the gabbroic host rocks. Locally, the vein margins may exhibit grain-size reduction indicating shear. The felsic veins are commonly 20 to 40 mm wide and exhibit compositional zonation with clinopyroxene + amphibole-rich cores and accessory phases consisting of apatite, zircon, and iron oxide minerals. The cores are rimmed by variably wide margins of plagioclase that have diffuse to sharp boundaries with the pervasively altered bounding host rock (Figs. 3, 30, and 35). Primary minerals within the veins are typically highly to pervasively replaced by variable amounts of coarse-grained actinolite and tremolite. Secondary plagioclase, granular epidote, and prehnite are common after plagioclase. Rare, strongly pleochroic anhedral and red-brown hornblende may be a primary phase locally in the veins.

The wall rocks near these veins are variably altered with actinolite, chlorite, secondary plagioclase, and traces of epidote as common secondary phases (Figs. 3, 30, and 35). Brown hornblende forms well

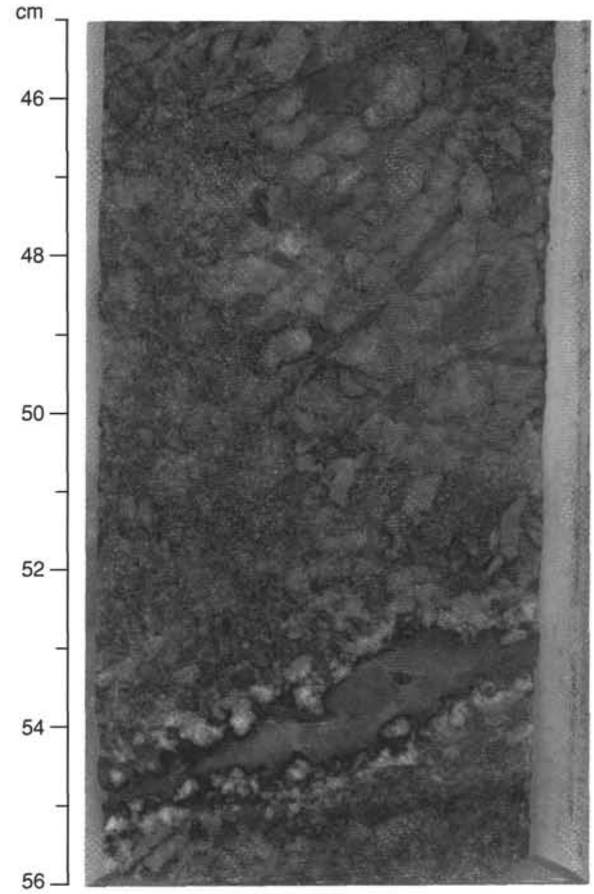

Figure 35. Subhorizontal, altered clinopyroxenite vein rimmed by a margin of brown amphibole, plagioclase, and apatite cuts highly altered gabbro in Unit 2 of Hole 922B. The brown amphibole and chlorite form a corona-like rim on the edge of the vein. Clinopyroxene in the vein is pervasively replaced by actinolite, and plagioclase is highly altered to secondary plagioclase (Sample 153-922B-4R-3, Piece 3, 45–56 cm).

developed rims around clinopyroxene adjacent to the veins and locally rims host-rock olivine grains. In the olivine gabbros and poikilitic olivine gabbros, intrusion of these veins and attendant alteration results in development of coarse-grained talc and magnetite ± smectite-rich pods after olivine. The pods enclose anhedral plagioclase grains, which are rimmed by a fine band of green chlorite. Plagioclase in the veins and adjacent host rock is highly to pervasively altered to secondary plagioclase, which rims grain boundaries and occurs along jagged and irregularly shaped fractures cutting plagioclase. Typically the plagioclase in these zones is dusty in appearance because of abundant fine grains of clay minerals(?) and liquid-dominated fluid inclusions. Titanomagnetite grains with exsolved ilmenite exsolution lamellae, which are common in the evolved pockets and in felsic veins, are pervasively altered with exsolved ilmenite exsolution lamellae enclosed by variable amounts of green to colorless amphibole, and titanite (Fig. 31).

Hydrothermal Veins

Composite mesoscopic hydrothermal veins throughout the gabbroic rocks recovered from Holes 922A and 922B commonly contain variable amounts of actinolite, actinolite + chlorite, and chlorite. Less common veins contain epidote and epidote + prehnite; clay minerals are rare. The veins are locally densely distributed and commonly cut discrete shear zones. Vein orientations are highly variable. On the basis of crosscutting relationships three to four distinct vein generations have been recognized within the gabbroic intervals (see "Structural Geology," this chapter). Each of these vein sets is described below.

Actinolite Veins

This earliest vein set observed in all rock types recovered from Holes 922A and 922B is characterized by pale green, blue-green to dark green amphiboles, tentatively identified as actinolite. The actinolite veins are common throughout the gabbroic rocks where they form singular, isolated veins, and vein networks. Vein morphologies are highly variable and range from distinct sharp-sided, continuous features to irregular wispy, discontinuous structures. The mineralogy of this vein set locally changes on a submillimeter scale, where vein mineralogy is based on the mineral being cut (e.g., Sample 153-922A-2R-3, Piece 8, 15–18 cm). In plagioclase this vein set is locally composed of blue-green amphibole. Where these veins cut olivine, they are lined by iron oxide minerals, and the mineralogy changes to tremolite. The amphibole-filled veins are most common where associated with oxide-rich shear zones, where they form a dense network both parallel and almost perpendicular to the shear zones (Fig. 36). Fine veinlets of amphibole are common in plagioclase and are associated with coronitic replacement of olivine and clinopyroxene. They form a ubiquitous component of highly altered and highly deformed gabbros in some sections, and clearly govern the static metamorphism observed in these deformed intervals. In the more continuous veins, intense wall-rock alteration results in the pervasive replacement of bounding olivine and clinopyroxene grains by amphibole ± chlorite and iron oxide minerals. Alteration halos, where present, are commonly 1–2 mm in width. Plagioclase grains in the alteration halos are commonly chalky white due to moderate- to high-intensity alteration by secondary plagioclase. Actinolite veins cut magmatic felsic veins and are cut by later chlorite and actinolite + chlorite veinlets.

Actinolite + Chlorite Veins

Actinolite + chlorite veinlets are similar in nature to the actinolite veinlets and when combined with the actinolite veins, they govern the background static metamorphism observed in the gabbroic rocks. The veins are typically ~1 mm or less wide and dark green, and associated alteration halos are rare. The composite actinolite + chlorite veins are the most common veins in the gabbroic rocks and commonly form fine, anastomosing networks that locally pervasively crosscut plagioclase grains. As with the actinolite veins, this vein set is most abundant in shear zones, where they both run parallel and crosscut the preferred direction of mineral alignment. In one sample, these veins are cut by a later epidote + prehnite-bearing vein (e.g., Sample 153-922A-2R-3, Piece 3, 67–93 cm).

Chlorite Veins

Fine chlorite veins, generally <1 mm wide, form anastomosing networks in plagioclase and highly deformed samples. These veinlets are commonly discontinuous and generally contain dark green, well-crystallized chlorite; associated wall-rock alteration is typically absent.

Epidote ± Prehnite Veins

Epidote and epidote + prehnite veinlets (1–2 mm wide) are rare in the gabbroic rocks and where present are associated with pervasive alteration of the adjacent host rock. They form subvertical veins that cut highly deformed zones, and in one sample crosscut an actinolite + chlorite vein (Sample 153-922A-2R-3, Piece 2, 59–67 cm). Wall-rock alteration associated with this vein set includes pervasive replacement of plagioclase grains by medium-grained apple-green epidote, prehnite, and lesser amounts of secondary plagioclase.

Fluid Inclusions in the Gabbroic Rocks

Multiple populations of fluid inclusions in the variably altered and deformed gabbroic samples indicate that fluid circulation at Site 922 involved fluids of widely varying compositions and temperatures, starting at late magmatic conditions. Inclusions are abundant in apatite hosted in oxide-rich gabbros, gabbronorites, and gabbros, and are locally abundant in hydrothermal clinopyroxene associated with evolved melt pockets and magmatic veins. The inclusions typically occur along anastomosing arrays of healed microfractures in plagioclase and as primary inclusions trapped during growth of magmatic apatite and hydrothermal clinopyroxene. Primary and secondary inclusions are not common in secondary and vein-filling minerals, which likely reflects the inherent difficulty of minerals such as actinolite, chlorite, and prehnite to trap inclusions. Based on petrographic analyses at room temperature, the inclusions were classified into three main types.

Type 1: Liquid-dominated, daughter-mineral-absent inclusions: Type 1 inclusions are liquid-dominated inclusions, which are moderately common in plagioclase and less common in apatite and secondary amphibole. Inclusion sizes are widely variable, ranging from <1 μm to 20 μm. The liquid-dominated inclusions occur as two subtypes within the gabbroic rocks. Type 1A inclusions are hosted in plagioclase, amphibole, and apatite (Fig. 37). They exhibit negative to anhedral crystal habits, contain a small liquid-rimmed vapor bubble (<50 vol%), and commonly form anastomosing crosscutting arrays along healed microfractures. These inclusions are typically secondary in origin. In apatite, these inclusions occur both as primary and secondary inclusions and exhibit a very small vapor-to-liquid ratio. Type 1B inclusions form concentrated zones of irregularly shaped ragged inclusions and are common in highly altered patches of plagioclase. The inclusions most commonly occur in alteration halos associated with intrusion of magmatic veins and veins of actinolite and chlorite but are present locally away from the veins as well. They may be primary in origin; however, textural evidence for primary origin is not conclusive.

Type 2: Vapor-dominated, daughter-mineral-absent inclusions: Vapor-dominated inclusions are moderately common in oxide gabbro, gabbronorite, and gabbro and are rare in mylonite intervals. They are extremely abundant as primary and secondary inclusions in apatite (Fig. 62, "Site 920" chapter, this volume) and are less common as secondary inclusions in olivine (Fig. 38). In apatite the inclusions range in size from <1 to 15 μm and are characterized by containing ~100% of a vapor phase. The large extent of vapor-filling indicates that the inclusions likely contain CO_2 ± H_2O; however, shore-based studies can confirm their compositions. In olivine, vapor-dominated secondary inclusions range in size from <1 to 20 μm, and are similar to inclusions hosted in apatite. In highly deformed zones, trails of the secondary inclusions along healed microfractures in olivine terminate at the porphyroclast boundaries, indicating that they were likely entrapped previous to the high-temperature deformation. Hydrothermal clinopyroxene grains are characterized by containing extremely abundant primary vapor-dominated inclusions that give the clinopyroxene a turbid appearance.

Type 3: Daughter-mineral-bearing inclusions: Daughter-mineral-bearing inclusions in the gabbroic rocks are common in plagioclase, where they occur along healed microfractures. Daughter phases locally fill the inclusions so that little liquid is visible. Four to five daughter minerals may be present in a single inclusion, with fibrous elongate birefringent daughter phases common. Vapor to liquid ratios are highly variable in these inclusions, though vapor-rich to vapor-dominated inclusions are common. Similar inclusions are observed in gabbros collected from the ridge-transform massif in the MARK area and from Hole 735B, which commonly contain methane (Kelley et al., 1993).

Down- and Intra-hole Variation in Alteration

There is no apparent difference in the occurrences of alteration minerals between Holes 922A and 922B, and alteration intensities are broadly similar between the two holes (Figs. 25 and 26). Alteration is most intense in the top of Hole 922A and near the bottom of Hole

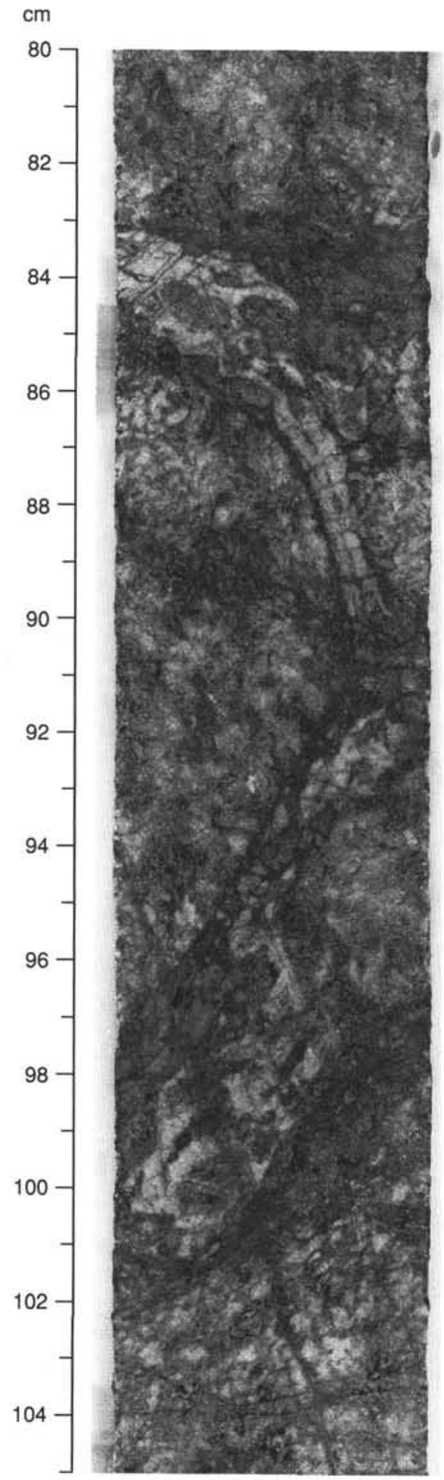

Figure 36. Sample 153-922A-2R-5 (Piece 2, 80–105 cm). Oxide-rich shear zones in coarse-grained, highly altered olivine gabbro in Unit 2 of Hole 922A. Shear zones visible between 83 and 90 cm and between 90 and 102 cm dip in opposite directions. The piece is densely veined by a network of dark green actinolite and actinolite + chlorite veins and veinlets, which are both parallel and highly discordant to the fabric in the shear zones.

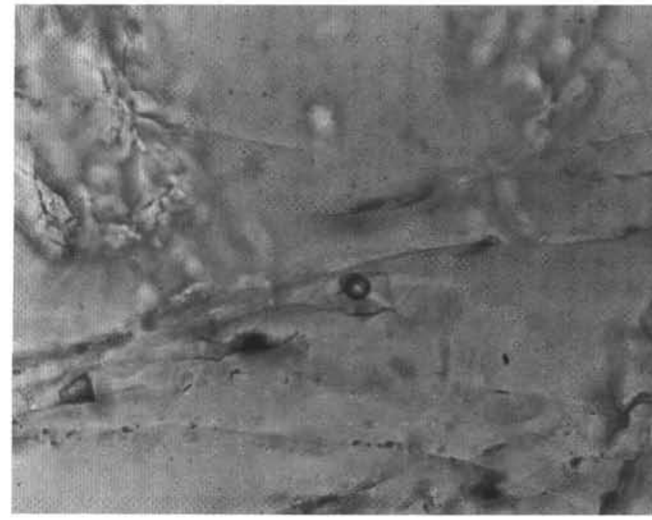

Figure 37. Liquid-dominated low-salinity fluid inclusion in plagioclase along healed microfracture (Sample 153-922B-4R-3, Piece 4, 70–76 cm). The inclusion contains a small vapor bubble, rimmed by a low-salinity liquid. The inclusion is 10 µm wide.

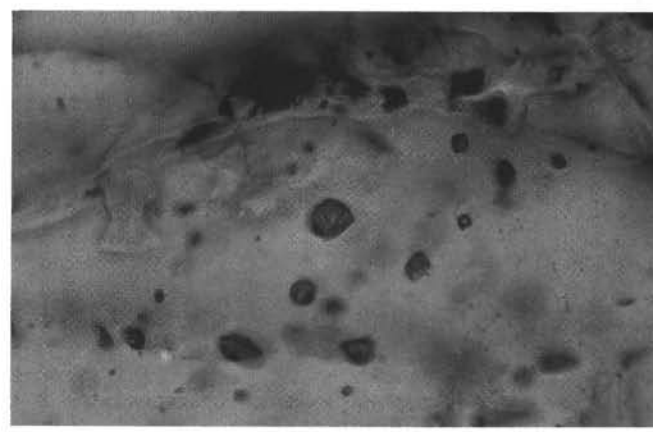

Figure 38. Vapor-dominated fluid inclusions in olivine. These inclusions occur along healed microfractures that terminate at the boundaries of the olivine grains that are rimmed by neoblastic plagioclase (Sample 153-922B-2R-1, Piece 1A, 12–17 cm). The central inclusion is 15 µm wide.

922B and is generally associated with brittle deformation in the form of anastomosing actinolite and actinolite + chlorite-filled veins in both of these areas. A general but poorly defined increase in alteration appears near the base of Hole 922A. Alteration intensities of Units 1 and 2 in Holes 922A and 922B are similar, though isolated intervals of gabbro and olivine gabbro locally exhibit somewhat higher alteration intensities (Fig. 24).

Discussion

Deformational and metamorphic relationships in the gabbroic rocks recovered from Holes 922A and 922B reflect the integrated effects of polyphase deformational episodes, intrusion of felsic veins, and progressive strain localization and metamorphic recrystallization that occurred under conditions of decreasing temperatures and increasing hydration. The effects of these processes have resulted in variable styles, grades, and intensities of alteration both within individual lithologies and throughout the cores recovered.

In the gabbroic suite, magmatic and metamorphic processes exhibit a progressive evolution with the merging of crystal fabrics that are strictly magmatic to those associated with lower temperature deformation. The crystal-plastic fabric observed in discrete and heterogeneously distributed shear zones throughout the core is commonly associated with synkinematic hornblende and recrystallization of olivine, plagioclase, and pyroxene, indicating that recrystallization and deformation probably occurred at temperatures of 700°–900°C (Spear, 1981; Liou et al., 1974). The high-temperature deformation zones typically exhibit slight to moderate retrograde alteration effects, with limited overprinting of actinolite-tremolite, talc, and minor chlorite after the mafic phases. Slight veining by hydrothermal minerals in these zones is consistent with the low alteration intensities in these intervals. In contrast, where actinolite ± chlorite veins form a dense network that crosscuts and overprints the high-temperature fabric, neoblasts and porphyroclasts are pervasively altered and the synkinematic hornblende is extensively replaced by green amphibole. Retrograde mineral assemblages in these zones of well developed talc, tremolite-actinolite, chlorite, and minor brown amphibole is consistent with penetration of hydrothermal fluids into these zones under greenschist facies conditions. The scarcity of low-temperature phases such as zeolite minerals in these rocks suggests that sealing of the circulation system occurred at temperatures of ~300°–400°C (Liou et al., 1974). The fact that synkinematic minerals in ductile shear zones are largely restricted to amphibolite facies, and the fact that greenschist and zeolite facies mineral assemblages are scarce and always represent a post-kinematic static overprint, indicate that the shear zones ceased to be operative at high temperatures and did not act as conduits for fluids circulating under lower temperature greenschist to zeolite facies conditions.

Away from the zones of intense deformation, high-temperature static background alteration is limited to brown amphibole as blebs and rims around clinopyroxene and olivine and talc after olivine. The relative absence of these high-temperature phases may reflect limited circulation of hydrothermal fluids in the gabbroic rocks under amphibolite facies conditions. Complex coronitic replacement of olivine in these rocks suggests that the aureoles may have been influenced by chemical diffusion at low water-to-rock ratios in response to compositional gradients between plagioclase and olivine (Ito and Anderson, 1983). In contrast to the general absence of high-temperature secondary phases in these rocks, the gabbros commonly exhibit moderate to high intensities of alteration by abundant tremolite-actinolite and chlorite, with lesser amounts of hydrothermal clinopyroxene, secondary plagioclase, and traces of epidote and prehnite. The close association of these lower temperature phases with well-developed networks of actinolite and actinolite + chlorite veinlets is consistent with brittle failure and increased circulation of fluids at temperatures of 300°–450°C.

The deformational and hydrothermal history of the gabbroic suite of rocks recovered from Site 922 is broadly similar to rocks recovered by dredge and submersible from the ridge-transform massif in the MARK area. However, there is a general tendency for better development and preservation of high-temperature secondary phases and deformation zones in the drilled gabbroic rocks than what has been previously observed in rocks recovered from this area (Gillis et al., 1993b; Marion et al., 1991; Marion, 1992; Gallinatti, 1984; Karson and Dick, 1983). This may reflect a relative sampling bias in which dredge and submersible samples have preferentially sampled rocks affected by brittle deformation.

STRUCTURAL GEOLOGY

Introduction

The cores recovered from the two holes at Site 922 contain medium- to coarse-grained rocks that consist mainly of troctolite and olivine gabbro with various degrees of alteration, metamorphism, and deformation. Mesoscopic core observations record the occurrence of primary magmatic foliations, discrete shear zones, distributed microfractures, fracture networks, veins, and vein arrays indicating several successive tectonic events. Crystal-plastic and brittle deformation have locally overprinted the magmatic textures. Cores from Hole 922A are described in terms of a single structural domain characterized mainly by heterogeneous crystal-plastic deformation with superimposed fracturing. Core from Hole 922B can be divided into two domains on the basis of structural style. The upper domain is marked by discrete crystal-plastic shear zones and locally densely distributed microfractures indicating that an early episode of crystal-plastic deformation was overprinted by an episode of brittle deformation. In the lower domain, crystal-plastic fabrics are less extensive and microfractures and veins are more widespread relative to the upper domain.

Magmatic Fabrics

Fabrics observed in the cores that are interpreted to result from crystal growth and accumulation or magmatic flow include cumulate to poikilitic textures with either a random orientation of primary igneous minerals or a faint mineral shape-fabric related to alignment of the long axes of grains. Magmatic flow fabric is defined by plagioclase laths with a weak shape preferred orientation or where pyroxene and/or olivine grains are crudely aligned (e.g., Fig. 8). Rocks that display magmatic fabrics show no sign of dynamic recrystallization or distortion of minerals. The medium- to coarse-grained olivine gabbro in Section 153-922B-3R-1, for example, shows a weakly developed preferred orientation of subhedral plagioclase laths with no development of neoblasts. The magmatic foliation defined by the shape preferred orientation of plagioclase grains in the lower part of Piece 3 in the same section has a dip of 15°. A weak preferred orientation of plagioclase grains also is observed in Sections -4R-1 and -4R-2 from Hole 922B.

Thin-section observations from several gabbroic samples with primary igneous textures support interpretations from mesoscopic observations regarding the magmatic fabrics. The coarse-grained olivine gabbro in Sample 153-922A-2R-3, 15–18 cm, displays a well-preserved, primary igneous texture characterized by a weak preferred orientation of large plagioclase laths and interstitial olivine grains. The occurrence of polygonal neoblasts along grain boundaries and intracrystalline deformation bands reflects limited recrystallization in this sample. Similarly, the coarse-grained troctolite in Sample 153-922A-2R-1, 122–129 cm, shows a weak shape preferred orientation of plagioclase laths, which display minor development of deformation twins.

Crystal-plastic Fabric

A crystal-plastic fabric defined by a preferred alignment of elongated olivine and pyroxene crystals appears in many of the gabbroic rocks (Fig. 39). This fabric predominantly occurs in millimeter- to decimeter-scale, discrete shear zones (Figs. 40 and 41). These shear zones generally have sharp and well-defined boundaries and are commonly bounded by undeformed rock (Fig. 40). Locally, they coincide with lithological boundaries between gabbros and troctolitic gabbros, and in other places they are overprinted by actinolite + chlorite veins (e.g., Section 153-922B-3R-2, Pieces 3A and 3B). Strong grain-size reduction in the shear zones leads to the development of porphyroclastic textures. The dip of shear zones is highly variable, ranging from subhorizontal to subvertical. Anastomosing branches splay out from them (e.g., Section 153-922A-2R-5, Piece 2B).

Shear zones are particularly well-developed in some intervals of the cores in both holes. In Section 153-922A-2R-2 the homogeneous troctolite of Unit 2 displays two closely spaced shear zones in the upper part of Piece 2 in which asymmetric plagioclase grains, clinopyroxene grains, and bands of iron oxide minerals define a gneissic texture (Fig. 40). The foliation plane within these shear zones has a dip of 55°. The shape preferred orientation of the minerals decreases progressively in intensity downsection away from the shear zones and is not visible in the middle of the piece. Section 922A-2R-4 similarly contains several discrete shear zones. A 10-mm-wide shear zone at the top of Piece 1 has a dip of 36° and contains lenses of recrystallized

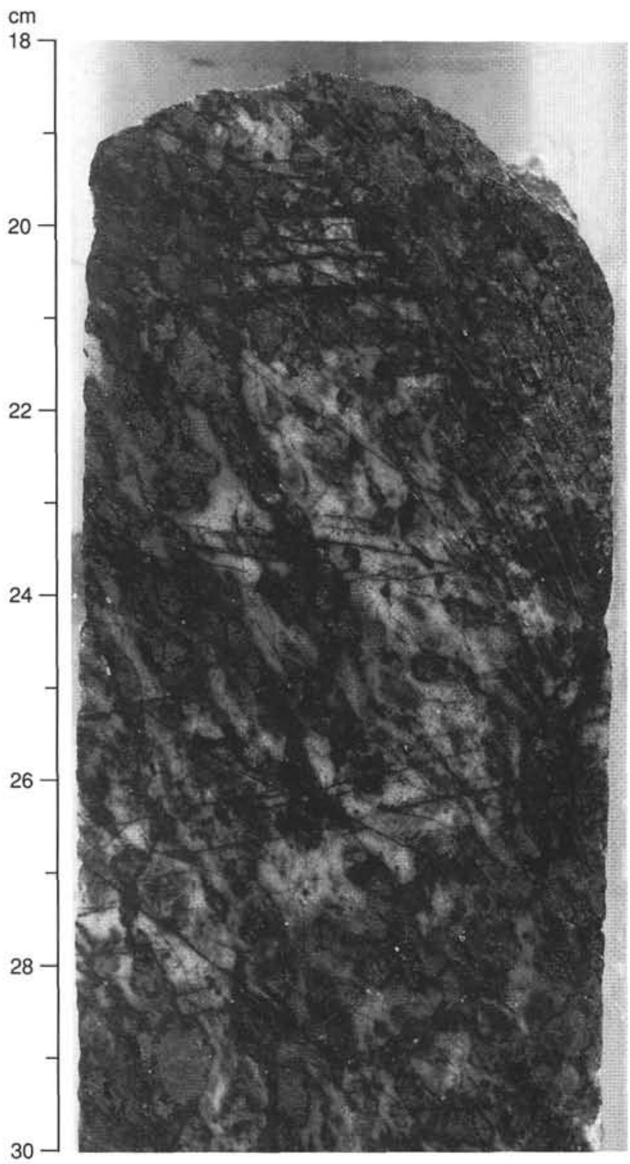

Figure 39. Shape preferred orientation of the long axes of elongated pyroxene grains, plagioclase stringers, and oxide mineral veinlets define a typical porphyroclastic fabric dipping steeply in a coarse-grained olivine gabbronorite from Unit 1 (Sample 153-922B-2R-2, Piece 3, 18–30 cm). This fabric is part of a decimeter-scale shear zone developed in the upper part of the piece. Conjugate sets of chlorite + actinolite veins (black) cross-cut the crystal-plastic fabric at oblique angles. Notice the dense distribution of chlorite + actinolite veins in the uppermost part of the piece.

plagioclase, chlorite, and brown amphibole. The host rock immediately below the shear zone is a coarse-grained olivine gabbro with no shape preferred orientation fabric. In Section 153-922A-2R-5 (Piece 2A), three discrete shear zones with widths ranging from 5 to 40 mm contain elongated pyroxene porphyroclasts in a sheared and possibly recrystallized matrix of plagioclase. The uppermost shear zone (at 75 cm) is subvertical, while the other two converge, forming a curved zone in the center of the piece (Fig. 36). The zone may consist of a folded, continuous shear zone with a subhorizontal axis and a subhorizontal axial plane or two oppositely dipping shear zones that intersect near the edge of the piece.

In Section 153-922B-1W-2, the olivine gabbro in Pieces 1 and 2 contains 5- to 20-mm-wide shear zones that have a well-developed mylonitic texture. The discrete shear zones in Piece 1 have gentle to

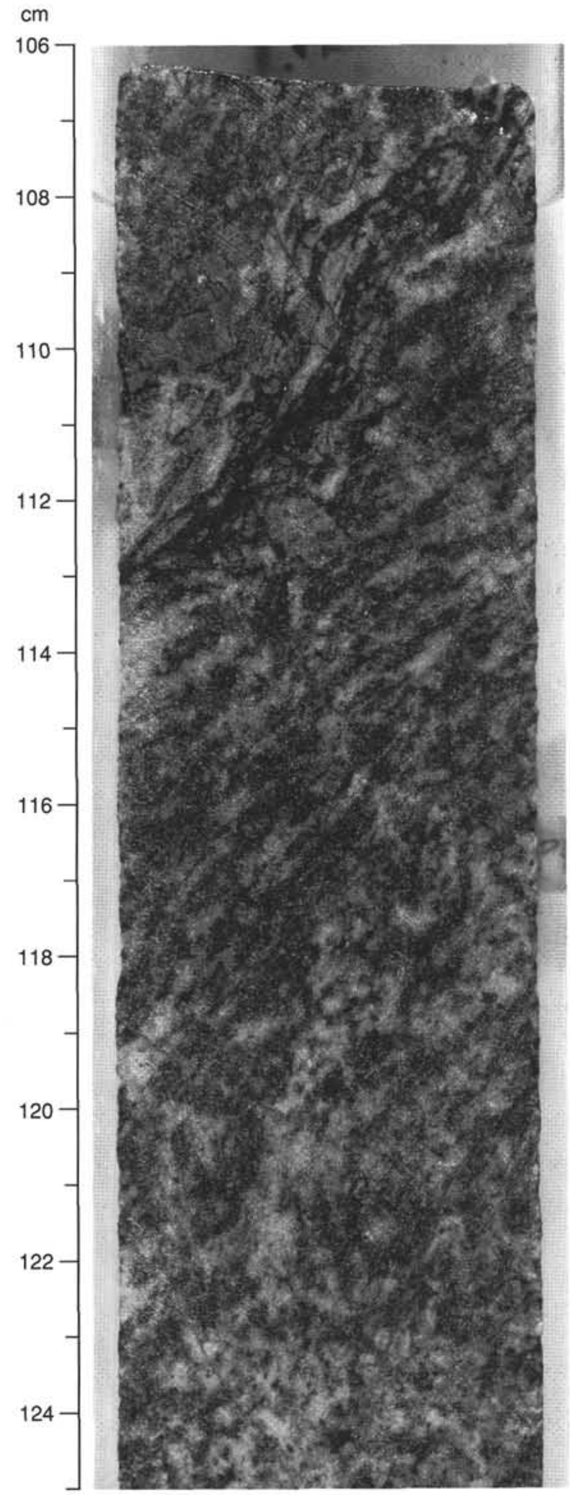

Figure 40. The troctolite of Unit 2 is transected by two moderately dipping (50°) subparallel shear zones at 107 and 120 cm, respectively, in Piece 2 of Sample 153-922A-2R-2, 106–125 cm. Whereas the lower shear zone is not clearly visible, the upper shear zone is 25 mm wide and contains abundant iron oxide minerals and large (to 13 mm) porphyroclasts of clinopyroxene and plagioclase. The shear zone foliation is cut at high angles by chlorite + actinolite veins. Note the relatively sharp boundaries between the shear zones and the rest of the rock.

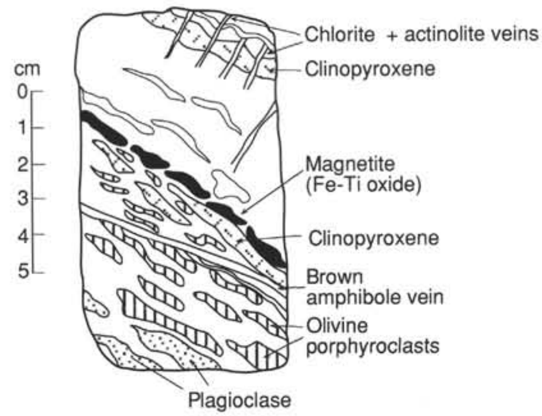

Figure 41. Line drawing of a decimeter-scale shear zone with a typical porphyroclastic fabric defined by elongated olivine and clinopyroxene grains in the olivine gabbro rock of Unit 1 in Sample 153-922B-1W-1 (Piece 8, 105–115 cm). Deformed Fe-Ti oxide minerals (black) occur as elongated stringers parallel to the shear zone fabric. A 2-mm-wide and moderately dipping actinolite + brown amphibole vein cuts across the shear zone fabric. A subset of parallel chlorite + actinolite veins transects the shear zone fabric at 90° in the upper part of the piece.

moderate dips (2°–44°) and anastomosing branches. They contain plagioclase, olivine, clinopyroxene, and orthopyroxene porphyroclasts in a fine-grained matrix containing thin seams of clinopyroxene, plagioclase, hornblende, and iron oxide minerals. The domain between the top two shear zones shows a strong lineation defined by elongated olivine and plagioclase grains that plunges gently (2°–16°) parallel to the shear zones. Similarly, Pieces 1, 4 , 5, and 9 in Section 153-922B-2R-2 contain discrete, steeply dipping shear zones that include highly elongated plagioclase and pyroxene porphyroclasts and deformed oxide minerals. Clinopyroxene grains in these shear zones are locally bent and display narrow rims of actinolite and minor chlorite along the tails.

The discrete shear zones are locally associated with sulfide and/or oxide mineral concentrations (Figs. 36 and 41). A 2-mm-wide shear zone in Section 153-922A-3R-1 (Piece 1) overprints the shape preferred orientation of plagioclase in the troctolite and contains fine-grained chlorite and oxide minerals. In Piece 2 in the same section a medium-grained oxide gabbro is weakly deformed with a crystal-plastic fabric deflected into a 2- to 3-mm-wide shear zone. Downsection in Piece 4A, a steeply dipping (75°–80°), 1- to 2-cm-wide curviplanar shear zone cuts across the troctolite and contains oxide minerals. In Section 153-922B-2R-1, a 5- to 15-mm-wide steeply dipping (60°) shear zone in the upper portion of Piece 2A separates anorthositic, deformed olivine gabbro from relatively undeformed olivine gabbro below and contains a small patch of oxide, sulfide minerals, and apatite.

Microscopic observations in rocks from the discrete shear zones show strongly developed, multimodal grain-size distributions (Fig. 42). Plagioclase grains commonly have cores with patchy extinction and mantles with "necklaces" of neoblasts. Pyroxene porphyroclasts are kinked and have neoblasts along their edges, whereas olivine is generally recrystallized into neoblasts with subgrains and irregular sutured boundaries. A steeply dipping shear zone in a gabbronorite in Sample 153-922A-2R-2 (Piece 2, 106–111 cm) shows a fine-grained (200–500 μm) matrix with relict euhedral orthopyroxene (~5 mm) and anhedral plagioclase grains. Subhedral plagioclase porphyroclasts (~1 mm) display a moderately developed preferred orientation of mechanical twins. Olivine neoblasts form elongated clusters or are scattered in the matrix. A coarse-grained olivine gabbro in Sample 153-922B-4R-1 (Piece 6, 59–63 cm) contains a narrow shear zone in which pyroxene is replaced by green-brown amphibole aligned parallel to the foliation.

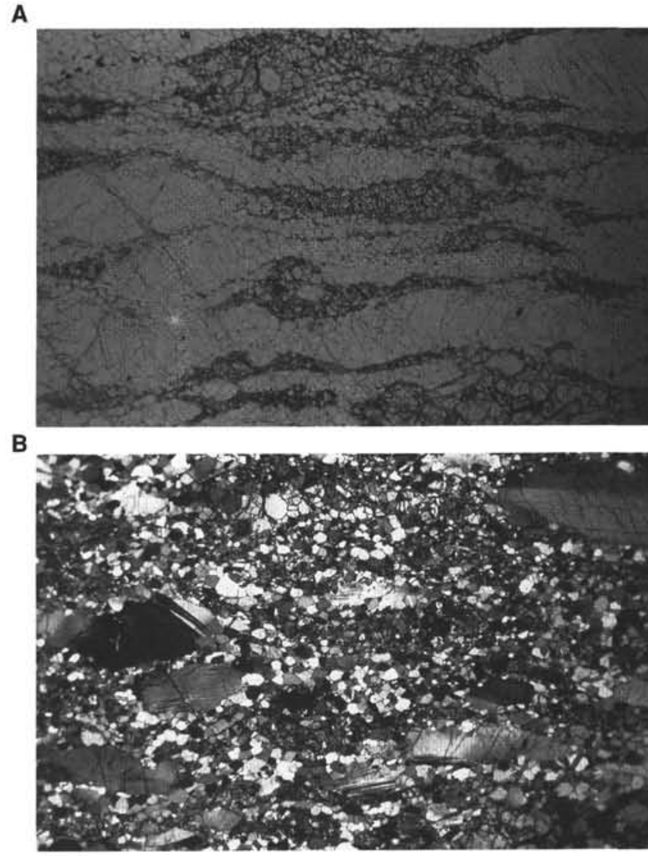

Figure 42. Photomicrographs of Sample 153-922B-1W-1 (Piece 8, 105–112 cm). **A.** Plane polarized light. **B.** Crossed polarized light. Field length is 9 mm. Bimodal grain-size distribution in plagioclase. Porphyroclasts are 1–5 mm and contain twins aligned parallel to mesoscopic foliation. Olivine is strongly recrystallized, and one olivine shows porphyroclast asymmetric tails that indicate a sinistral sense of shearing.

Brittle Features

Faults and Joints

Mesoscopic faults and joints are developed only locally in the rocks recovered from Site 922. There are a few locations in Hole 922B where rubble fragments have been recovered in pieces adjacent to zones of strong microfracturing. For example, in Section 153-922B-1W-2, strong distributed microfractures occur at the base of Piece 2. Fragments of rubble in Piece 3 of this section may represent a very poorly recovered fault zone immediately below Piece 2. Similarly, in Section 153-922B-4R-3, distributed fractures in Piece 6 are followed by pieces of rubble with dense fracture arrays, and in Section 153-922B-4R-2 the three small pieces (Pieces 3, 4, and 5) have a high microfracture density.

Hole 922B also contains a few veins that preserve evidence for minor fault displacements. One measured offset suggests a separation of about 2.5 cm across a 7-mm-thick chlorite + actinolite vein (Section 153-922B-3R-2, Piece 3A). An actinolite-bearing 3-mm-wide fault occurs in Section 153-922B-2R-1 (Piece 5) and truncates two chlorite + actinolite veins.

A few joints, coated with clays, chlorite, and oxide minerals, are also found in Hole 922B core (e.g., Sections 153-922B-1W-1, Pieces 1 and 2, -2R-1, and -4R-2, Pieces 1, 2, and 6). The dominant joint sets generally dip steeply (e.g., Section 2R-1, Piece 1A).

Distributed Microfractures

Structures resulting from brittle deformation at Site 922 include distributed microfractures and fracture networks, discrete veins and vein arrays, rare faults, and some joints. Much of the alteration in Hole 922A is controlled by closely spaced fracture networks with variable degrees of preferred fracture orientation. Microfracturing is particularly distinct in some plagioclase grains where light green chlorite and white clay mineral aggregates have crystallized (e.g., Section 153-922A-1R-1, Pieces 5, 7, and 8); plagioclase also has a brown color when microfractures are filled with smectite. Zones of microfracturing (1 to 10 cm wide) are localized within core pieces. For example, in Section 153-922A-2R-1 a high density of chlorite veins appears at the top of Piece 6, and vein "swarms" occur at the base of Section 153-922A-2R-4 (Piece 1). Some of the most extensive microfracturing occurs in Section 153-922A-3R-1 where all pieces are crosscut by a network of microfractures filled by chlorite and amphibole at a high angle to the foliation. In this section, irregular arrays of chlorite and amphibole veins (<1 mm wide) cut the troctolite and the compositional and textural banding (Section 153-922A-3R-1, Pieces 3 and 4).

Hole 922B displays similar types of microfracturing and associated alteration characteristics to those in Hole 922A. Alteration in some pieces has localized along microfracture arrays. For example, Section 153-922B-1W-1 (Piece 4) contains a diffuse band (12 mm wide) that is composed of concentrated hairline veins of actinolite and chlorite. These tiny veins have altered the bounding wall rock to secondary plagioclase, actinolite, and chlorite. A similar type of veining occurs in Piece 10 in the same section. Olivine is also affected by dense microfracture arrays that are commonly filled with clay minerals (e.g., Section 153-922B-1W-2, Piece 2).

In several locations, there is also a spatial association between microfracture arrays and crystal-plastic shear zones, where a penetrative foliation, defined by shape preferred orientation of plagioclase and pyroxene is overprinted by distributed fractures. In these cases, the microfractures commonly have a weak preferred alignment subparallel to the shape preferred orientation of minerals (Section 153-922A-2R-5, Piece 2). The microfracture orientations contrast with some discrete arrays of chlorite and actinolite veins that dip in the opposite direction to penetrative foliations. For example, in Section 153-922A-2R-2, arrays of chlorite veins dip about 45°, perpendicular to the foliation. These veins, however, are oriented parallel to an oxide mineral–bearing shear zone at the top of Piece 2. Similar geometries are seen in Section 153-922A-2R-3. In Section 153-922A-2R-5, the shear zones in Piece 2 are cut by veins of chlorite and actinolite (1 to 4 mm wide). Discrete veins are oriented at a high angle to these zones of microfractures. In some places, microfractures overprint shear zones and are filled with smectite and oxide minerals (e.g., Section 153-922A-2R-6). Core from Hole 922B also exhibits similar overprinting relations to that of Hole 922A, where networks of chlorite and actinolite veins overprint strong crystal-plastic fabrics (e.g., Section 153-922B-2R-1, Piece 3; Fig. 39). Furthermore, dense veining in Hole 922B locally coincides with the occurrence of shear zones (e.g., Section 153-922B-4R-1, Pieces 7 and 8; see the section on veins, this chapter).

In other areas, the alignment of microfractures defines a weakly developed foliation, which forms a penetrative subhorizontal planar fabric that is predominantly due to closely spaced microfractures with coatings of chlorite (e.g., Section 153-922A-2R-5, Piece 1). Similar zones are present in Section 153-922A-2R-2 where 20-mm-thick bands contain subhorizontal microveins within a 12 cm length.

Veins

The magmatic and crystal-plastic deformation fabrics are overprinted by several generations of veins and vein arrays. Some well-developed conjugate sets of vein arrays and vein networks result in extensive alteration in the host rock. Most individual veins and vein arrays appear to be pure-extensional fractures whereas other veins, particularly those spatially associated with shear zones, show evidence for minor shear displacements, as suggested by fibers of filling minerals that are oblique to the vein walls and by apparent offset of mineral grains and other features along and across the vein planes.

In general, the gabbroic rocks from both Site 922 holes contain similar vein types and generations. These vein types include chlorite + actinolite, felsic veins commonly filled with plagioclase + actinolite + iron oxides and, epidote + plagioclase + prehnite ± quartz-bearing veins. The relative timing of different vein generations is discussed below.

Actinolite + Chlorite Veins

These veins are the most common vein type in the recovered gabbroic rocks. These generally occur as discrete veins in all rock types ranging from olivine gabbro, gabbronorite to troctolite, and they commonly have planar geometry with sharp to diffuse boundaries with the host rock (Fig. 3). There are also anastomosing veinlets and veins in conjugate sets and vein networks. Some undeformed actinolite + chlorite veins are present within discrete shear zones (Sections 153-922B-2R-2, Piece 5, -4R-1, Piece 8, and -3R-1, Piece 3), whereas others are found to cut across the shear zones at small to high angles (Fig. 41). The actinolite + chlorite vein in Section 153-922A-2R-5 (Piece 2A), for instance, is 2 mm wide and 160 mm long, with three en-echelon strands that dip steeply (74°) on the cut surface of the core, and the vein cuts the gently dipping shear zone at a high angle. One actinolite + chlorite vein (Section 153-922B-4R-2, Piece 6) occurs as a discrete 10-mm-wide vein with fine-grained apatite near its margins. It is bounded on each side by a 1- to 2-mm-wide chalky plagioclase zone. It dips gently (12°) and is cut by a later 1-mm-wide chlorite + actinolite vein. The host rock along the margins of this vein displays extensive alteration.

Some chlorite + actinolite veins are also spatially associated with shear zones that locally correspond to lithological and/or textural boundaries in the host rock (e.g., Sections 153-922A-3R-1, Piece 4, and -922B-2R-3, Piece 1). Extensive alteration of the bounding wall rock to secondary plagioclase, actinolite, and chlorite is observed around a 12-mm-wide zone along chlorite + actinolite hairline veinlets in Section 153-922B-1W-1 (Piece 4). In conjugate sets, it is usually difficult to establish the crosscutting relations between subhorizontal and subvertical vein generations; in one particular case (Section 153-922A-1R-1, Piece 4A), however, subhorizontal veins with overlapping segments consistently intersect and cut across the subvertical ones. The chlorite + actinolite veins are commonly highly oblique to the shape preferred orientation of the clinopyroxene grains in and near the shear zones (Sections 153-922A-3R-1, Piece 3A, -2R-5, Piece 1, and -2R-2, Piece 1). They appear to cut across magmatic veins and shear zones (e.g., Section 153-922B-1W-1, Piece 7; Fig. 43) but are cut by epidote-bearing composite veins in other sections (e.g., Section 153-922A-2R-3, Piece 3).

Felsic Veins

In general, felsic veins have either subhorizontal (2°–20°) or subvertical (72°–80°) dip angles with only a small number of veins dipping moderately (35° and 52°). They are interpreted as magmatic features (see "Igneous Petrology," this chapter; Figs. 30 and 43). These veins mainly consist of plagioclase + actinolite ± clinopyroxene ± chlorite ± zeolite with actinolite in the core of the veins. They commonly have alteration halos consisting of chalky white plagioclase and fine-grained chlorite (e.g., Section 153-922B-4R-3, Pieces 1 and 2). One vein that is included in this group because of its likely magmatic origin consists of clinopyroxene + brown amphibole + apatite and cuts across the metagabbro of Section 153-922B-4R-1 (Pieces 8A and 8B; Fig. 1). The minerals in this vein are in turn cut at a high angle by subparallel, intra-vein chlorite + actinolite veins.

Felsic veins commonly have sharp boundaries with the host rock and are locally sheared internally and/or along their margins. Some

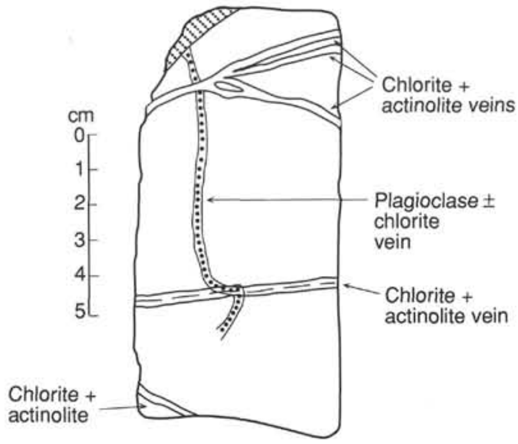

Figure 43. Line drawing depicting the crosscutting relations of veins in the olivine gabbro of Unit 1 in Sample 153-922B-1W-1 (Piece 7, 92–104 cm). Gently dipping and branching chlorite + actinolite veins cut across a subvertical felsic vein composed mainly of plagioclase and chlorite. This felsic vein is also cut by and sheared along a gently dipping (~20°), 3-mm-wide chlorite + actinolite vein; sense of shearing is top to the left.

veins display evidence of shear displacements along their boundaries and of grain-size reduction in the wall rock (e.g., Section 153-922A-2R-2, Piece 1; Fig. 30). Other veins contain asymmetric clinopyroxene grains suggesting normal shear sense. The 8- to 10-mm-wide felsic vein in Section 153-922B-3R-1 (Pieces 3 and 4), for example, cuts across and separates a chlorite + actinolite vein by as much as 12 mm. Chlorite + actinolite veins generally cut felsic veins (Fig. 43). Detailed microscopic investigations of these veins and their relative timing of development await shore-based studies.

Epidote-bearing Veins

These veins are scarce throughout the cores in both holes, and they occur as thin (1–2 mm), individual veins along which the rocks are commonly cut by later fractures and/or joints. They typically contain plagioclase, quartz, prehnite, or magnetite, in addition to epidote, and in some cases clay-mineral-rich assemblages occur along their traces (e.g., Section 153-922B-2R-1, Pieces 1A and 1B). They generally have subvertical (70° to 87°) dips and cut across shear zones at high angles (e.g., Sections 153-922B-2R-1, Pieces 1A and 1B, and -922A-2R-4, Piece 2B). One epidote-bearing vein cuts an actinolite + chlorite vein at an oblique angle (Section 153-922A-2R-3, Piece 3), suggesting that the epidote-bearing composite vein development might have postdated other vein generations documented at Site 922.

Downhole Variations

Hole 922A contains two lithologic units consisting of metatroctolite (Unit 1; Section 1R-1, Piece 1, to 2R-3, Piece 3) and troctolite and olivine gabbro (Unit 2; Section 2R-1, Piece 4, through 3R-1, Piece 4). These rocks are mainly medium- to coarse-grained and show varying degrees of alteration and metamorphism overprinting the early structures and textures (see "Metamorphic Petrology," this chapter). The upper part of Unit 1 displays a faint subhorizontal shape preferred orientation defined by inequant plagioclase grains and a background texture developed by extensive microfracturing and associated alteration. Conjugate sets of chlorite + actinolite veins are common in this core. Unit 2 starting with Section 2R-1 shows well-preserved compositional and/or textural boundaries (Fig. 6; also see "Igneous Petrology," this chapter) that are locally sheared and/or veined. Discrete shear zones are widespread throughout the core, and both the shear zones and compositional and textural boundaries are cut at oblique to high angles by chlorite + actinolite veins. Oxide gabbro and/or oxide minerals occur near and within the shear zones in this core. The top of Core 3R consists of troctolite and olivine gabbro belonging to Unit 2 and show extensive alteration around a chlorite + actinolite vein network. The poikilitic olivine gabbro in the rest of the core displays subhorizontal plagioclase-rich layers and magmatic veins with less developed discrete shear zones. Chlorite + actinolite veins are the most common types crossing various structures.

Hole 922B contains troctolite and olivine gabbro on top (Unit 1; Section 1W-1, Piece 1, to 2R-3, Piece 4), and poikilitic olivine gabbro making up the remainder of the core (Unit 2; Section 3R-1, Piece 1, through 5R-1, Piece 1). Unit 1, near the top of Core 1W, displays steeply dipping compositional layers with a faint olivine shape preferred orientation (Fig. 6). Discrete shear zones with anastomosing branches are widespread throughout the core and nearly all shear zones dip moderately. Microfractures, distributed fractures, and network veins are locally well developed in the rock, and the occurrence of rubble fragments coincides with these zones of intense fracturing in the core. Core 2R includes minor intrusions of oxide gabbro and anorthositic gabbro into the host troctolite-olivine gabbro rock of Unit 1, and the intrusive contacts are locally sheared (Section 2R-1, Piece 2). Discrete shear zones with varying dip angles and directions are common throughout the core. The vertical contact between the olivine gabbronorite and olivine gabbro of Unit 1 in Section 2R-2 (Piece 7) (Fig. 15) is both sheared and veined obscuring the nature of the primary relations between these two lithologies. Networks and conjugate sets of chlorite veins exist in the upper and lower parts of Section 2R-2. Unit 2 consists mainly of a poikilitic olivine gabbro and shows evidence of less shearing and more microfracturing in Core 3R compared to the earlier cores in this hole and includes an increased number of magmatic veins and anorthositic layers. Core 4R starts on top with an aphyric diabase and continues with poikilitic olivine gabbro of Unit 2 with no shape preferred orientation fabric. Felsic veins and pegmatitic gabbros are common in this part of Unit 2. The small number of discrete shear zones have evidence for normal shear sense. Core 5R includes a small piece of olivine gabbro with widespread chlorite veins and no shape preferred orientation.

In general, all of Hole 922A can be considered as a single structural domain characterized by heterogeneous crystal-plastic deformation (Fig. 44) and locally well-developed distributed microfractures and fractures. Microstructures of rocks from Site 922 are described briefly below. For more detailed descriptions of various textural types see the "Structural Geology" section and Figure 17 in the "Explanatory Notes" chapter (this volume). Textural "groups" in parentheses refer to Figure 17 of the "Explanatory Notes" chapter. There is no evidence for discrete cataclastic zones in Hole 922A rocks. The existing igneous textures include isotropic and foliated fabrics (textural Group 1), and they are subequally represented and distributed throughout the cores from this site (Table 6). Crystal-plastic deformation is partitioned into discrete shear zones ranging from a millimeter to a decimeter wide. Grain-size distribution and textural characteristics of the rocks within these shear zones are typical of the porphyroclastic textures seen in gabbros elsewhere (textural Group 4). However, it is important to note that thin sections of shear zone rocks for shipboard studies were limited, and the downhole distribution of microstructural groups as shown in Table 6 may simply be an artifact of sampling bias.

Hole 922B has two structural domains based on structural style (Fig. 44). The upper part of core from Hole 922B in igneous Unit 1 (Cores 1R and 2R) contains numerous discrete shear zones and some distributed fractures. Rubble fragments are very common. The lower part of core from this hole, corresponding broadly with Unit 2 (Cores 3R through 5R) shows a limited number of shear zones and widespread closely spaced microfractures and vein arrays. Felsic veins are also more common. Primary igneous textures are variably preserved in the cores; the subhorizontal magmatic shape preferred orientation (textural Group 2) is common in Cores 2R (Unit 1) and 4R (Unit 2),

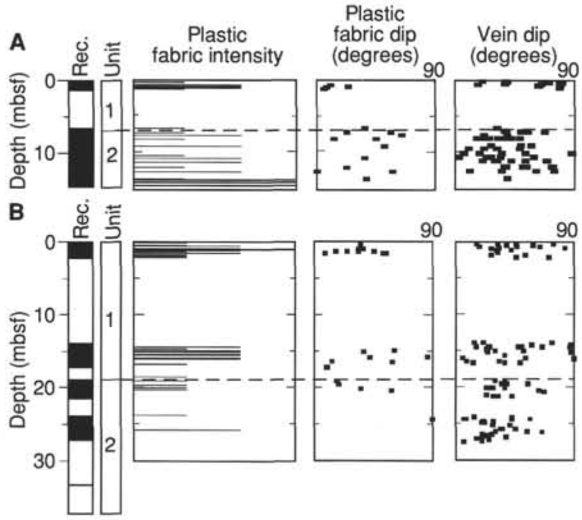

Figure 44. Summary diagram of core recovery, igneous units, crystal-plastic fabric dip and intensity (3 intensity levels are shown; Fig. 13, "Explanatory Notes," this volume), and vein dip vs. depth for (**A**) Holes 922A and (**B**) 922B.

whereas the isotropic magmatic texture (textural Group 1) is well represented in Core 3R (Unit 2). Crystal-plastic deformation microstructures (textural Group 4) are conspicuously less common downhole (Table 6).

Figure 44 shows the distribution of fabric intensity, dips of different fabric elements, and dips of all vein generations with depth in both holes. The intensity scales for different fabric elements and veins are given in the "Explanatory Notes" chapter, this volume. Whereas magmatic and crystal-plastic deformation intensities increase with depth in rock from Hole 922A, there is an apparent decrease in intensity of related structures in rock from Hole 922B. Dip angles of different fabric elements do not change significantly with depth in either hole, but shear zones tend to have lower dip angles in core from near the top of Hole 922A. Veins do not show any systematic pattern in their dip angles with depth.

Discussion

Lithological units recovered in Holes 922A and 922B are similar to those recovered from Site 921 holes. However, some of the structures observed and documented in Site 921 rocks are absent or less well-developed in the rocks from Site 922. In both Holes 921B and 921C a weakly to moderately lineated gabbro occurs immediately below a relatively undeformed diabase. The lineation in these rocks is defined by shape preferred orientation of elongated clinopyroxene grains and plunges gently to steeply. In the case of the lineated gabbro in Hole 921B this structure seems to persist in at least two cores downhole (from Core 2R through the first five pieces of Section 4R-1). In contrast, elongation of clinopyroxene and olivine mainly is limited to the vicinity of discrete shear zones in Site 922 gabbroic rocks; the rocks away from these shear zones are devoid of such lineations. The rock unit immediately below the only recovered diabase unit in Section 153-922B-4R-1 (Piece 1) consists of a medium-grained olivine gabbro and does not display any lineation or a penetrative shape preferred orientation.

The crystal-plastic fabric in gabbroic rocks from Holes 921B and 921C is locally overprinted by cataclastic zones, which show intense grain-size reduction (gouge) and microvein development. Less intense and thinner cataclastic zones were also encountered in Pieces 5 and 6 of Section 153-921D-5R-1. These kinds of brittle deformation features do not exist in Site 922 gabbros.

A vein chronology has been established based on scarce crosscutting relations in core pieces which suggest that vein types may become relatively younger in the descending order of felsic, chlorite + actinolite, and epidote-bearing veins. Some of these crosscutting relations are somewhat ambiguous. The widespread occurrence of chlorite + actinolite veins within and along the discrete shear zones indicates reactivation of these zones during the subsequent brittle deformation. The mineralogy of vein-filling material and inferred vein chronology suggest the circulation of hydrothermal fluids with progressively lower temperatures through time (see "Metamorphic Petrology," this chapter).

Table 6. Classification of microstructures in gabbroic rocks from Holes 922A and 922B.

Thin-section location (cm)	Textural group
153-922A-	
1R-1, 9	6/1a
1R-1, 130	Weak 6 on 4
2R-1, 122	2a
2R-1, 125	2b
2R-2, 38	2b
2R-2, 106	4a
2R-3, 15	1a
2R-4, 33	1a
2R-5, 2	1a
2R-5, 5	1b
2R-5, 30	1a
2R-5, 50	1a
3R-1, 104	6/2a
153-922B-	
1W-1, 37	1b
1W-1, 51	1b
1W-1, 66	4a/1b/1a
1W-1, 105	4 on 2
1W-1, 134	5/4 b
1W-2, 41	4a
1W-2, 51	5a / 4a
2R-1, 12	1a
2R-1, 27	4a
2R-1, 128	1b/4 a
2R-2, 20	4a
2R-2, 45	5a/4a
2R-2, 87	5a/4a
3R-1, 44	1a
3R-2, 0	Weak 6 on 1a
3R-2, 54	2a
4R-1, 20	Weak 6 on 1a
4R-1, 59	4a on 1a
4R-2, 16	5b
4R-3, 0	Strong 6/1a
4R-3, 70	6 on 1a

Notes: The sections are classified based on criteria summarized in "Structural Geology" section of "Explanatory Notes," and Figure 17 of that chapter. Numbers separated by slashes indicate more than one textural group is present. "On" indicates a textural group that overprints an earlier one.

PALEOMAGNETISM

Introduction

Paleomagnetic measurements were made on the archive half-rounds and 21 minicores taken from Holes 922A and 922B. The remanent magnetization of these gabbro samples appears to be generally less complex than Site 921 gabbros (which come from 2 km north of Site 922). Although both normal and reversed polarity samples are present, the majority of the core recovered is apparently of normal polarity. The presence of reversed polarity magnetizations at Site 922 is broadly compatible with the available sea surface magnetic anomaly data (Schulz et al., 1989), which suggest an age of approximately 1 Ma for this portion of the median valley wall.

Whole-core Measurements

Whole-core susceptibility was measured at 3 cm spacing for all core sections from Holes 922A and 922B. Susceptibilities were typically 10^{-2} SI with rare peaks (up to 0.1 SI) that are generally attributable to oxide gabbros. Metatroctolite at the top of Hole 922A and metagabbro at the base of Hole 922B have much lower susceptibilities (<0.001 SI).

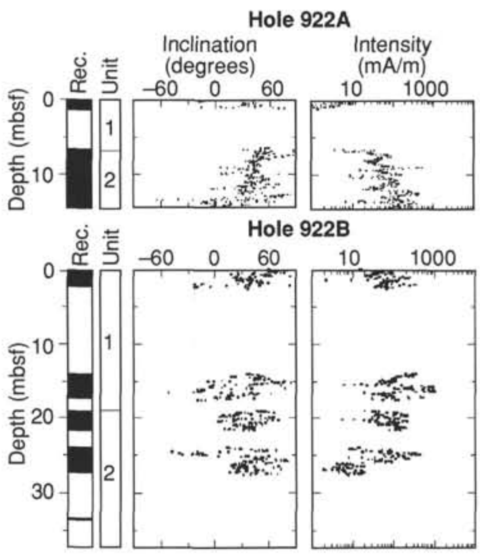

Figure 45. Downhole remanence data for archive half-cores from Holes 922A and 922B after demagnetization at 20 mT. Inclinations are predominantly positive and near the expected axial dipole inclination (41°) at the site. The lower intensities at the base of Hole 922B and the top of Hole 922A are associated with intervals of metagabbro and metatroctolite.

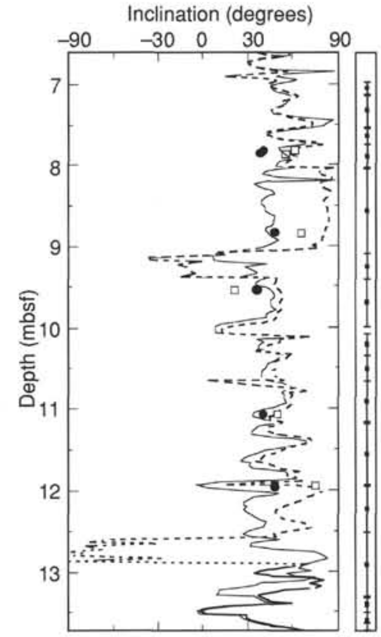

Figure 46. Correlation of archive half-core 10 mT (dashed line) and 20 mT (solid line) inclination data with discrete sample results from Core 153-922A-2R. Discrete sample NRM (squares) and high-stability magnetization components (filled circles) agree well with the archive half-core data. Continuous core pieces longer than 15 cm are shown in the column at the right.

Archive half-cores from Site 922 were measured at an interval of 3 cm with the pass-through cryogenic magnetometer. Reliable natural remanent magnetization (NRM) data were obtained for only 25% of the cores, which had intensities ranging from approximately 0.005 to 3.0 A/m. The lower end of this range corresponds to the highly altered gabbros and troctolites at the base of Hole 922B and top of Hole 922A. The remaining sections, many containing oxide gabbros, were too highly magnetized to measure. NRM inclinations were often steep (60°–80°). Comparison with discrete sample data suggests that these initial steep inclinations represent a drilling-induced remanence contamination of the NRM, as noted for gabbros from Site 921. Demagnetization of the archive half-cores to 20 mT yields predominantly positive inclinations that are similar (~40°) to the expected dipole inclination (41°) at the site (Fig. 45). The results from the archive half-cores are corroborated by the inclinations determined from discrete sample demagnetization (Fig. 46).

Discrete Sample Measurements

Remanent magnetization and initial susceptibility were determined for 21 discrete samples from Holes 922A and 922B (Table 7). NRM intensities of the 21 samples have a geometric mean of 0.62 A/m ± 0.8 log units and an arithmetic mean of 1.45 A/m ± 1.35. The mean NRM intensity is similar to that of the gabbros recovered at Site 921 (1.1 A/m). Shipboard sampling was primarily restricted to olivine gabbros, troctolites, and metagabbros, with no samples from shear zones or strongly veined regions. Volume susceptibility for the discrete samples from Site 922 range from 4×10^{-2} to 3×10^{-4} (SI units), representing the range from olivine gabbros to metagabbros respectively. The corresponding mean Koenigsberger ratio (the ratio of the remanent to induced magnetization, Q) for the gabbros is 3.55 ± 0.2 log units (arithmetic mean = 3.95).

Demagnetization of discrete samples from Site 922 indicates the predominance of normal polarity magnetizations, with variable degrees of steeply oriented, drilling-induced overprints (Fig. 47). This drilling-related overprint is readily removed by AF demagnetization at 10 mT and is less distinct in thermally demagnetized samples (Fig. 47), possibly reflecting blocking temperatures that significantly overlap that of the higher stability magnetization component. The majority of samples are of normal polarity, with a mean inclination of 42.2° (alpha = 3.6°, n = 15; McFadden and Reid, 1982) similar to the expected dipole inclination (41°). However, two samples have high-stability components of shallow negative inclinations. These negative inclinations may reflect either tectonic rotations or the incomplete isolation of reversed polarity characteristic remanence as a result of a significant normal polarity low-stability component (Fig. 47). The maximum unblocking temperatures (near 575°–600°C) in thermally demagnetized samples (e.g., Fig. 47) are compatible with magnetite as the dominant carrier of remanence.

Approximately one third of the samples from Site 922 have demagnetization behavior that suggests that the characteristic magnetization has not been isolated. For example, Sample 153-922A-2R-1, 122–125 cm, apparently decays toward the origin (Fig. 48A) although the final demagnetization steps when analyzed in detail clearly do not trend toward the origin (Fig. 48B). Steps above 30 mT represent the vector average of two individual measurements after demagnetization along opposite axial directions. The similarity of these duplicate measurements (which deviate by less than 15°) effectively rules out a spurious magnetization at these demagnetization steps. The directions at the highest demagnetization levels lie along a great circle (Fig. 48C), suggesting that an additional reversed polarity component may be present.

Anisotropy of magnetic susceptibility was also determined for the majority of the discrete samples (Table 7). The degree of anisotropy ($P = K_1/K_3$ where K_1 and K_3 are the maximum and minimum principal susceptibility axes, respectively) is comparable to that of gabbros from Site 921 (Fig. 49). There is no strong tendency toward either oblate or prolate magnetic fabrics, and no simple correlation with rock type exists. However, one strongly prolate sample (Sample 153-922B-3R-1, 47–50 cm) is a gneissic gabbro.

Discussion of Paleomagnetic Results

Site 922 was drilled at a location offset ~2 km south of Site 921. Although the two sites are the same distance from the ridge axis, Site 921 gabbros are predominantly of reversed polarity whereas Site 922 are primarily normally magnetized. The presence of well-defined negative inclination components in samples from both sites indicates

Table 7. Summary of magnetic properties of discrete samples from Site 922.

Core, section, interval (cm)	Piece	Rock name	Depth (mbsf)	NRM Dec.	NRM Inc.	NRM Int. (A/m)	K (SI)	AMS P	AMS L	AMS F
153-922A-										
1R-1, 130–133	9	Metatroctolite	01.30	302.1	66.7	0.018	0.00030	—	—	—
2R-1, 122–125	8	Troctolite	07.82	235.5	61.8	0.570	0.00348	1.077	1.067	1.010
2R-1, 126–129	8	Troctolite	07.86	225.6	54.7	0.471	0.00297	1.138	1.050	1.084
2R-2, 81–84	1C	Troctolite	08.83	321.8	66.4			1.087	1.026	1.059
2R-3, 15–18	1A	Troctolite	09.54	343.5	22.8	5.204	0.03712	1.203	1.106	1.088
2R-4, 43–46	1	Olivine gabbro	11.08	168.5	50.2			1.101	1.058	1.041
2R-5, 2–5	1B	Olivine gabbro	11.96	283.4	73.9	0.829	0.00433	1.086	1.056	1.028
2R-5, 6–9	1B	Olivine gabbro	12.00	311.1	71.0	2.751	0.01421	1.185	1.165	1.017
153-922B-										
1W-1, 37–40	2B	Troctolite	00.37	158.8	53.0	0.644	0.00556	1.151	1.110	1.037
1W-2, 41–44	2	Olivine gabbro	01.79	194.9	58.6	2.051	0.02698	1.173	1.049	1.118
2R-1, 76–79	1C	Troctolite	14.76	122.6	63.1	2.913	0.01736	1.131	1.106	1.022
2R-2, 20–23	3	Olivine gabbronorite	15.69	183.4	85.2	3.442	0.04732	1.179	1.047	1.125
2R-3, 14–17	1	Olivine gabbro	16.90	295.4	56.4	0.398	0.00272	1.337	1.138	1.175
3R-1, 44–47	3	Olivine gabbro	19.44	166.5	74.3	1.919	0.02956	1.077	1.065	1.012
3R-1, 47–50	3	Olivine gabbro	19.47	173.4	64.5	1.710	0.01581	1.270	1.204	1.055
3R-2, 49–41	2	Olivine gabbro	20.69	318.1	53.9	2.144	0.01597	1.201	1.183	1.015
4R-1, 43–46	5	Olivine metagabbro	24.43	205.1	71.7	2.188	0.02035	1.158	1.058	1.094
4R-2, 16–20	1A	Olivine metagabbro	25.45	252.5	57.7	0.044	0.00059	—	—	—
4R-2, 19–21	1A	Olivine metagabbro	25.48	258.8	65.6	0.562	0.00629	1.146	1.092	1.050
4R-3, 70–73	4B	Meta gabbro	27.27	1.8	58.2	0.012	0.00034	—	—	—
4R-3, 73–76	4B	Meta gabbro	27.30	2.9	52.8	0.019	0.00039	—	—	—

Note: Table includes volume susceptibility (K), natural remanent magnetization (NRM), magnetic fabric parameters ($P = K_1/K_3$, $L = K_1/K_2$, $F = K_2/K_3$; where K_1, K_2, and K_3 are the maximum, intermediate, and minimum axes of the susceptibility ellipsoid, respectively). Rock names (see "Igneous Petrology," this chapter) are defined for whole piece and may not be descriptive of minicore samples.

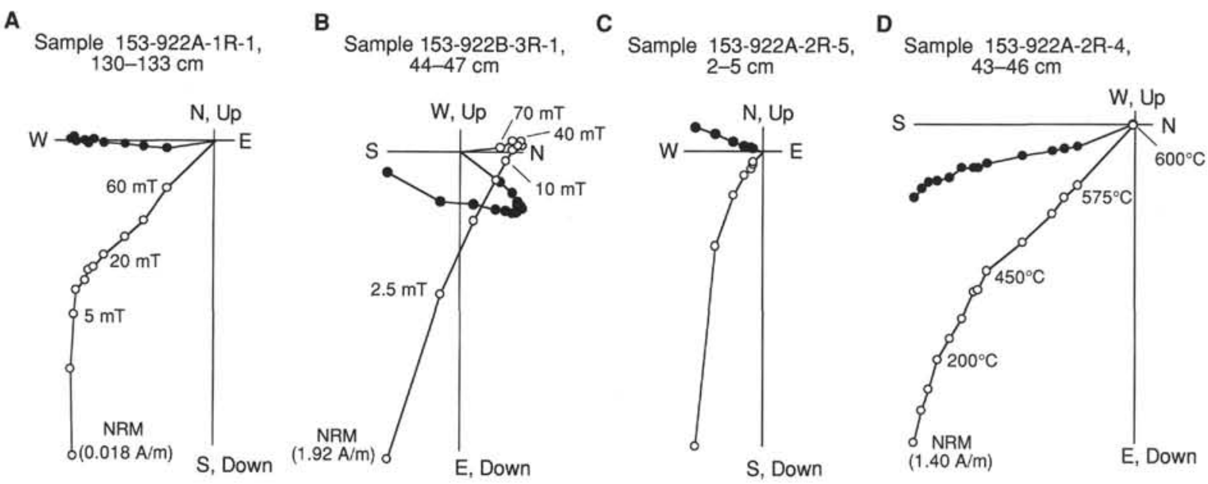

Figure 47. Vector endpoint diagrams for AF and thermal demagnetization of representative discrete samples from Site 922. The majority of samples have a high stability magnetization component of normal polarity (**A, C, D**), with a variable steeply inclined low-stability component probably related to drilling. Samples with a reversed polarity final magnetization direction (**B**) have significant normal polarity overprints. Filled (open) circles are projections of the vector onto the horizontal (vertical) plane. NRM intensity for each sample given in parentheses.

the presence of at least some material older than 0.78 Ma, the age of the last magnetic reversal (Cande and Kent, 1992). There are at least two possible interpretations of the discrepancy in dominant polarity at Sites 921 and 922. The difference in polarity between the two sites may represent a temporal difference, with original magnetizations acquired during normal and reversed polarity intervals. This scenario is plausible given the slow spreading rate and nominal 1 Ma crustal age inferred from sea-surface magnetic anomaly lineations (Schulz et al., 1989). The generally high stability to both AF and thermal demagnetization of some normal polarity samples from Site 922 (e.g., Fig. 47) strongly supports their interpretation as an original normal polarity remanence. Alternatively, samples with apparent normal polarity from the two sites may reflect the inability to adequately isolate an original reversed polarity magnetization. Many samples from Sites 921 and 922 exhibit demagnetization behavior in which the individual steps lie along great circle paths, consistent with the presence of a higher stability, reversed polarity component (Fig. 48). The failure to isolate a final characteristic magnetization direction in these samples demonstrates the viability of low-stability normal polarity overprints in generating apparent normal polarity directions. Distinction between these two alternative interpretations is not possible with the available shipboard data. The origin of such intimately associated normal and reversed polarity intervals will be the subject of shore-based studies.

PHYSICAL PROPERTIES

Introduction

Nineteen minicore samples were analyzed for horizontal compressional wave velocity (V_p), resistivity, and a determination of index properties (bulk density, grain density, water content, porosity,

Table 8. Physical property measurements from Site 922.

Core, section interval (cm)	Piece	Depth (mbsf)	V_p (m/s)	Resistivity (Ωm)	Wet-bulk density (g/cm^3)	Dry-bulk density (g/cm^3)	Grain density (g/cm^3)	Void ratio	Porosity (%)	Water content (%)	Alteration estimate (%)	Rock type	Unit
153-922A-													
1R-1, 130–132	9	1.30	5299	1534	2.834	2.822	2.854	0.0114	1.126	0.408	100	MT	1
2R-1, 122–124	8	7.82	5766	861	2.970	2.967	2.975	0.0027	0.266	0.092	17	T	2
2R-1, 126–128	8	7.86	5536	439	2.904	2.900	2.911	0.0036	0.358	0.126	17	T	2
2R-3, 15–17	1A	9.54	5774	384	3.024	3.021	3.030	0.0030	0.303	0.102	37	T/OG	2
2R-5, 2–4	1A	11.96	5009	188	2.831	2.820	2.852	0.0115	1.135	0.411	47	OG	2
2R-5, 6–8	1A	12.00	5139	741	2.833	2.826	2.845	0.0067	0.666	0.241	17	OG	2
153-922B-													
1W-1, 37–39	1	0.37	6167	192	2.907	2.904	2.913	0.0029	0.291	0.102	54	MT	1
1W-2, 41–43	2	1.79	5441	132	2.950	2.939	2.971	0.0108	1.073	0.373	25	OG	1
2R-1, 76–78	1C	14.76	5462	289	2.860	2.858	2.864	0.0023	0.233	0.083	8	T	1
2R-2, 20–22	3	15.69	5462	687	2.962	2.955	2.978	0.0078	0.774	0.268	21	OGN	1
2R-3, 14–16	1	16.90	5448	241	2.912	2.900	2.936	0.0124	1.225	0.432	44	OG	1
3R-1, 44–46	3	19.44	5805	236	2.875	2.865	2.892	0.0094	0.936	0.334	18	OG	2
3R-1, 47–49	3	19.47	6090	329	2.845	2.840	2.854	0.0047	0.472	0.170	18	OG	2
3R-2, 49–51	2	20.69	6110	925	2.826	2.820	2.836	0.0060	0.596	0.216	16	OG	2
4R-1, 43–45	2	24.43	6026	194	2.820	2.814	2.831	0.0062	0.616	0.224	63	MOG	2
4R-2, 16–18	1A	25.45	5797	163	2.828	2.819	2.846	0.0096	0.955	0.346	68	MOG	2
4R-2, 19–21	1A	25.48	5582	274	2.835	2.825	2.852	0.0096	0.952	0.345	68	MOG	2
4R-3, 70–72	4B	27.27	5823	112	2.837	2.829	2.852	0.0080	0.798	0.288	52	MG	2
4R-3, 73–75	4B	27.30	6082	302	2.829	2.822	2.843	0.0077	0.761	0.276	52	MG	2

Note: MT = metatroctolite, T = troctolite, OG = olivine gabbro, OGN = olivine gabbronorite, MOG = meta-olivine gabbro, MG = metagabbro.

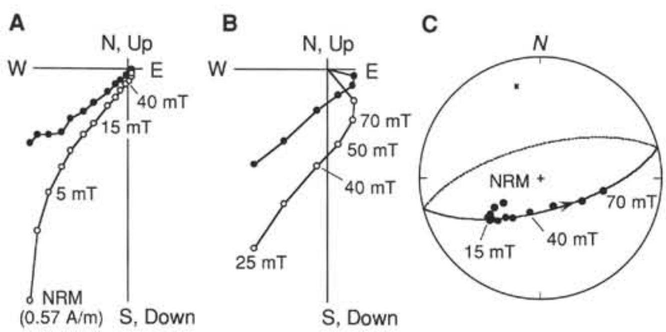

Figure 48. Vector endpoint diagram and equal area plot for Sample 153-922A-2R-1, 122–125 cm. Filled (open) circles in (**A**) and (**B**) are projections of the vector onto the horizontal (vertical) plane. **C.** Following removal of a drilling remanence (by 5 mT), the remanence directions during demagnetization lie along a great circle path consistent with the presence of a higher stability reversed polarity component. Lower hemisphere projections shown by filled circles and solid line.

Table 9. Thermal conductivity measurements from Site 922.

Core, section, interval (cm)	Piece	Depth (mbsf)	Thermal conductivity (W/m°C)	Alteration (%)	Rock type	Unit
153-922A-						
1R-1, 121–139	9	1.21	3.045	(65)*	MT	1
2R-1, 92–113	7	7.52	2.997	(17–24)*	T	2
2R-5, 1–18	1	11.95	2.981	47	OG	2
3R-2, 29–38	2A	13.79	2.773	35	OG	2
153-922B-						
1W-1, 30–43	2B	0.30	2.975	23	MT	1
1W-2, 23–43	2	1.61	2.462	25	OG	1
2R-2, 81–99	8	16.30	2.981	38	OGN	1
3R-2, 34–53	2	20.54	2.810	16	OG	2
4R-1, 32–47	5	24.32	2.910	(41–63)*	MOG	2
4R-3, 69–80	4B	27.26	3.038	(52–56)*	MG	2

Notes: * = not measured in this sample (nearby value). MT = metatroctolite, T = troctolite, OG = olivine gabbro, OGN = olivine gabbronorite, MOG = meta-olivine gabbro, MG = metagabbro.

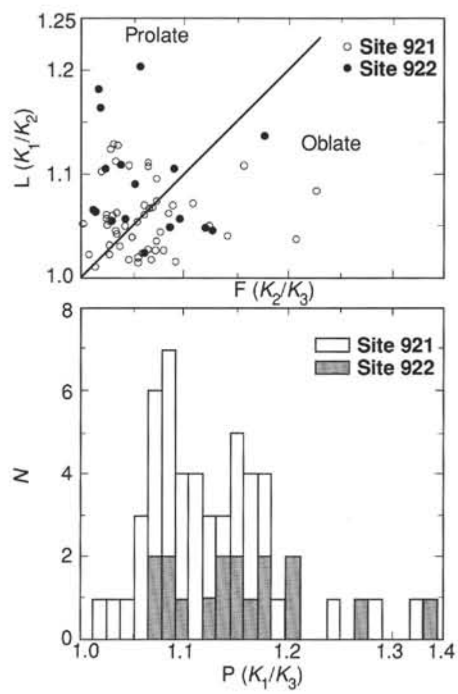

Figure 49. Magnetic fabric of gabbros from Site 922. Magnetic fabric lineation (L) vs. foliation (F) illustrating dominantly triaxial susceptibility ellipsoid shape. Anisotropy degree (P) for Site 922 gabbros.

and dry density; Table 8) at Site 922. Ten half-round archive sections of core were measured for thermal conductivity (Table 9). Bulk whole-core densities were measured using the gamma-ray attenuation porosity evaluator (GRAPE) component of the multisensor track. Descriptions of experimental methods are provided in the "Physical Properties" section of the "Introduction" and "Explanatory Notes" (this volume) and in the "Explanatory Notes" of the Leg 147 *Initial Reports* (Shipboard Scientific Party, 1993).

The following discussion incorporates a summary of index properties for this site, downhole variations in properties of core from Holes 922A and 922B, and consideration of relationships between various physical properties examined at this site and Site 921.

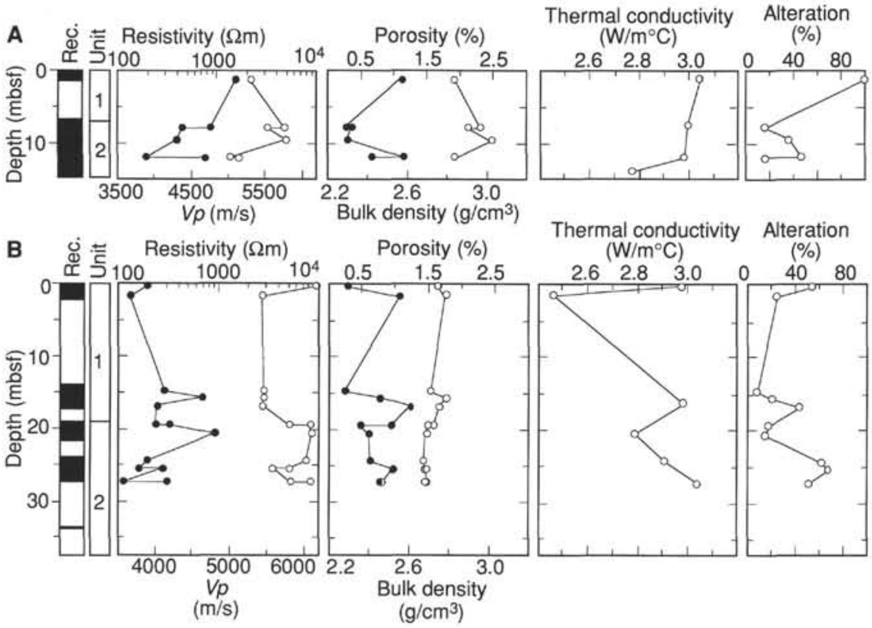

Figure 50. Physical property determinations, core recovery, and unit identification vs. depth for (**A**) Hole 922A and (**B**) Hole 922B. Circles represent locations of physical properties determinations. First panel from left: left curve is resistivity (filled circles), right curve is velocity (open circles). Second panel: left curve is porosity (filled circles), right curve is density (open circles).

GRAPE data have not been incorporated because of limited core recovery (see also "Site 921" chapter, "Physical Properties" section). While the measurements are believed to accurately characterize the samples studied, the coarse grain size and variability inherent in these gabbroic rocks does limit the extent to which results from the analysis of small samples can be extrapolated to larger-scale downhole characteristics at each location (as was also the case for Site 921).

Data

Wet and dry mass and volume measurements were taken for the determination of bulk densities, porosity, water content, and void ratio (with salt volume corrections for a salinity of 0.032) from the predominantly olivine gabbroic rock recovered at Site 922 (Table 8). Bulk densities range from 2.82 to 3.024 g/cm^3 with a median value of 2.878 g/cm^3; grain densities are essentially indistinguishable from bulk densities (2.831 to 2.978 g/cm^3 with a median value of 2.854 g/cm^3), reflecting the relatively low porosity (0.23%–1.23%, median value 0.77%) of these rocks. V_p ranges from 4722 to 5863 m/s in these rocks, with a median value of 5414 m/s. The densities and velocities of these rocks are similar to those observed in metagabbro exposed in fracture zones of the Atlantic (e.g., compilation of Christensen, 1982), and are generally less than values determined from Site 921. The rocks display thermal conductivities ranging from 2.46 to 3.05 W/m°C with a median value of 2.97 W/m°C, somewhat greater than that observed at Site 921 and toward the higher end of the range of values observed by Clark (1966).

Hole 922A

Variations in rock resistivity, V_p, porosity, density, thermal conductivity, and alteration as a function of depth for Hole 922A are shown in Figure 50, with bars indicating core recovery and unit boundaries determined from considerations of primary mineralogy and texture (see also "Igneous Petrology" section, this chapter).

Resistivities of the gabbroic rock recovered from Hole 922A range from about 100 to 10^3 Ωm (Fig. 50). The resistivity of the metatroctolite of Unit 1 is relatively high (1543 Ωm) compared to that measured in the troctolite and olivine gabbro of Unit 2 (188–861 Ωm). The resistivity low observed at nearly 12 mbsf (Unit 2) corresponds to the relatively altered Sample 153-922A-2R-5 (Piece 1A, 2–4 cm).

V_p (Fig. 50) is observed to be rather low (about 5300 m/s) in the metatroctolite of Unit 1 (see also Table 8) and increases to 5500–5800 m/s in the troctolite of Unit 2. Velocities in the olivine gabbro at about 12 mbsf (Unit 2) are the lowest observed in this site (5000–5100 m/s).

Porosity (Fig. 50) is highest (1.13%) in rock recovered from within Unit 1 at the top of Hole 922A. Porosity at the top of Unit 2 is much lower (about 0.3%) and increases to about 1% near 12 mbsf.

Density variations with depth (Fig. 50) are generally inverse to those described for porosity (above). Higher densities (2.9–3.0 g/cm^3) correspond to the higher velocity, lower porosity material located at 7.8–9.5 mbsf.

Thermal conductivity (Fig. 50) remains relatively constant near 3.0 W/m°C to 12 mbsf (see also Table 9). Olivine gabbro from 13.79 mbsf (Section 153-922A-3R-2, Piece 2A, Unit 2) displays a slightly lower conductivity of 2.77 W/m°C.

Estimates of alteration with depth (corresponding to most of the physical property sample locations) from visual core descriptions also are shown in Figure 50. Alteration is greatest in the metatroctolite (100%) at the top of the hole (Unit 1) and appears moderate (17%–47%) within Unit 2.

Hole 922B

Downhole diagrams of Hole 922B physical properties measurements are shown in Figure 50 with bars indicating core recovery and unit identification. These are plotted at the same scale as the upper series of panels (Hole 922A) for direct comparison of these nearly coincident hole locations.

The moderately altered (about 50%) metatroctolite sampled at the top of Unit 1 in Hole 922B (Sample 153-922B-1W-1, Piece 1, 37–39 cm) shows relatively low resistivity and porosity and comparatively high velocity, thermal conductivity, and alteration. The slight decrease in resistivity and alteration, more dramatic decreases in velocity and thermal conductivity, and modest increases in porosity and bulk density with depth correspond to a lithologic change from troctolite to olivine gabbro near the top of Unit 1. Resistivity ranges from 250 to 700 Ωm in the troctolite, and olivine gabbronorite and olivine gabbro from 14.7 to 19.4 mbsf in Unit 1, whereas velocity and bulk density remain constant at about 5450 m/s and 2.9 g/cm^3, respectively, through this depth interval. Porosity and alteration appear to increase with depth toward the base of Unit 1, with a relative high in

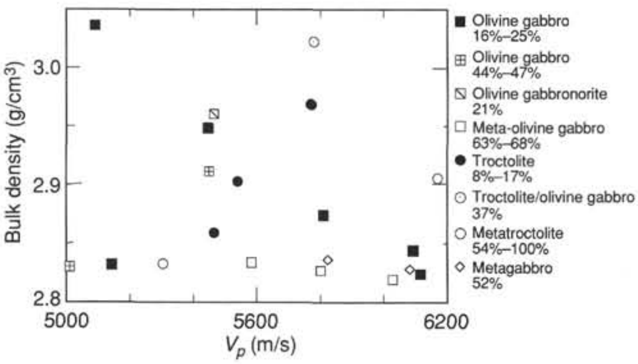

Figure 51. Velocity (V_p) vs. density for rocks recovered at Site 922.

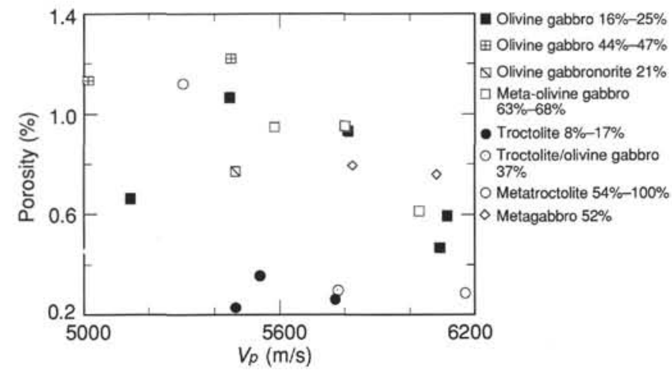

Figure 53. Velocity (V_p) vs. porosity for rocks recovered at Site 922.

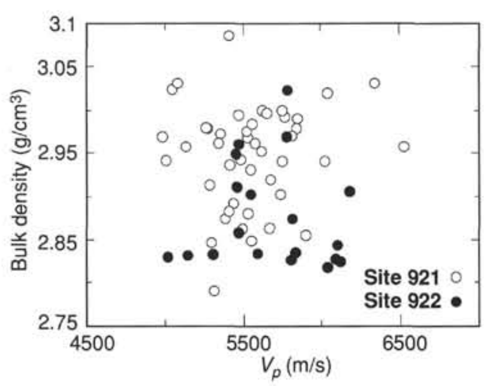

Figure 52. Velocity (V_p) vs. density for rocks recovered at Sites 921 and 922.

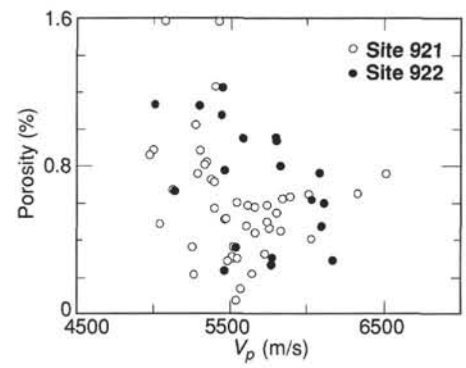

Figure 54. Velocity (V_p) vs. porosity for rocks recovered at Sites 921 and 922.

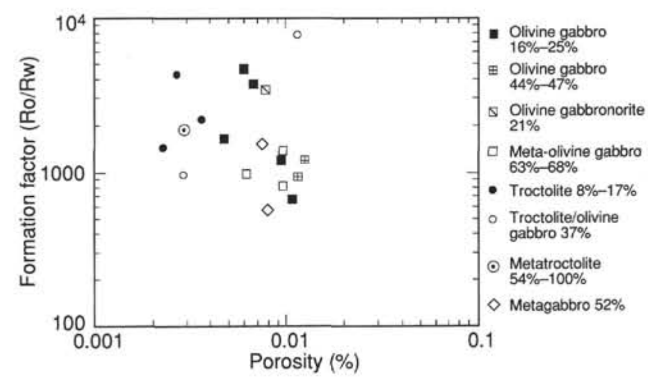

Figure 55. Formation factor (ratio of rock and water resistivity) vs. porosity (corrected for salt) for rocks recovered at Site 922.

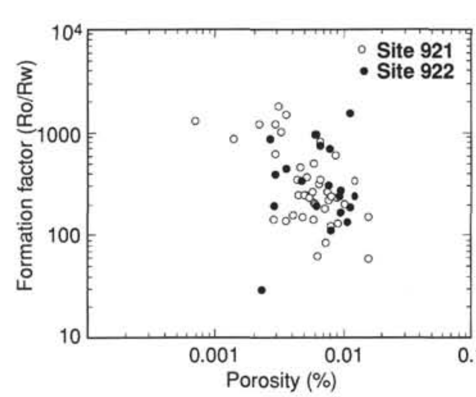

Figure 56. Formation factor (ratio of rock and water resistivity) vs. porosity (corrected for salt) for rocks recovered at Sites 921 and 922.

thermal conductivity occurring in the moderately altered (38%) olivine gabbronorite at 16.3 mbsf.

The olivine gabbro sampled at the top of Unit 2 is a relatively high-velocity (6000 m/s), low-porosity (0.6%) body with a density of 2.7 g/cm^3. A resistivity high is observed in the high-velocity, low-porosity olivine gabbro Sample 153-922B-3R-2 (Piece 2, 49–51 cm) at 20.7 mbsf. The lower thermal conductivity appears to correspond with lower degrees of alteration at this depth. Slight drops in velocity and increases in porosity and resistivity are observed at 25.5 mbsf within the moderately altered (68%) meta-olivine gabbro of Unit 2.

Site 922 Data Analysis

Downhole fluctuations observed in physical properties measurements from this site appear to correlate relatively well with unit boundaries as defined by igneous textures and lithologies. The troctolitic and olivine gabbroic rocks sampled at this site are characterized by velocities typically associated with seismic Layer 2. Fluctuations in velocity do not generally appear to correlate with observed bulk densities (Fig. 51); densities for olivine gabbro, meta-olivine gabbro, and metagabbro fall between 2.8 and 2.9 g/cm^3, with the highest observed densities corresponding to troctolitic lithologies. Densities and velocities observed at this site are similar to those observed in rocks exposed in fracture zones of the Atlantic (e.g., Christensen, 1982). As was the case for Site 921, velocities remain significantly less than were observed in similar density, low- to moderate-porosity gabbroic rocks recovered from Hole 735B in the Southwest Indian Ocean (Robinson, Von Herzen, et al., 1989) or from the Hess Deep area (Gillis, Mével, Allan, et al., 1993a). The predominance of relatively low-density material at this site (even compared to Site 921) is illustrated in Figure 52. With the exception of troctolitic samples, variations in velocity appear to correlate inversely with variations in porosity (Fig. 53). Velocities decrease from 6200 m/s to 5200 m/s as porosity increases from 0.2%

to 1.3%. Observed porosities for Site 922 fall within the range of observed values for Site 921 (Fig. 54), although they generally display higher porosities (except for the troctolitic samples) than were observed at similar velocities in Site 921.

Variations in porosity as a function of formation factor (the ratio of rock and seawater resistivities) for Site 922 are plotted in Figure 55. Samples showing higher degrees of alteration generally show lower resistivities, as has been observed elsewhere (Pezard et al., 1991). Troctolitic samples show relatively high resistivities. The combined array of observations from Sites 921 and 922 are shown in Figure 56. Although there is considerable scatter, the observations appear to cluster in a linear array, suggesting that electrolytic conduction in pore spaces may be a dominant conduction mechanism in many of these rocks (e.g., Pezard et al., 1991).

REFERENCES*

Cande, S.C., and Kent, D.V., 1992. A new geomagnetic polarity time scale for the Late Cretaceous and Cenozoic. *J. Geophys. Res.,* 97:13917–13951.

Christensen, N.I., 1982. Seismic velocities. *In* Carmichael, R.S. (Ed.), *Handbook of Physical Properties of Rocks:* Boca Raton, FL (CRC Press), 2:1–228.

Clark, S.P. (Ed.), 1966. *Handbook of Physical Constants.* Mem.—Geol. Soc. Am., 97.

Gallinatti, B.C., 1984. Initiation and collapse of active circulation in a hydrothermal system at the Mid-Atlantic Ridge, 23°N. *J. Geophys. Res.,* 89:3275–3289.

Gillis, K.M., Mével, C., Allan, J.F., et al., 1993a. *Proc. ODP, Init. Repts.,* 147: College Station, TX, (Ocean Drilling Program).

Gillis, K.M., Thompson, G., and Kelley, D.S., 1993b. A view of the lower crustal component of hydrothermal systems at the Mid-Atlantic Ridge. *J. Geophys. Res.,* 98:19597–19619.

Ito, E., and Anderson, A.T., Jr., 1983. Submarine metamorphism of gabbros from the Mid Cayman Rise: petrographic and mineralogic constraints on hydrothermal processes at slow-spreading ridges. *Contrib. Mineral. Petrol.,* 82:371–388.

Karson, J.A., and Dick, H.J.B., 1983. Tectonics of ridge-transform intersections at the Kane Fracture Zone. *Mar. Geophys. Res.,* 6:51–98.

Kelley, D.S., Gillis, K.M., and Thompson, G., 1993. Fluid evolution in submarine magma-hydrothermal systems at the Mid-Atlantic Ridge. *J. Geophys. Res.,* 98:19579–19596.

Liou, J.G., Kuniyoshi, S., and Ito, K., 1974. Experimental studies of the phase relations between greenschist and amphibolite in a basaltic system. *Am. J. Sci.,* 274:613–632.

Manning, C.E., and Bird, D.K., 1986. Hydrothermal clinopyroxenes of the Skaergaard intrusion. *Contrib. Mineral. Petrol.,* 92:437–447.

Marion, E., 1992. Interactions croûte océanique profonde/eaau de mer dans les gabbros de la zone MARK (Mid-Atlantic Ridge/Kane Fracture Zone) [Thèse de Doctorat]. Univ. de Paris VI.

Marion, E., Mével, C., and Cannat, M., 1991. Evolution of oceanic gabbros from the MARK/Kane fracture intersection massif. *Terra Abstr.,* 3:310.

McFadden, P.L., and Reid, A.B., 1982. Analysis of paleomagnetic inclination data. *Geophys. J. R. Astron. Soc.,* 69:307–319.

Mével, C., and Cannat, M., 1991. Lithospheric stretching and hydrothermal processes in oceanic gabbros from slow-spreading ridges. *In* Peters, T., Nicolas, A., and Coleman, R.G. (Eds.), *Ophiolite Genesis and Evolution of the Oceanic Lithosphere:* Dordrecht (Kluwer), 293–312.

Mével, C., Cannat, M., Gente, P., Marion, E., Auzende, J.-M., and Karson, J.A., 1991. Emplacement of deep crustal and mantle rocks on the west median valley wall of the MARK area (MAR 23°N). *Tectonophysics,* 190:31–53.

Pezard, P.A., Howard, J.J., and Goldberg, D., 1991. Electrical conduction in oceanic gabbros, Hole 735B, Southwest Indian Ridge. *In* Von Herzen, R.P., Robinson, P.T., et al., *Proc. ODP, Sci. Results,* 118: College Station, TX (Ocean Drilling Program), 323–332.

Robinson, P.T., Von Herzen, R., et al., 1989. *Proc. ODP, Init. Repts.,* 118: College Station, TX (Ocean Drilling Program).

Schulz, N.J., Detrick, R.S., and Miller, S.P., 1989. Two and three-dimensional inversions of magnetic anomalies in the MARK area (Mid-Atlantic Ridge, 23°N). *Mar. Geophys. Res.,* 10:41–57.

Shipboard Scientific Party, 1993. Explanatory notes. *In* Gillis, K., Mével, C., Allan, J., et al., *Proc. ODP, Init. Repts.,* 147: College Station, TX (Ocean Drilling Program), 15–42.

Spear, F.S., 1981. An experimental study of hornblende stability and compositional variability in amphibole. *Am. J. Sci.,* 281:697–734.

Stakes, D., Mével, C., Cannat, M., and Chaput, T., 1991. Metamorphic stratigraphy of Hole 735B. *In* Von Herzen, R.P., Robinson, P.T., et al., *Proc. ODP, Sci. Results,* 118: College Station, TX (Ocean Drilling Program), 153–180.

Wadsworth, W.J., 1961.The ultrabasic rocks of southwest Rhum. *Philos. Trans. R. Soc. London B,* 244:21–64.

*Abbreviations for names of organizations and publications in ODP reference lists follow the style given in *Chemical Abstracts Service Source Index* (published by American Chemical Society).

Ms 153IR-104

NOTE: For all sites drilled, core-description forms ("barrel sheets"), and core photographs can be found in Section 3, beginning on page 277. Thin-section data are given in Section 4, beginning on page 665. The CD-ROM (back pocket, this volume) contains the complete set of spreadsheets with piece-by-piece data for all structural features identified and measured. A set of summary spreadsheets that are linked to the igneous and metamorphic spreadsheets are also contained on the CD-ROM. Keys, summary tables, checklists, and thin-section summaries and notes are also archived. Compressed versions of the figures created for this volume, compatible with Macintosh computers, are located in the directories labeled REPT92X in the "Structure" directory. Scanned TIFF images of all the SVCD drawings are archived in the "STRCDRAW" file. Apparent dip data and true strike and dip data for all measurable features are contained in the "STR_DIP" subdirectory. This directory also contains the LinesToPlane documentation and program that converts the apparent dip data to true strike and dip in an archived form. GRAPE, MST, and index properties are also reported on the CD-ROM.